

**TECHNISCHE
UNIVERSITÄT
WIEN**
Vienna University of Technology

MASTER THESIS

Synthesis and Characterization of Triarylamine Based Materials as Two Photon Absorption Photoinitiators

conducted at the

Institute of Applied Synthetic Chemistry
at the **Vienna University of Technology**

under supervision of

Univ.Prof. Dipl.-Ing. Dr.techn. Johannes **Fröhlich**

advised by

Univ.Ass. Dipl.-Ing. Brigitte **Holzer**,

Univ.Ass. Dipl.-Ing. Dr.techn. Daniel **Lumpi**,

and

Senior Lecturer Dipl.-Ing. Dr.techn. Ernst **Horkel**

by

Markus **Lunzer**, BSc.

Matr.Nr.: 0709583

Heinzelmanngasse 22/22, 1200 Wien

Vienna, September 1, 2014

Danksagung

An dieser Stelle möchte ich mich bei Univ.Prof. Dr. Johannes Fröhlich für die Möglichkeit bedanken, diese Masterarbeit in seiner Forschungsgruppe durchzuführen. Sowohl den Freiraum bei der Durchführung der wissenschaftlichen Arbeit, als auch die nicht obligatorische Unterstützung für die Teilnahme an Konferenzen weiß ich sehr zu schätzen.

Im Besonderen möchte ich mich bei Univ.Ass Dipl.-Ing. Brigitte Holzer für die herausragende praktische Betreuung und Unterstützung während dieser Arbeit bedanken. Auch gilt mein Dank Univ.Ass. Dr. Daniel Lumpi für die ausgezeichnete Betreuung. Beiden danke ich für die Erreichbarkeit auch außerhalb üblicher Bürozeiten.

Senior Lecturer Dr. Ernst Horkel und Ass.Prof. Dr. Christian Hametner möchte ich für Beratung und Hilfestellungen im Zuge dieser Arbeit danken.

Bei Dipl.-Ing. Paul Kautny bedanke ich mich für die Hilfe bei der Messung der Absorptions- und Emissionsspektren und anderen Fragestellungen.

Für die gute Zusammenarbeit und die Unterstützung bei den Strukturierungsversuchen möchte ich Dipl.-Ing Maximilian Tromayer danken.

Frau Elisabeth Eitenberger danke ich für die Aufnahmen der SEM-Bilder, sowie Andreas Gaubitzer für das Anfertigen von Lichtmikroskop-Aufnahmen.

Des Weiteren möchte ich mich bei meinen Laborkollegen Florian Glöcklhofer und Babara Sohr sowie den vielen weiteren Mitgliedern der Forschungsgruppe für das gute Arbeitsklima und die unbeschwerte Zeit bedanken.

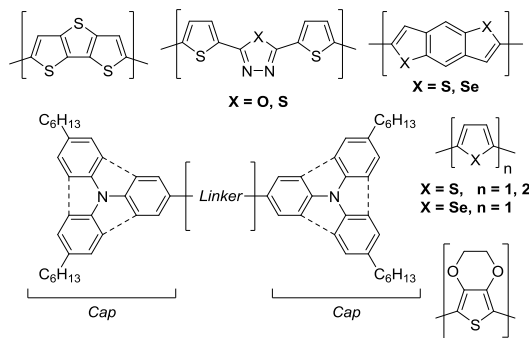
Besonders möchte ich mich bei meinen Eltern Josef und Birgit für die Ermöglichung eines Studiums, den mir entgegengebrachten Freiraum sowie die großzügige Unterstützung in den letzten Jahren bedanken.

Im Speziellen möchte ich mich bei meiner Freundin Julia für ihr großes Verständnis während dieser besonders arbeitsintensiven Zeit am Ende des Studiums bedanken.

Kurzfassung

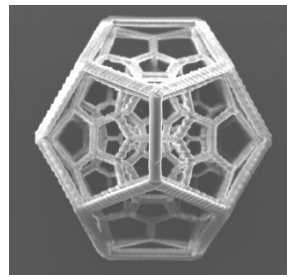
Zweiphotoneninduzierte Photopolymerisation (2PIP) ermöglicht die Fabrikation von 3D-Strukturen mit Dimensionen im Submicrometerbereich. Da bei dieser Technologie Probleme im Zusammenhang mit linearer Absorption umgangen werden, kann der Anregungsstrahl unter der Oberfläche der Monomerformulierung fokussiert werden, ohne dabei die Schichten ober- und unterhalb der fokalen Ebene zu beeinflussen.

Aufgrund großer Fortschritte in den vergangenen Jahren steht die 2PIP kurz vor der Marktreife. Um diese Entwicklung weiter voranzutreiben, werden hocheffiziente 2PA-Photoinitiatoren (2PA-PIs) benötigt. Hierfür geeignete Moleküle beinhalten üblicherweise starke π -Donor- (D) oder Akzeptor- (A) Gruppen sowie ein delokalisiertes π -Elektronensystem.



Struktur motive von 2PA-PIs.

Diese Arbeit beschäftigt sich mit der Synthese und Charakterisierung symmetrischer D- π -D Moleküle auf Basis von Triphenylamin-Donor-Gruppen und heterocyclischen π -Linkern als potentielle 2PA-PIs.



Komplexe 3D-Struktur aus 2PIP-Test.

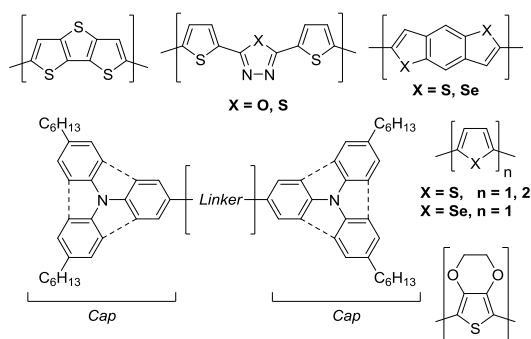
Strategien zur Erhöhung der 2PA und damit der 2PIP-Effizienz dieser Cap-Linker-Cap Strukturen sind (i) Erhöhung der Elektronendichte der Linker, sowie (ii) Planarisierung der Linker, (iii) und der Caps. Weiters wurden D- π -A- π -D Verbindungen basierend auf Oxadiazol and Thiadiazol hergestellt. Um die Löslichkeit an Monomerformulierungen anzupassen, erfolgte eine Modifizierung der Triarylaminbausteine mit *n*-Hexylresten.

Neben photophysikalischer Charakterisierung wurden die Zielsubstanzen mittels 2PIP Strukturierungstests evaluiert und zeigten dabei hohe Effizienz im Vergleich zu etablierten 2PA-PIs.

Abstract

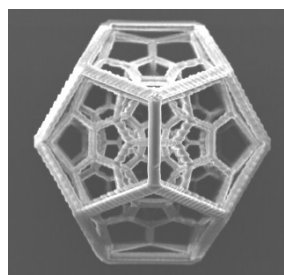
Two-photon induced photopolymerization (2PIP) enables the fabrication of 3D structures with dimensions in the submicrometer range. As this technique avoids the problems associated with linear absorption, the excitation beam can penetrate deeply into the monomer formulation, leaving layers above and beyond the focal plane unaffected.

Owing to great advances in recent years 2PIP is on the edge of commercialization. To further promote this progress highly efficient two-photon absorption photoinitiators (2PA-PIs) are strongly required. Suitable initiator compounds usually contain strong π -donor (D) or acceptor (A) groups and an extended delocalized π -system.



Structural motifs of 2PA-PIs.

This work focuses on the synthesis and characterization of potential 2PA-PIs based on symmetric D- π -D type molecules containing triphenylamine donor groups and heterocyclic π -linkers.



Complex 3D-model fabricated applying a resin from the structuring tests.

Strategies to increase 2PA and thus the 2PIP efficiency of these cap-linker-cap type molecules are (i) increasing the electron density of the linker, (ii) planarization of the linker, (iii) and the caps. Additionally, D- π -A- π -D type compounds based on oxadiazole and thiadiazole are investigated. To adjust the solubility to the respective monomer formulation *n*-hexyl residues are introduced to the triarylamine building blocks.

Besides photophysical characterization, target molecules are evaluated *via* 2PIP structuring tests revealing good efficiencies as 2PA-PIs.

Abbreviations

Besides common abbreviations in the English language and chemical element symbols the below listed short forms are used.

1PA	one-photon absorption
1PIP	one-photon induced photopolymerization
2PA	two-photon absorption
2PA-PIs	two-photon absorption photoinitiators
2PIP	two-photon induced photopolymerization
3D	three dimensional
A	π -acceptor
ACN	acetonitrile
AOM	acousto-optic modulator
APT	attached proton test
BET	back electron transfer
<i>n</i> -BuOH	<i>n</i> -butanol
CCD	charge-coupled devise
conc.	concentrated
D	π -donor
DACH	(\pm)- <i>trans</i> -1,2-diaminocyclohexane
DCM	dichloromethane
DDQ	2,3-dichloro-5,6-dicyano-1,4-benzoquinone
DMAc	dimethylacetamide
DMF	dimethylformamide
DTT	ithieno[3,2- <i>b</i> :2',3'- <i>d</i>]thiophene
EDOT	2,3-dihydrothieno[3,4- <i>b</i>]-1,4-dioxin
EA	ethyl acetate
eq	equivalents
Et ₃ N	triethylamine
EtOH	ethanol
GC-MS	gas chromatography-mass spectrometry
IC	internal conversion
ICT	intramolecular charge transfer
IR	infrared

KO ^t Bu	potassium <i>tert</i> -butoxide
LAH	lithium aluminium hydride
M	monomer
MeOH	methanol
Me ₃ SnCl	trimethyltin chloride
NBS	<i>N</i> -bromosuccinimide
NIS	<i>N</i> -iodosuccinimide
NA	numerical aperture
NMP	<i>N</i> -methyl-2-pyrrolidone
NMR	nuclear magnetic resonance
<i>n</i> -BuLi	<i>n</i> -buthyllithium
<i>n</i> -HexLi	<i>n</i> -hexyllithium
PE	light petrol, b.p.: 45-60 °C
PI	photoinitiator
ⁱ PrOH	isopropanol
sat.	saturated
SEM	scanning electron microscopy
<i>t</i> -BuLi	<i>tert</i> -buthyllithium
THF	tetrahydrofuran
TMS	trimethylsilyl
TLC	thin-layer chromatography
TMEDA	tetramethylethylenediamine
UV	ultraviolet

General remarks

Labeling of substances

Identification of substances is achieved by strict sequential numbering. Structurally similar substances receive same numbers combined with additional small Latin letters for further differentiation. Substances previously reported in literature receive Arabic numerals, whereas substances unknown to literature are labeled in Roman numerals.

References to literature citations

References to literature are given within the text by Arabic numbers in square brackets.

Nomenclature

The nomenclature of chemical compounds not described in literature is based on the rules of Chemical Abstracts. Other compounds, reagents and solvents may be described by simplified terms, trivial or trade names.

Table of Contents

A. FORMULA SCHEME	1
A.1 Synthesis of Cap-systems	2
A.1.1 Synthesis of Triphenylamine Cap-system	2
A.1.2 Synthesis of Hexyl-substituted Cap-systems	2
A.1.3 Synthesis of Pinbop®	3
A.1.4 Cap Abbreviations	3
A.2 Synthesis of Linkers	4
A.2.1 Linker Synthesis	4
A.2.2 Synthesis of Acceptors	4
A.2.3 Acceptor Abbreviations.....	4
A.3 Synthesis of 2PA-PIs	5
A.3.1 Synthesis of Linker-based 2PA-PIs	5
A.3.2 Synthesis of Acceptor-based 2PA-PIs	6
B. GENERAL PART	7
B.1 Multiphoton-absorbing Materials	8
B.1.1 The Effects of Two-photon Absorption (2PA).....	8
B.1.2 Physical Principles.....	10
B.1.3 The 2PA Cross-section - δ_{2PA}	13
B.2 Applications and Molecular Design	15
B.3 Two-photon Induced Photopolymerization	16
B.3.1 Two-photon Microfabrication	16
B.3.2 Radical Photopolymerization	18
B.3.3 One-photon Induced Radical Photopolymerization	18
B.3.4 Two-photon Induced Radical Photopolymerization	20
B3.5 State of the Art 2PA-PIs for Radical Photopolymerization.....	22
B.3.5 Electron Rich Heterocycles as Structural Motifs in 2PA-PIs	26
B.4 Goal of the Thesis	27
C. SPECIFIC PART	29
C.1 Introduction	30
C.2 Synthesis	34
C.2.1 Synthesis of Cap-systems	34
C.2.1.1 Synthesis of Boronic Acid Esters	34
C.2.1.2 Synthesis of Brominated 5,11-Dihexylindolocarbazole	34
C.2.1.3 Synthesis of Triphenylamine Cap-systems.....	35
C.2.1.4 Synthesis of 1-Hexyl-4-iodo-benzene.....	38
C.2.1.5 Synthesis of 3,6-Dihexyl-9 <i>H</i> -carbazole.....	39
C.2.2 Synthesis of Linkers	40

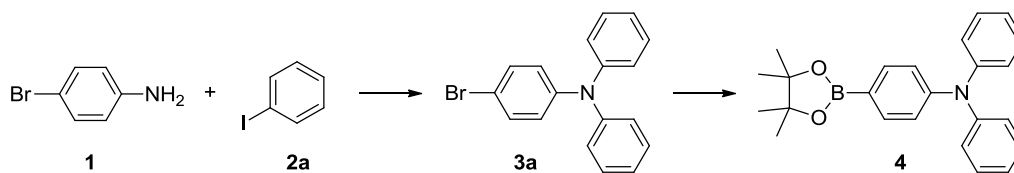
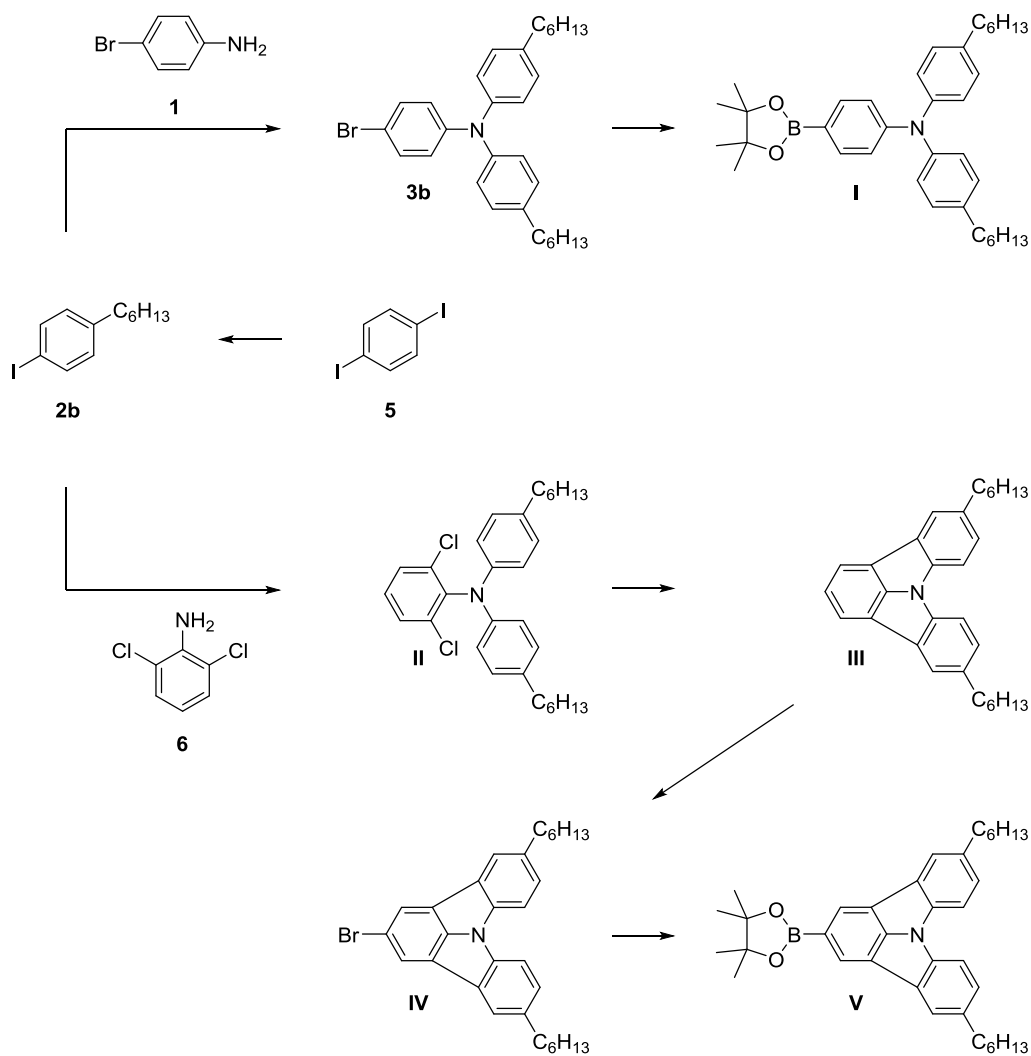
Table of Contents

C.2.2.1 Synthesis of BBT and BBS	40
C.2.2.2 Synthesis of the Selenophene Linker	44
C.2.2.3 Synthesis of Acceptors	44
C.2.3 Synthesis of 2PA-PIs	45
C.2.3.1 Synthesis of Linker-based 2PA-PIs	46
C.2.3.3 Synthesis of Acceptor-based 2PA-PIs.....	49
C.3 Photophysical Characterization of Target Molecules.....	50
C.3.1 Absorption and PL-Emission Spectra of Linker Based 2PA-PIs	50
C.3.2 Absorption and PL-Emission Spectra of Acceptor Based 2PA-PIs.....	52
C.4 2PIP-Structuring Tests.....	53
C.5 Conclusion and Outlook.....	61
D. EXPERIMENTAL PART	63
D.1 General Remarks	64
D.2 Chromatographic Methods.....	64
D.2.1 Thin Layer Chromatography.....	64
D.2.2 Column Chromatography	64
D.3 Analytical Methods.....	65
D.3.1 GC-MS Measurements.....	65
D.3.2 NMR-Spectroscopy	65
D.3.3 Absorption Spectroscopy.....	65
D.3.4 Fluorescence Spectroscopy	65
D.4. 2PIP-Structuring Tests.....	66
D.4.1 Laser Device.....	66
D.4.2 2PIP-sample Preparation	67
D.4.3 Functionalization of Glass Substrates	68
D.5 Synthesis and Characterization of the Compounds.....	68
D.5.1. General Reaction Procedures	68
GP1: Ligand-accelerated Catalyzed Ullmann Condensation	68
GP2: Synthesis of the Boronic Acid Esters	69
GP3: Suzuki Cross-coupling Reaction Using (NHC)Pd(allyl)Cl as Catalyst	70
GP4: Stille Cross-coupling Reactions Using Pd(PPh ₃) ₄ as Catalyst.....	70
D.5.2 Synthesis of Cap-systems	71
D.5.2.1 Synthesis of Triphenylamine Cap-system	71
4-Bromo- <i>N,N</i> -diphenylbenzeneamine (3a).....	71
D.5.2.1 Synthesis of Hexyl-substituted Cap-systems	72
4-Bromo- <i>N,N</i> -bis(4-hexylphenyl)benzeneamine (3b).....	73
<i>N,N</i> -Bis(4-hexylphenyl)-4-(4,4,5,5-tetramethyl-1,3,2-dioxaborolan-2-yl)-benzeneamine (I).....	74
2,6-Dichloro- <i>N,N</i> -bis(4-hexylphenyl)benzeneamine (II)	75
5,11-Dihexylindolo[3,2,1- <i>jk</i>]carbazole (III)	76
2-Bromo-5,11-dihexylindolo[3,2,1- <i>jk</i>]carbazole (IV)	77
5,11-Dihexyl-2-(4,4,5,5-tetramethyl-1,3,2-dioxaborolan-2-yl)indolo[3,2,1- <i>jk</i>]carbazole (V)	77
1,1'-(9 <i>H</i> -Carbazole-3,6-diyl)bishexan-1-one (8).....	78
3,6-Dihexyl-9 <i>H</i> -carbazole (9).....	79
9-(4-Bromophenyl)-3,6-dihexyl-9 <i>H</i> -carbazole (VI)	80

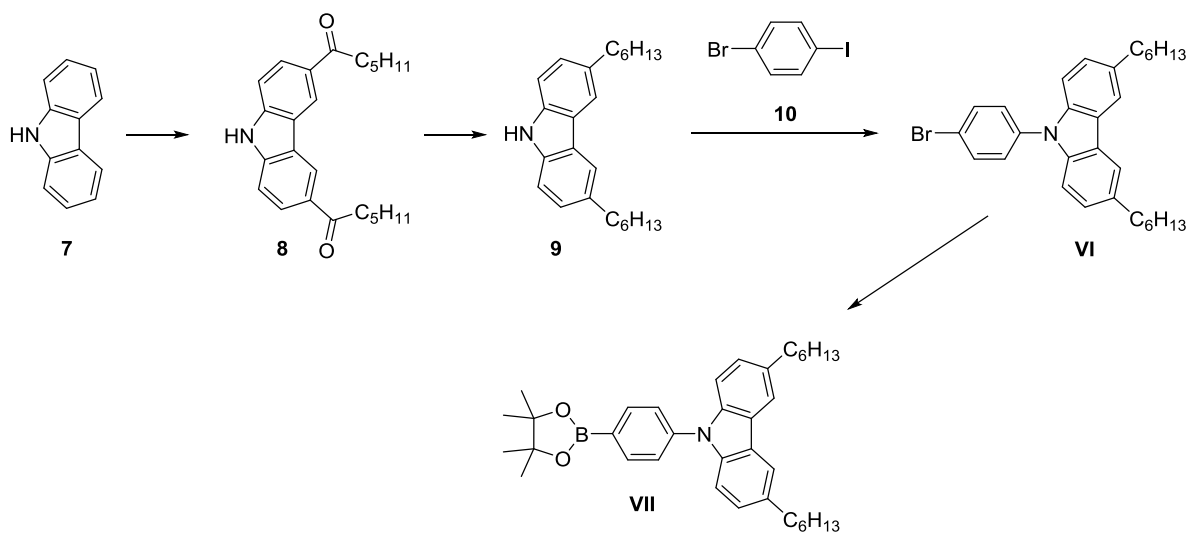
Table of Contents

3,6-Dihexyl-9-(4-(4,4,5,5-tetramethyl-1,3,2-dioxaborolan-2-yl)phenyl)-9 <i>H</i> -carbazole (VII).....	81
D.5.3. Synthesis of Pinbop [®]	82
4,4,5,5-Tetramethyl-2-(1-methylethoxy)-1,3,2-dioxaborolane (Pinbop [®]) (12)	82
D.5.4 Synthesis of Linkers	82
1,1'-Benzo[1,2- <i>b</i> :4,5- <i>b'</i>]dithiophene (14a)	82
1,1'-Benzo[1,2- <i>b</i> :4,5- <i>b'</i>]diselenophene (14b)	83
1,1'-Benzo[1,2- <i>b</i> :4,5- <i>b'</i>]dithiophene-2,6-diylbis(1,1,1-trimethylstannane) (15a)	84
1,1'-Benzo[1,2- <i>b</i> :4,5- <i>b'</i>]diselenophene-2,6-diylbis(1,1,1-trimethylstannane) (15b)	85
2,5-Dibromoselenophene (17).....	85
1,1'-(2,5-Selenophenediyl)bis(1,1,1-trimethylstannane) (18)	86
D.5.5 Synthesis of acceptors	87
5-Bromo-2-thiophenecarboxylic acid ethyl ester (20).....	87
5-Bromo-2-thiophenecarboxylic acid (21)	87
5-Bromo-2-thiophenecarbonyl chloride (22).....	88
5-Bromo-2-thiophenecarboxylic acid, 2-(5-bromo-2-thienylcarbonyl)hydrazide (23)	89
2,5-Bis(5-bromo-2-thienyl)-1,3,4-oxadiazole (24a).....	89
2,5-Bis(5-bromo-2-thienyl)-1,3,4-thiadiazole (24b).....	90
D.5.6 Synthesis of 2PA-PIs	91
D.5.6.1 Synthesis of linker-based 2PA-PIs	91
4,4'-(2,3-Dihydrothieno[3,4- <i>b</i>]-1,4-dioxine-5,7-diyl)bis [<i>N,N</i> -bis(4-hexylphenyl)benzeneamine] (VIII, HxTPA-1E).....	91
4,4'-(2,5-Thiophenediyl)bis[<i>N,N</i> -bis(4-hexylphenyl)benzeneamine] (IXa, HxTPA-1T).....	92
4,4'-(2,2'-Bithiophene-5,5'-diyl)bis[<i>N,N</i> -bis(4-hexylphenyl)benzeneamine] (IXb, HxTPA-2T).....	93
2,2'-(2,2'-Bithiophene-5,5'-diyl)bis(5,11-dihexylindolo[3,2,1- <i>jk</i>]carbazole) (X, HxICz-2T).....	94
9,9'-(2,2'-Bithiophene-5,5'-diyl)di-4,1-phenylene)bis-3,6-dihexyl-9 <i>H</i> -carbazole (XI, HxPCz-2T) ...	94
4,4'-(2,5-Selenophenediyl)bis[<i>N,N</i> -bis(4-hexylphenyl)benzeneamine] (XII, HxTPA-1S)	95
4,4'-(Dithieno[3,2- <i>b</i> :2',3'- <i>d</i>]thiophene-2,6-diyl)bis [<i>N,N</i> -bis(4-hexylphenyl)benzeneamine] (XIII, HxTPA-1DTT).....	96
4,4'-(1,1'-Benzo[1,2- <i>b</i> :4,5- <i>b'</i>]dithiophene-2,6-diyl)bis [<i>N,N</i> -bis(4-hexylphenyl) benzeneamine] (XIVa, HxTPA-1BBT).....	97
4,4'-(1,1'-Benzo[1,2- <i>b</i> :4,5- <i>b'</i>]diselenophene-2,6-diyl)bis [<i>N,N</i> -bis(4-hexylphenyl)benzeneamine] (XIVb, HxTPA-1BBS).....	98
D.5.6.2 Synthesis of acceptor-based 2PA-PIs	99
4,4'-(1,3,4-Oxadiazole-2,5-diyl)di-2,5-thiophenediyl)bis[<i>N,N</i> -diphenylbenzeneamine] (29, TPA-TOxD).....	99
4,4'-(1,3,4-Thiadiazole-2,5-diyl)di-2,5-thiophenediyl)bis[<i>N,N</i> -diphenylbenzeneamine] (XV, TPA-TThD)	100
4,4'-(1,3,4-Oxadiazole-2,5-diyl)di-2,5-thiophenediyl)bis [<i>N,N</i> -bis(4-hexylphenyl)benzeneamine] (XVIa, HxTPA-TOxD).....	101
4,4'-(1,3,4-Thiadiazole-2,5-diyl)di-2,5-thiophenediyl)bis [<i>N,N</i> -bis(4-hexylphenyl)benzeneamine] (XVIb, HxTPA-TThD).....	102
E. BIBLIOGRAPHY.....	A
F. APPENDIX	- 1 -
F.1 NMR-spectra.....	- 2 -
F.2 SEM-images of 2PIP-structuring tests	- 21 -

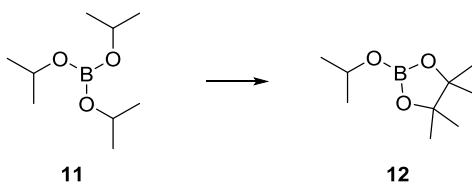
A. Formula Scheme

A.1 Synthesis of Cap-systems**A.1.1 Synthesis of Triphenylamine Cap-system****A.1.2 Synthesis of Hexyl-substituted Cap-systems**

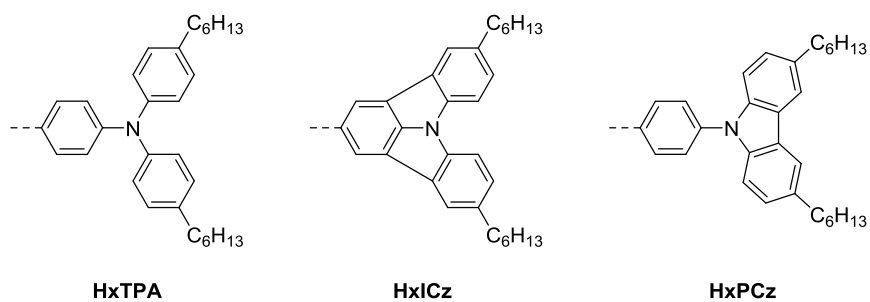
A. Formula Scheme



A.1.3 Synthesis of Pinbop[®]

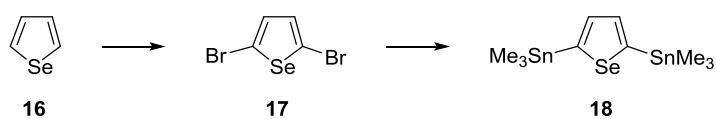
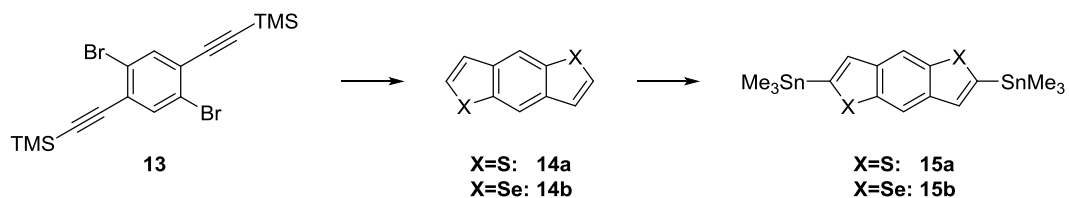


A.1.4 Cap Abbreviations

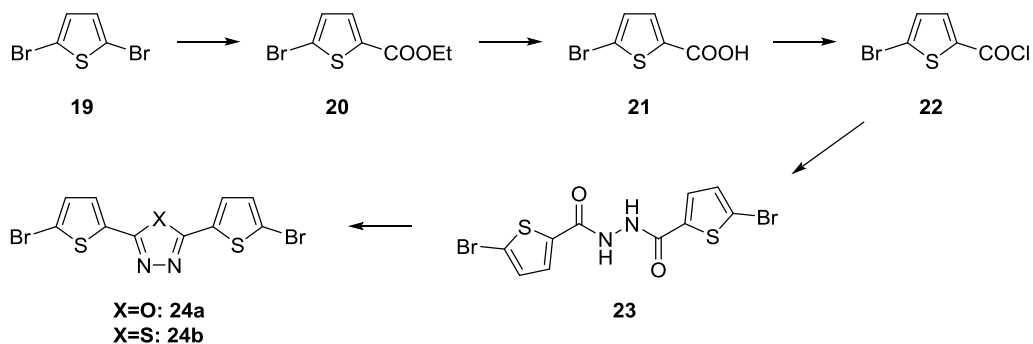


A.2 Synthesis of Linkers

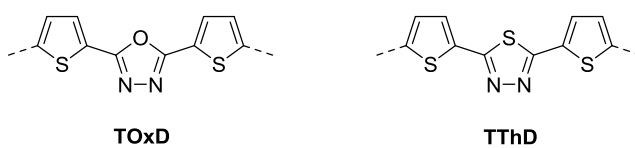
A.2.1 Linker Synthesis



A.2.2 Synthesis of Acceptors

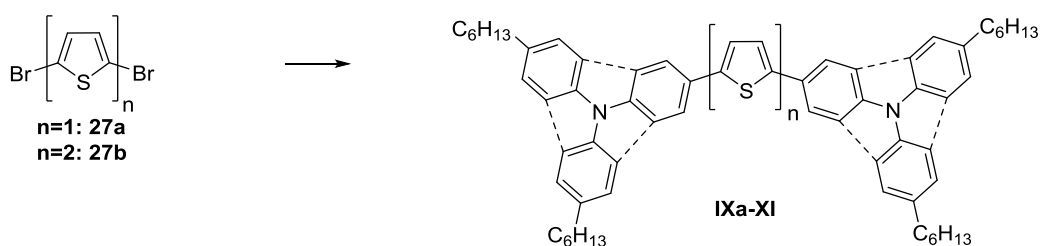
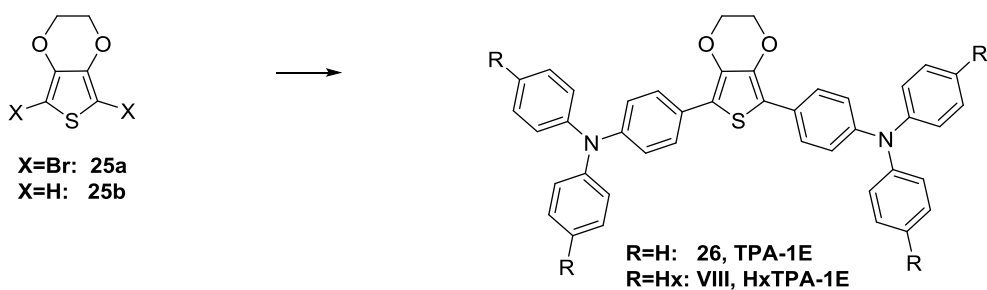


A.2.3 Acceptor Abbreviations

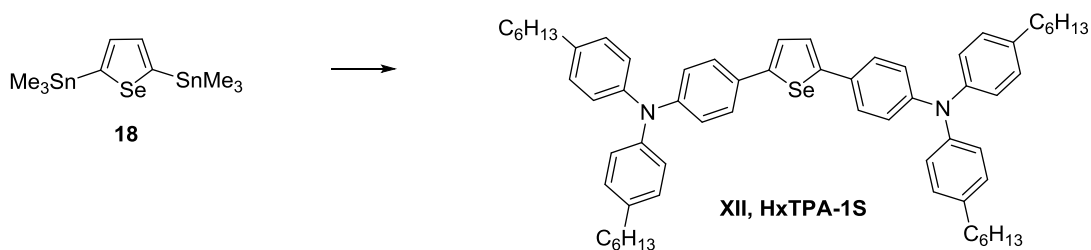


A.3 Synthesis of 2PA-PIs

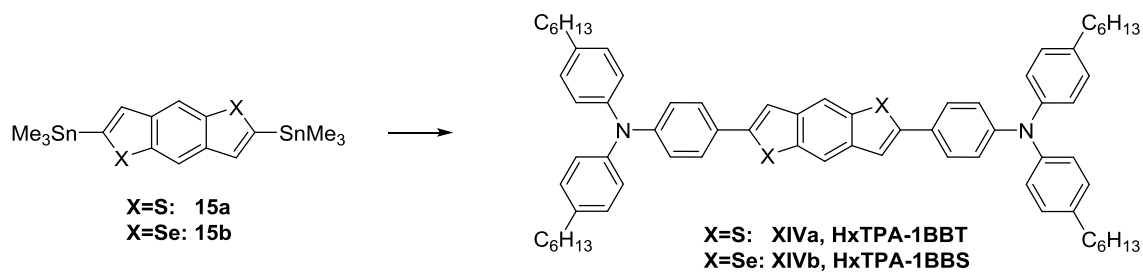
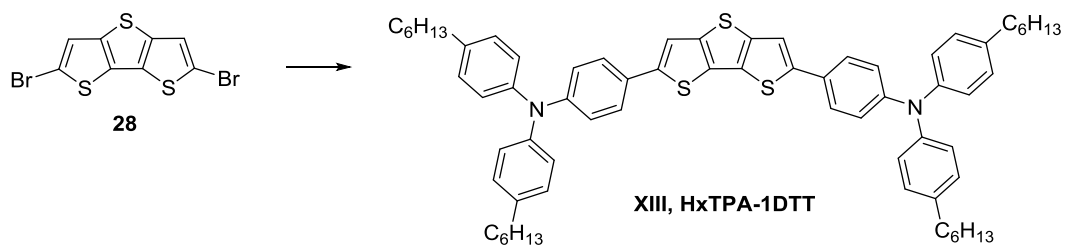
A.3.1 Synthesis of Linker-based 2PA-PIs



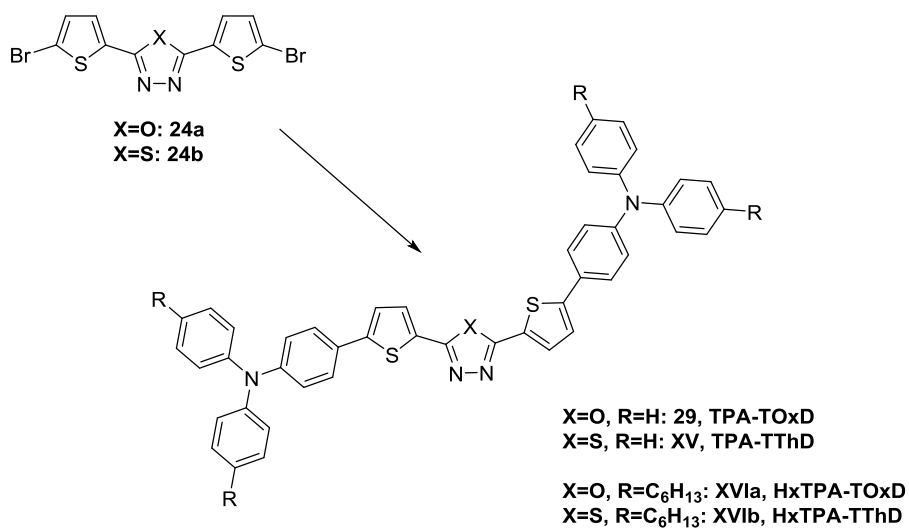
	number of thiophen units	cap system	substance abbreviation
XIa	n=1	HxTPA	HxTPA-1T
XIb	n=2	HxTPA	HxTPA-2T
X	n=2	HxCz	HxCz-2T
XI	n=2	HxPCz	HxPCz-2T



A. Formula Scheme



A.3.2 Synthesis of Acceptor-based 2PA-PIs



B. General Part

B.1 Multiphoton-absorbing Materials

B.1.1 The Effects of Two-photon Absorption (2PA)

The simultaneous absorption of two photons by the same molecule was first predicted in 1931 by Göppert-Mayer in her doctoral thesis,^[1] yet the first experimental confirmation of a 2PA induced process followed 30 years later, shortly after the invention of the laser.^[2] However, two-photon absorption processes did not gain much interest until femtosecond pulsed laser technology became forthcoming in the 1990s (particularly the Ti:sapphire laser).^[3]

In contrast to linear absorption processes, 2PA is a non-linear optical (NLO) event whereby a molecule instantaneously absorbs a pair of photons, whose sum of energy equals the transition energy. Nevertheless, the transition property of this process is inherently weak at normal light intensities.^[4-5]

However, in the presence of intense laser pulses, molecules can simultaneously absorb two or more photons with the transition probability for the absorption of two identical photons being proportional to I^2 ,¹ with I being the intensity of the resonant light (Figure 1).^[6] Since the intensity of a focused laser beam decreases quadratically with distance from the focal point, 2PA falls off as the fourth power of distance from the focal point^[4], which is a crucial characteristic for the application of 2PA.

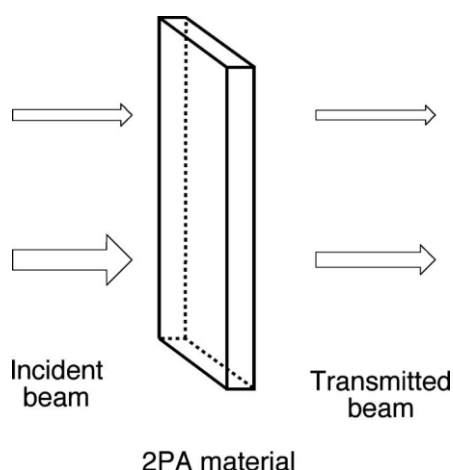


Figure 1: Schematic illustration of the attenuation of a beam incident on a volume element of material exhibiting 2PA. Due to the nonlinear nature of the phenomenon the transmittance of the material depends on the intensity of the incident beam: a weak beam (*above*) is absorbed to a smaller degree than an intense beam (*below*).^[5]

¹ In the case of two photons with different energies the transition probability is proportional to the product of their intensities.^[5]

As a consequence two-photon excitation provides several benefits. On the one hand 2PA is a powerful tool to activate chemical or physical processes with high spatial resolution in three dimensions by applying laser beams under tight focusing conditions to induce excitation. Any subsequent process, such as fluorescence or a photon-induced chemical reaction, is also localized within this small volume, where excitation takes place.^[7]

On the other hand a key feature of 2PA is the ability to create excited states with photons of half the actual excitation energy required for one-photon absorption. Hence, target molecules can be excited at some depth in regularly absorbing or scattering medium by excitation with photon energies certainly below those 1PA.^[4, 6]

The effect of these significant characteristics can be demonstrated by comparison of the excitations caused by application of an IR- and an UV-fs-pulsed laser beam respectively, each narrowly focused in a solution of a fluorescent dye (Figure 2).^[8] In the given case the IR-laser (2PA) emits photons of twice the wavelength λ and hence half the energy compared to the UV-laser (1PA). Fluorescence caused by 1PA can be observed throughout the solution along the entire light path of the hourglass shaped UV-laser beam, decreasing in intensity according to Beer-Lambert law. In the lower example, however, excitation due to 2PA is restricted to the center of the sharp focal point (voxel²) only, showing no fluorescence above and below the focal plane, since intensity decreases as the fourth power of distance from the center.^[4]

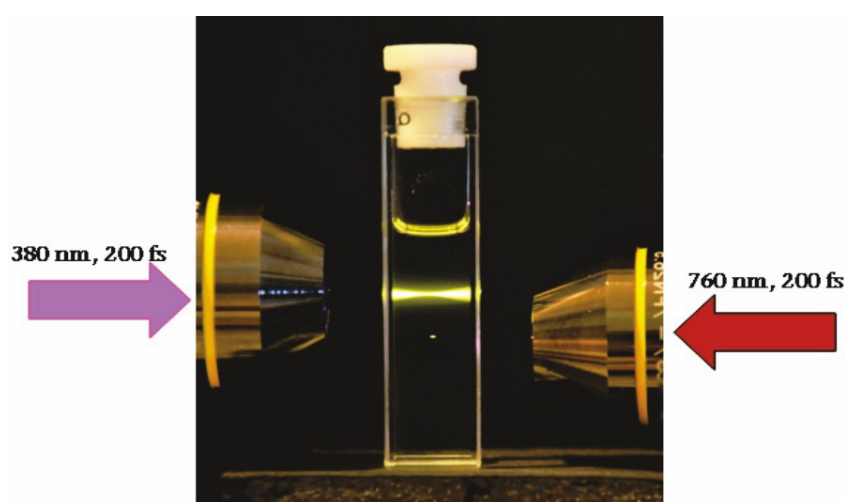


Figure 2: Excitation of a fluorescent dye solution *via* 1PA (*above*) and 2PA (*below*), using narrowly focused laser beams of respective wavelengths (UV, IR).^[8]

² Volume element

The diameter of a focused collimated beam of monochromatic light of uniform intensity is proportional to the wavelength and inversely proportional to the numeric aperture of the focusing lens (vocal volume). Indeed, the excitation density is no real spot but of ellipsoid shape and can be defined as the ellipsoid within which the density of excitation is more than 50% of that at the center of the focus. As a consequence of this geometry the resolution is much poorer in the direction longitudinal to the beam than radial (Figure 3).^[3, 9]

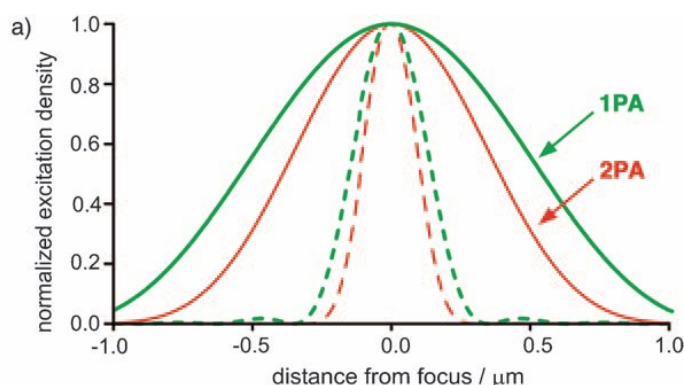


Figure 3: Excitation density as a function of axial and radial distance from the focal point (*green*: 1PA; *red*: 2PA; solid line: axial; dashed line: radial; NA = 1.4, $\lambda = 800$ nm).^[3]

Since the contraction in the excitation volume by going from 1PA to 2PA is less than a factor two and the size of the focal volume is proportional to the wavelength, the resolution achieved from 2PA at 800 nm will be less than that from 1PA at 400 nm. Nevertheless, 2PA is more advantageous as i) longer wavelengths show much smaller absorption and scattering losses and are less harmful to sensitive samples due to lower energy input and ii) the sharper contrast in the excitation density prevents the occurrence of disruptive emission or photochemical reaction outside the focal volume.^[3, 9]

B.1.2 Physical Principles

The act of two-photon absorption involves simultaneous absorption of a pair of photons (of energies E_1 and E_2) by a material (e.g. a molecule), which occurs when the sum of energies $E_1 + E_2$ is in resonance with one of the electronic states of the material system. As a consequence of the absorption process the excitation beam loses intensity and the molecule is brought to an excited state f at $E_1 + E_2 = E_f$ above the ground state g (Figure 4). This absorption process can be imagined as an initial

interaction of a photon of energy E_1 with the material, which is hence raised to a virtual state of energy E_1 above the ground state g . This virtual state is not an actual state (eigenstate) of the molecule and thus exists only for a short time interval τ_v .³ However, if a photon of energy E_2 interacts during this interval τ_v with the molecule, it can be excited to state f . The term “simultaneous” for 2PA indicates that the two photons interact with the respective molecule within the time interval τ_v and that no real intermediate states occur in this process.^[5]

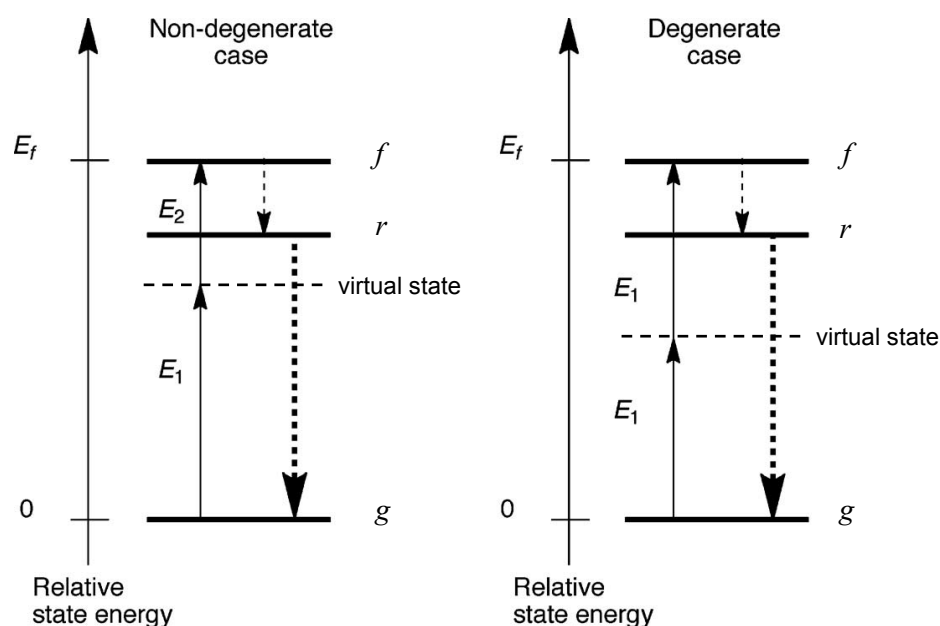


Figure 4: Schematic energy level diagram showing the excitation of a molecule from the ground state g to the excited state f for photons with differing energies (non-degenerated case, *left*) and the same energies (degenerated case, *right*). After excitation to state f the system relaxes quickly to state r , the lowest vibronic level of the lowest-energy excited state, by internal conversion (IC) or vibrational relaxation, from which further physical or chemical processes continue (e.g. relaxation to ground state g via fluorescence).^[5]

The photons inducing 2PA may have the same energy (degenerated case; $E_f = 2E_1$), or different energies (non-degenerated case; $E_f = E_1 + E_2$). The great majority of investigated examples in literature refer to degenerated cases where only one single (or two collinear) coherent linearly polarized excitation beam(s) is (are) used.^[5] In general, a molecule can be excited to state r by absorbing one photon (1PA) with energy equal to the energy difference between states g and r (thick arrow in Figure 5), presuming that this transition is allowed by the selection rules of quantum

³ The order of magnitude for τ_v is 10^{-15} - 10^{-16} s for photon energies in the VIS and NIR (estimated from the uncertainty principle).^[5, 10]

mechanics. In the case of many molecules without an inversion center (left panel in Figure 5), the same state r can be reached through the absorption of two identical photons, each with half the energy of the interval between the states.^[11]

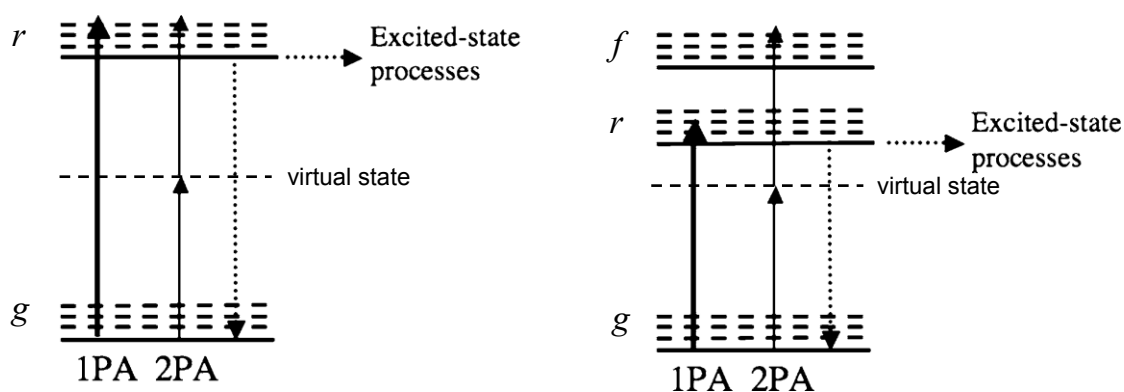


Figure 5: Energy diagrams illustrating the process of one-photon absorption (1PA) and two-photon absorption (2PA) for: (*left*) a molecule without an inversion center; (*right*) a molecule with an inversion center. The length of each arrow is proportional to the photon energy. The dotted arrows represent possible relaxation pathways.^[11]

However, for centrosymmetric molecules the selection rules for 1PA differ from those for 2PA and therefore the 1PA-allowed state r cannot be reached directly by 2PA.^[10] As a consequence, in centrosymmetric systems the lowest electronic state accessible through 2PA usually lies at higher energy f than the 1PA-allowed state r (right panel in Figure 5). After excitation by either 1PA or 2PA, a molecule typically undergoes rapid (ps timescale) internal conversion (IC) until the system reaches the lowest level of the state r . From this level, the system can revert to the ground state radiatively (up-converted fluorescence) or *via* non-radiative decay (dotted downward arrows in Figure 5), typically on a ns timescale.^[12] In addition, the molecule can lose the excess energy through other processes e.g. energy transfer or electron transfer, or can react with other molecular species in its surroundings.^[11]

B.1.3 The 2PA Cross-section - δ_{2PA}

A crucial parameter for the quantification of 2PA-efficiency is expressed by the 2PA cross-section δ_{2PA} , which will be discussed briefly below.^[13]

The attenuation of a light beam passing through an optical medium can generally be expressed by the phenomenological Equation 1,

$$\frac{dI(z)}{dz} = -\alpha I(z) - \beta I^2(z) - \gamma I^3(z) \dots \quad (1)$$

wherein $I(\lambda)$ is the intensity of the incident light beam propagating along the z-axis and α, β , and γ , are the one-, two-, and three-photon absorption coefficients of the transmitting medium, respectively.

Under the assumptions that the incident light has a uniform transverse intensity distribution, the initial intensity is not dependent on time and under the conditions that there is no linear absorption ($\alpha = 0$) at the wavelength λ of the incident light, and only 2PA takes place, equation 1 simplifies to Equation 2.

$$\frac{dI(z)}{dz} = -\beta I^2(z) \quad (2)$$

Expression 2 describes the proportionality of the 2PA probability of molecules to the square of the local light intensity. The solution of Equation 2 is

$$I(z, \lambda) = \frac{I_0(\lambda)}{1 + \beta(\lambda)I_0(\lambda)z} \quad (3)$$

Here, $I_0(\lambda)$ is the incident light intensity, z is the propagation length in the medium, and $\beta(\lambda)$ is the 2PA coefficient that is a material parameter depending on the wavelength of the incident light. $\beta(\lambda)$ (cm/GW) is a macroscopic parameter that depends on the concentration of the two-photon absorbing molecules and can further be expressed as

$$\beta(\lambda) = \sigma'_2(\lambda)N_0 = \sigma'_2(\lambda)N_A d_0 \times 10^{-3} \quad (4)$$

Here σ'_2 is the molecular 2PA cross-section (cm⁴/GW), N_0 is the molecular density (1/cm³), N_A is Avogadro's number, and d_0 is the molar concentration of the absorbing molecules (mol/dm³)⁴.

⁴ Equation 4 is precisely valid only when it can be assumed that the 2PA process is not too strong and most molecules are staying in their ground states. For further information see Ref.^[13]

B. General Part

Although the parameter $\sigma'_2(\lambda)$ is a directly measurable quantity (cm^4/GW) that characterizes the average two-photon absorbability per molecule, another parallel expression for the 2PA cross section is often found in literature, defined by

$$\delta_{2PA} = \sigma_2(\lambda) = \sigma'_2(\lambda) \cdot h\nu \quad (5)$$

with $h\nu$ being the photon energy of the input light beam. According to this definition, δ_{2PA} is in units of $\text{cm}^4 \text{ s} / \text{photon}$. In practice, most of the measured values of δ_{2PA} are in the range from 10^{-51} to $10^{-46} \text{ cm}^4 \text{ s}$. Therefore, another informal unit is often preferred in literature (GM, the abbreviation of Göppert-Mayer), defined by^[3]

$$1 \text{ GM} = 10^{-50} \text{ cm}^4 \text{ s photon}^{-1} \text{ molecule}^{-1} \quad (6)$$

Since the length of the delocalized π -system influences the δ_{2PA} intensively, the maximum of δ_{2PA} per number of conjugated π -electrons (δ_{max}/N_e)^[3] or per molecular weight ($\delta_{\text{max}}/\text{MW}$)^[14] are furthermore used for comparison between different molecules.

There are several methods for the measurement of δ_{2PA} described in literature.^[5] However, the two main techniques for measuring 2PA cross-sections, nowadays, are known as z-scan and two-photon excited fluorescence (2PEF).^[3] 2PEF has the advantage of being highly sensitive, requiring only marginal amounts of dilute 2PA material solutions. However, the method is applicable for materials exhibiting strong fluorescence.^[3] For some applications fluorescence is an undesired material feature, as it is the case with 2PA-photoinitiators (2PA-PIs), where emission dissipates energy, that is lost for photo-induced polymerization processes. Therefore, the z-scan technique is preferred for such materials, as it is even applicable for substances with extremely low fluorescence quantum yields. A disadvantage of the method is its relatively low sensitivity. In comparison to 2PEF considerable concentrations of the investigated substance are required to obtain appropriate signal intensities.^[15]

As δ_{2PA} -values are strongly dependent on the particular measurement setup, experimental conditions, and fitting algorithms applied, comparisons of measured values with those from literature are problematic. Consequently, even if the same method is used, fluctuant results can be obtained for the same compound.^[16]

B.2 Applications and Molecular Design

Based on its unique and beneficial characteristics the concept of 2PA has been exploited for a wide range of applications in many disparate fields, including micro-fabrication,^[17] 3D-data-storage,^[18-19] microscopy,^[9, 20] optical power limiting,^[21] up-converted lasing,^[22] photodynamic therapy,^[23] and the localized release of bio-active species.^[24] Although the utilization of 2PA suffered in its early days due to a lack of appropriated dyes for many applications, with only conventional fluorophores were being available⁵.^[4]

In the last decades, however, much effort has been dedicated to the design and synthesis of highly efficient 2PA materials.^[3, 11, 13-14, 25] This is especially the case because for each application materials need to be identified that satisfy a certain set of requirements. Typically these include the combination of a sizable probability of 2PA at the wavelength of interest (quantified by δ_{2PA}) and high sensitivity for a process to take place after the absorption of two photons, such as fluorescence emission, photochemical reactions, or the sensitization of another material.^[5]

Due to their inherent modularity, organic molecular systems offer a wealth of tuning possibilities in the ongoing search for adequate materials for specific applications. By comparison of electronic structures and photophysical processes, a strong correlation between intramolecular charge-transfer processes and two-photon absorptivity can be deduced.^[6] These findings suggest that the functionalization of molecules with an electron-rich (π -donor, D) component, an electron-withdrawing (π -acceptor, A) component, or both prove to be efficient.^[3] Additionally, the degree of conjugation has been determined as especially important to the δ_{2PA} , since it leads to states with extended charge separation.^[6, 26] Coplanarity is a further critical factor promoting the enhancement of an intramolecular charge transfer.^[27]

A summary of the requirements for maximizing the δ_{2PA} of 2PA active chromophores include:^[3]

- Long, π -conjugated chains with enforced coplanarity to ensure large conjugation lengths
- Strong donor and acceptor groups at the center and ends of the molecule

⁵ and had rather low efficiency for absorbing two photons, i.e. low TPA cross-sections.

- Centrosymmetric chromophores that possess a strong 1PA transition close to the 2PA laser wavelength
- Chromophores with narrow 1PA- and 2PA-bands

In order to increase the δ_{2PA} different molecular design strategies are commonly used as illustrated in Figure 6. As a consequence organic molecules that show two-photon activity can be grouped into four general classes: (i) dipolar, A- π -D; (ii) quadrupolar, A- π -A; D- π -D; A- π -D- π -A; D- π -A- π -D; and (iii) octupolar; 3-branched, A₃-(D-core) and D₃-(A-core); 4-branched, (iv) of higher complexity up to dendrimers (multipolar).^[13, 27]

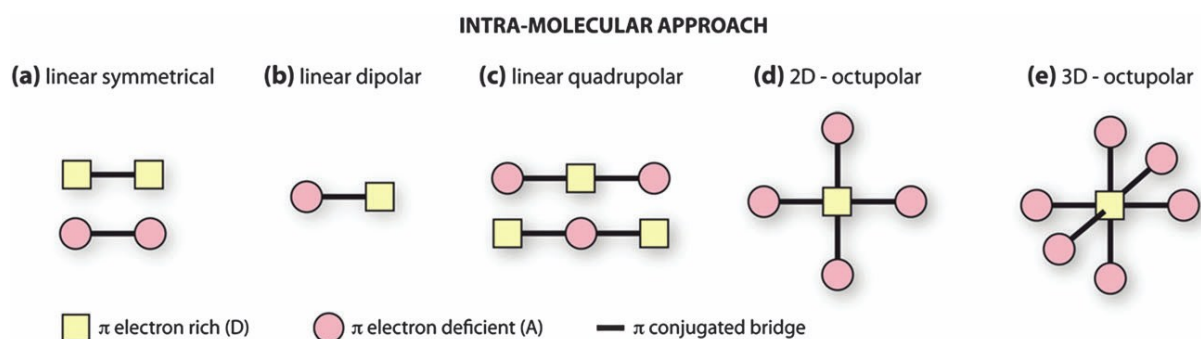


Figure 6: (a) Symmetrical chromophores, characterized by large changes in quadrupole moment during photoexcitation; (b) dipolar chromophores; (c) quadrupolar chromophores; (d) multibranch structures, where two or more dipolar molecules are joined together with an extended π -conjugation; (e) dendritic structures and hyperbranched polymers.^[27]

Besides this intramolecular strategy to highly efficient 2PA materials also intermolecular approaches have been reported^[27], but will not further be discussed as they exceed the scope of this work.

B.3 Two-photon Induced Photopolymerization

B.3.1 Two-photon Microfabrication

The possibility to activate chemical or physical processes within high spatial resolution in 3D by means of 2P excitation and the consequence that every subsequent process such as fluorescence or photoinduced chemical reaction is confined within the small focal excitation ellipsoid allows for the polymerization of suitable photoactive formulations within this small volume (voxel).^[7] Two-photon induced photopolymerization (2PIP) enables the computer-aided generation of

arbitrary 3D structures in a single step, operating at a wavelength beyond the single-photon absorption band of the resin. Since 2P-based approaches avoid the problems of linear absorption, the excitation beam can penetrate deeply into the resin without loss of intensity, yet leaving the layers above and beyond the focal plane unaffected (Figure 7, *left*).^[22] In contrast, for conventional one-photon induced photopolymerization (1PIP) based techniques layer-by-layer fabrication is essential, since 1P excitation can provoke substantial photochemistry outside the focal volume, due to linear absorption, attenuating lithographic contrast and definition, and decelerating the fabrication process (Figure 7, *right*).^[3]

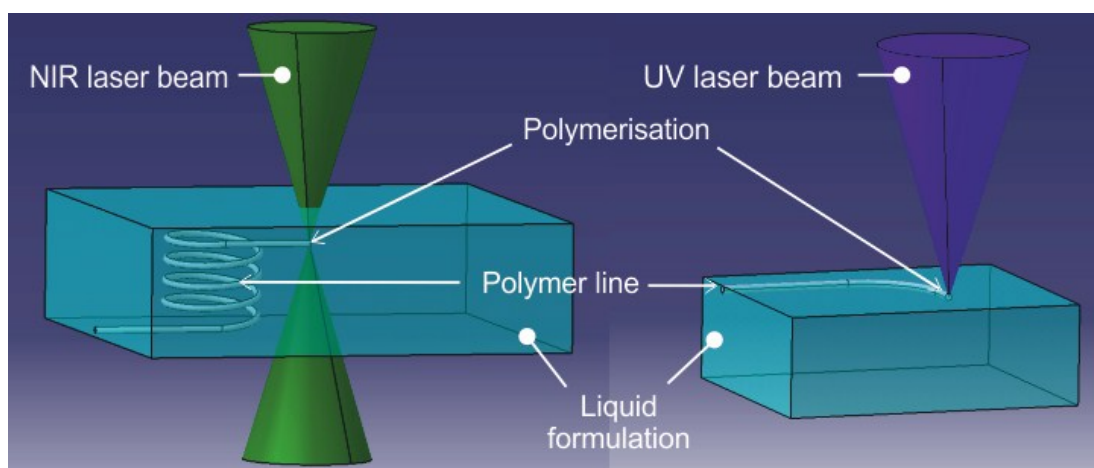


Figure 7: *left*: In a 2PIP process, IR light can be focused in some depth of the 2PA-sensitive resin, which enables direct 3D-structuring. *right*: In a 1PP process, UV light is absorbed at the surface of a photosensitive resin, allowing the fabrication of a planar structure within one manufacturing step only.^[28-29]

Due to the risk of quenching of the photopolymerization by molecular oxygen, high resolution 1PIP processes have to be performed under an inert gas atmosphere. However, 2P induced microfabrication occurs underneath the surface of the resin, diminishing this problem.^[30]

2PIP can be applied in stereolithography and rapid prototyping of structures with resolutions in the sub-micrometer range. Numerous potential applications of 2PIP have been reported, including 3D microfabrication of electronic and optical micro devices,^[31] photonic crystals,^[32] microfluidics channels,^[33] optical data storage,^[7] as well as polymer based optical waveguides on integrated circuit boards,^[34] and biological applications such as the fabrication of hydrogel-scaffolds for cell culturing and tissue engineering.^[35]

Different chemical methodologies for 2PIP have been reported, including (i) the radical polymerization of acrylates, (ii) the acid-catalyzed cationic polymerization of epoxides, and (iii) the polymerization of As_4S_6 glasses to give a cross-linked insoluble inorganic framework.^[3]

In the scope of this work only the former will be further discussed.

B.3.2 Radical Photopolymerization

In a radical photopolymerization monomers (M) and oligomers can be polymerized or cross-linked respectively, upon exposure to light of a suitable wavelength. The former reaction relates to the creation of a polymer by a chain reaction initiated by light, whereas the latter concerns the formation of cross-links between macromolecule chains. Both processes can occur, if a (macro)molecule contains more than one reactive functionality. In order to initiate radical polymerization processes, applicable formulations consist of monomers and photoinitiators (PI), usually photosensitive low-weight molecules, besides further additives and diluents.^[36] Thereby, the absorption band of the PI must overlap with the emission line of the deployed light source and more important, the dissociation energy necessary for bond cleavage must be lower than the excitation energy.

As a result of the excitation the photoinitiator to some degree converts the absorbed energy into chemical energy and forms a radical ($R\cdot$) as reactive intermediate, which subsequently initiates a polymerization reaction of monomers and oligomers.^[37]

Conventional PIs usually require excitation energies from the UV spectral range, absorbing photons *via* a linear 1PA process. Usual 1PIP processes consist of the following steps: ^[30]

- generation of starter radical: $h\nu_{UV} + initiator \rightarrow R\cdot$
- chain initiation: $R\cdot + M \rightarrow M\cdot$
- polymerization reaction: $M\cdot + M \rightarrow M-M\cdot$

B.3.3 One-photon Induced Radical Photopolymerization

Generally, PIs can be classified into type I (cleveable) or type II (hydrogen abstraction), according to their mechanism of radical formation.

The various pathways of activation and deactivation of photoinitiators are exemplified for the commercial PI Irgacure 369 illustrated in Figure 8.

After excitation by common 1PA (UV) or unusual 2PA (IR, simplified illustration), the PI is transferred from the ground state to an excited singlet state and further to a triplet state. A fraction of the absorbed energy may be lost as heat due to internal conversion from the singlet state back to the ground state. Additionally a part of the reactive intermediates can also be quenched by present oxygen, monomer,⁶ or recombination of intermediates. While a minor fraction of the triplet excited PIs abstracts hydrogen from a hydrogen donor and consequently undergoes a transfer and fragmentation process to efficient reactive intermediates, the residual triplet energy is high enough to induce the cleavage of a carbon-hydrogen bond (α - or β -cleavage) the majority of PIs. The formed radicals interact with reactive functionalities of monomers and oligomers, hence initiating a polymerization reaction.^[30, 37-38]

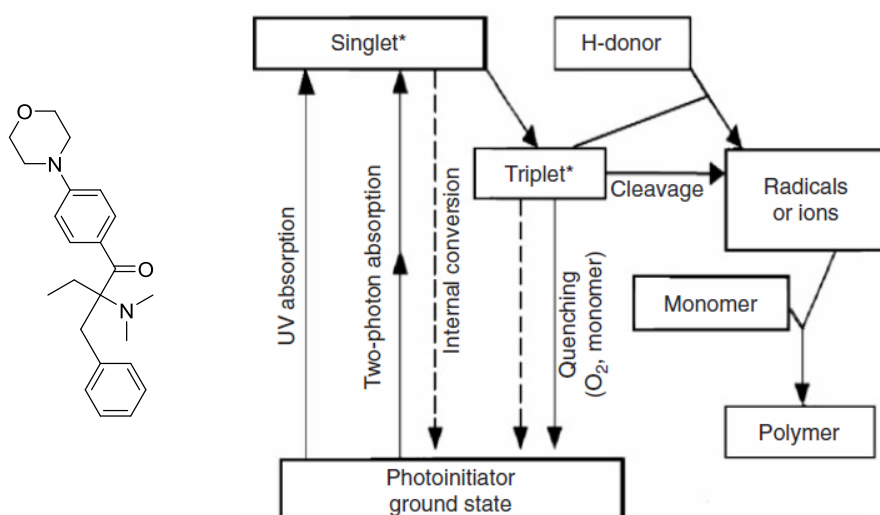


Figure 8: Various pathways for activation and deactivation of PIs upon excitation by the example of the commercial PI Irgacure 369 (left).^[37-38]

Factors that influence the polymerization rate besides the intensity of the light source are the concentration of the PI, the presence of oxygen and additives, the quantum yield for the generation of radicals, as well as the initiation efficiency of the formed radicals. Whereas the polymerization rate generally increases with the light intensity, it does not with the concentration of PI. Requirements for ideal PIs are high molar absorption efficiency, a properly adapted absorption spectral range, and the generation of highly reactive intermediates, while producing non-toxic by-products.

⁶ by inefficient electron or energy transfer to the monomer

For processing reasons it should be compatible with monomers and oligomers, and should be dispersed in the monomer homogeneously before the photo-reaction.^[30]

B.3.4 Two-photon Induced Radical Photopolymerization

For common UV-photoinitiators the 2P cross-sections are usually very small (<10 GM),^[7] resulting in low two-photon sensitivity. Consequently, resins containing initiators of this kind can be structured by means of long exposure times and high excitation intensities only, leading to long writing times and frequently structural damage.^[3, 39]

Consequently, highly efficient 2PA-photoinitiators are required for the application of 2P microfabrication. For this purpose, adequate molecules need to have high δ_{2PA} values, but also high efficiency to produce reactive intermediate radicals. Therefore, competitive deactivation pathways, as fluorescence, should be minimized.

Since only the maximum intensity in the center of the focal volume is high enough to effectively initiate a polymerization process, 2PIP offers the possibility to achieve voxel dimensions significantly smaller than expected from the size of the focal ellipsoid.^[3] Currently, realistic lateral resolutions of about 100 nm and even below can be achieved, though lower resolutions lead to substantially distorted structures.^[40-42] Due to the tiny voxel sizes, it is inherently difficult to investigate mechanisms of 2PIP by means of spectroscopic methods. Thus, exact mechanisms of radical formation and initiation of polymerization are still matters of discussion.

A precise control of the intensity and irradiation time allows for the polymerization of structures below the diffraction limit. As fundamental requirement for functional 2P-microfabrication, the laser intensity has to stay within the boundaries of polymerization, illustrated in Figure 9. The polymerization threshold is defined by the intensity (or irradiation time) at which polymerization initially sets in. By rising the intensity, the voxel size can be increased, resulting in broader lines, as far as the damage threshold is reached. From that intensity on, the formulation gets overexposed and as a consequence bubbles start to form, consequently resulting in damage to the fabricated structures.

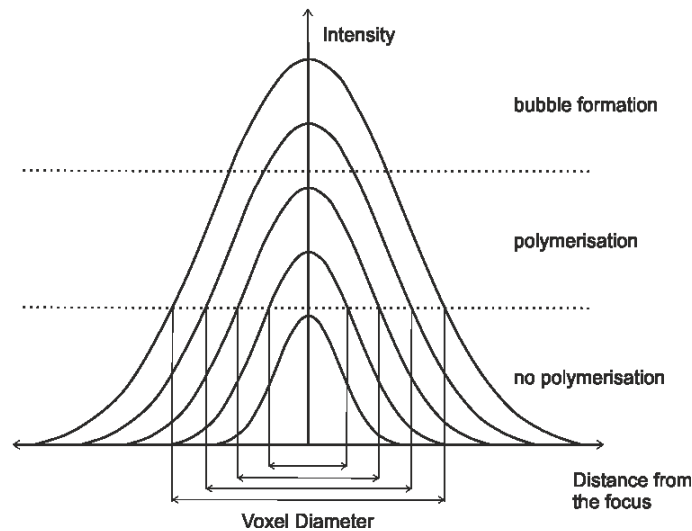


Figure 9: Relation of the laser intensity on the voxel diameter.^[43]

By variation of the laser power and writing speed, a photoactive formulation can be benchmarked according to its lower and upper threshold as well as its process window. By leaving the processing parameters identical for different resin formulations, different performances can be compared regarding their efficiency and reactivity, utilizing speed-power screenings.^[43-44]

Despite its promising benefits, 2P-microfabrication nowadays still suffers from some disadvantages, particularly low writing speed,^[3] holding it off commercialization. Further hindrances are high costs of laser devices,⁷ fluctuant laser stabilities, and high output intensities required, as well as shrinkage of fabricated structures. Thus, research and development in this field are still highly required, both in improving 2PA-PIs as well as advancing structuring devices.

⁷ e.g. sold by Nanoscribe GmbH or LZH in Europe

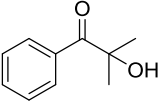
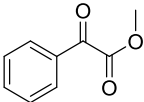
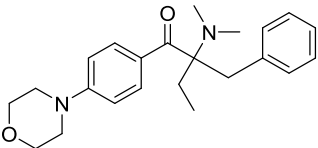
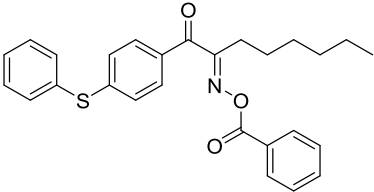
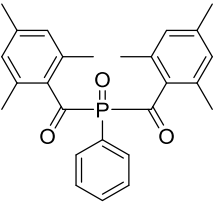
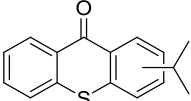
B3.5 State of the Art 2PA-PIs for Radical Photopolymerization

Besides the efforts that have been dedicated to the development of efficient photo-acid generators for cationic 2PIP, free radical based 2PIP is still a beneficial method owing to the large variety of appropriated monomers, fast polymerization rates, and ease of processing.^[17]

As already mentioned above, initially only conventional one-photon initiators have been deployed in 2PIP, which hindered this method from broad application. Since PIs of that kind offer rather small δ_{2PA} , their energy uptake in 2PA processes was inefficient. Table 1 represents an arbitrary selection of commercial 1PA-PIs examined by Schafer *et al.*^[45] concerning their δ_{2PA} . Although high quantum yields of radical formation slightly outweigh their low 2PA, still high excitation powers and long exposure times are required for their excitation, frequently resulting in damage to the polymerized patterns.

B. General Part

Table 1: List of 1PA maxima λ_{abs}^{1PA} , wavelength used for z-scan measurement λ_{z-scan} and δ_{2PA} values of several commercial 1PA-PIs.^[45]

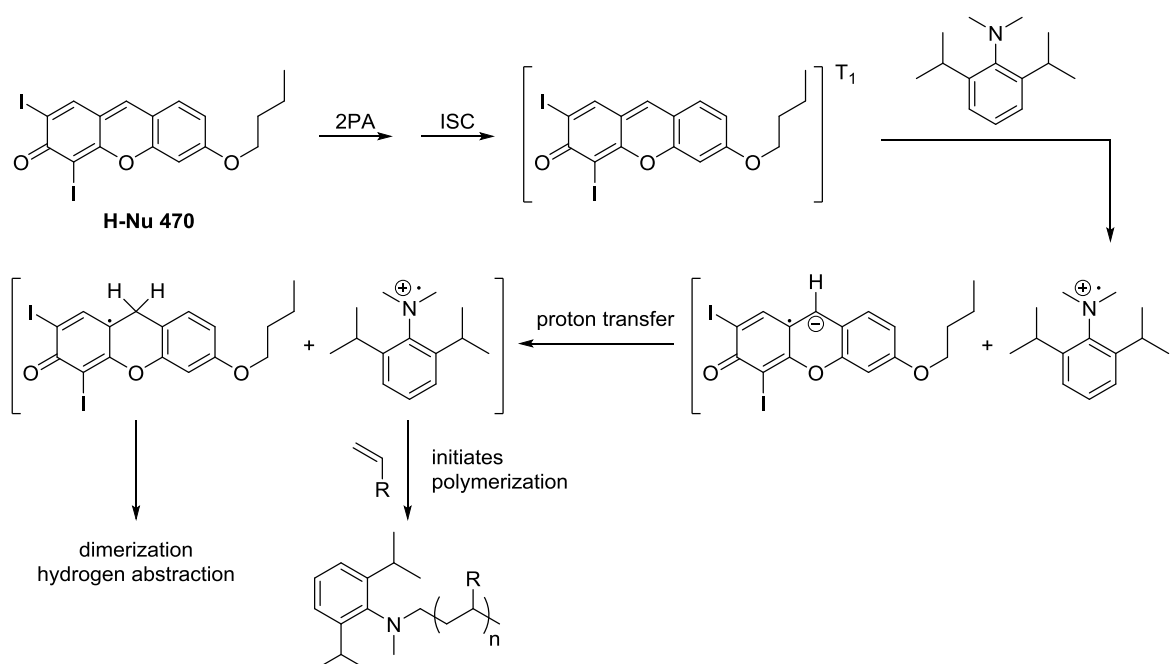
Compound	λ_{abs}^{1PA} (nm)	λ_{z-scan} (nm)	δ_{2PA} (GM)	
Darocure 1173		244	530	< 20
Darocure MBF		255	530	27
Irgacure 369		324	670	7
Irgacure OXE01		328	660	31
Irgacure 819		295	600	< 4
ITX		382	760	5

Several different approaches have been reported to overcome these limitations inherently to 1PA-PIs.

One concept to increase the sensitivity of PIs is the application of adequate chromophors as photosensitizers in combination with common 1PA-PIs or amines as co-initiators. Belfield *et al.*, developed a commercial 2PI system by combining the chromophore **H-Nu 470** with *N,N*-dimethyl-2,6-diisopropyl-benzeneamine.^[46] The working mechanism of this system is comparable to classical type II 1PA-PIs,

B. General Part

operating by hydrogen absorption (Scheme 1). By addition of a diaryliodonium salt as co-initiator to the formulation the rate of polymerization can further be increased.^[47]



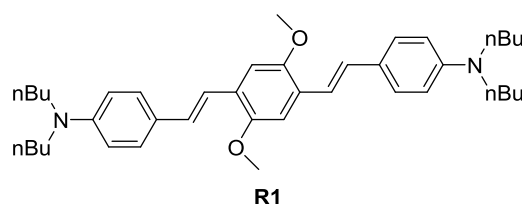
Scheme 1: Mechanism of the dye/amine PI-system applying H-NU 470^[28, 47]

Another approach to increased efficiency of 2PIP was the development of specialized 2PA-PIs that feature a large δ_{2PA} and do not resemble classical 1PA anymore.

Very high δ_{2PA} can be achieved by multipolar push-pull-systems in which π -acceptors and π -donors are interconnected *via* extended highly planar π -systems.^[3] Nevertheless, high 2PA cross-sections do not necessarily account for high efficiency of 2PIP processes only, since absorbed energy of excited states can be dissipated by various other pathways, competing with the formation of radicals, such as fluorescence, phosphorescence, thermal relaxation, as well as isomerization and rearrangement processes, and in the case of systems with bimolecular reaction steps also back electron transfer (BET). So far, the establishing of reliable concepts explaining structure-property relationships of TPIP efficiency, still remains a challenge. Besides some efforts to increase δ_{2PA} through rational molecular design, the most efficient 2PA-PIs up to now have been the outcome of fortunate discoveries, as the efficiency of 2PIP is affected by a multitude of parameters in complex relationship to each other.^[3] Several reviews have been published, highlighting efficient compounds of this kind, including those by Lin *et al.*,^[22] Lee *et al.*,^[48] and Rumi *et al.*^[11]

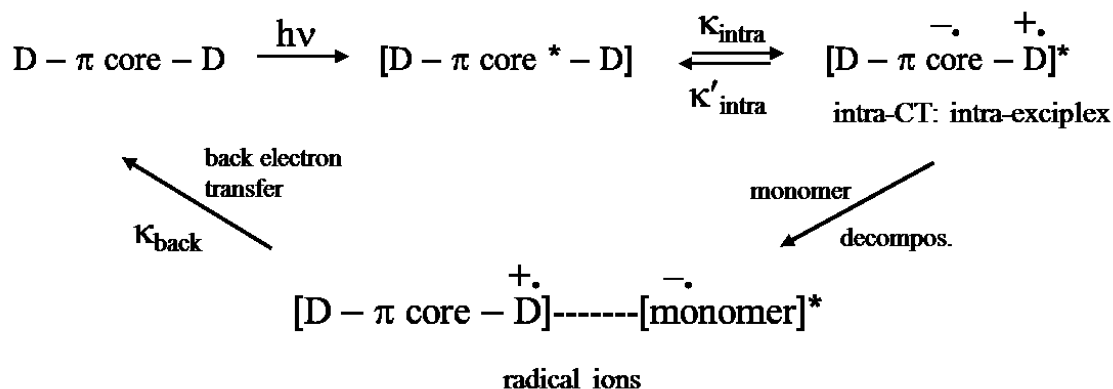
B. General Part

Since fs-pulsed lasers only generate a marginal number of radicals in a very small voxel at any point of time, the mechanism of 2PIP is inherently difficult to investigate by means of spectroscopic methods. Thus, exact mechanisms of radical formation and initiation of polymerization are still matters of discussion. However, since some well working 2PA-PIs, like **R1** (Scheme 2),^[7] do not contain molecular motifs, as weak cleavable bonds or functionalities known to efficiently undergo hydrogen abstraction, classical mechanisms of type I and type II PIs seem unrealistic in those cases.^[7]



Scheme 2: Molecular structure of **R1**^[7]

However, an activation mechanism for D- π -D type 2PA-PIs was proposed by Lu *et al.*^[49] As depicted in Scheme 3, an electron-rich PI forms an intra-excplex upon excitation by 2PA *via* an intramolecular charge transfer. Consequently, an electron is transferred from the excited 2PA-PI to a monomer molecule, resulting in the formation of a pair of radical ions. The radical anion formed from the monomer can subsequently add to a further monomer and initiate the propagation of the polymer chain. This mechanism appears to require a good capability of the monomer to abstract electrons from the intra-excplex. As a matter of fact that is in accordance with the successful appliance of acrylates in 2PIP. The α,β -unsaturated carboxyl group in this class of monomers is an electron acceptor and furthermore ensures a mesomeric stabilization of the formed radical anion. Though, analogical to classical type II PIs, such mechanism may suffer from a possible back electron transfer from the generated monomer radical anion to the 2PA-PI radical cation, resulting in deactivation and therefore a decrease in efficiency.^[28]

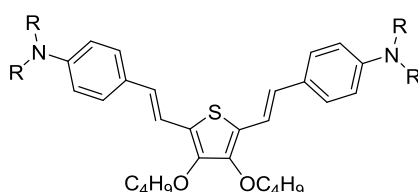


Scheme 3: Proposed mechanism for the activation of 2PA-PIs based on D- π -D structures.^[49]

Nevertheless, electron-rich symmetrical D- π -D type compounds represent potential candidates for 2PA-PIs, as they offer large changes in their quadrupolar moment upon excitation.^[7, 27]

B.3.5 Electron Rich Heterocycles as Structural Motifs in 2PA-PIs

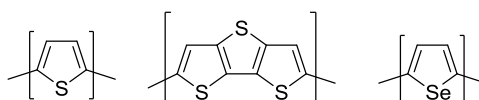
As thiophene features higher electron density compared to benzene, it is a structural motif, often applied in 2PA materials. For instance, substitution of the 1,4-dimethoxybenzene unit by 3,4-dialkyloxythiophene-2,5-yl in derivatives of **R1** (Scheme 2) have been reported, leading to potential 2PA-PI compounds (Scheme 4).^[50]



Scheme 4: 2PA materials derived from **R1**. R = p-MeOC₆H₄, phenyl, n = 1, 2.

Furthermore 2PA characteristics of molecules containing 2,5-thiophene, both as π -core^{8, [51]} and π -bridging units,^[52] as well as thiophene dendrimers,^[53] and macrocyclic thiophene derivatives,^[54-55] have been investigated, showing promising 2PA properties. Moreover, a distinct role in the contribution of the fused thiophene system dithienothiophene (DTT) as π -center to high δ_{2PA} has been observed, both experimentally and theoretically.^[56-57] Also selenophene has been applied in 2PA materials, as π -bridge in polymeric structures^[58] and π -core in small molecules.^[59]

⁸ besides 2,2'-bithiophene, and 2,2':5,2'-terthiophene

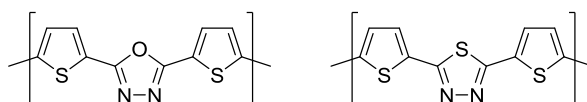


Scheme 5: Selected examples of structural building blocks applied as π -core or π -bridge.

Nevertheless, the application of 3,4-unsubstituted thiophene as conjugated π -linker in D- π -D type 2PA compounds is rarely found in literature.^[59-60]

B.4 Goal of the Thesis

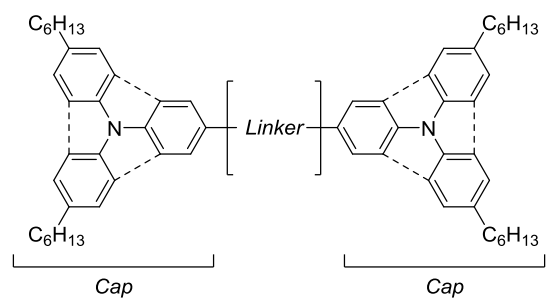
On the basis of preliminary studies the aim of this work is to synthesize, characterize, and evaluate symmetrical α,ω -bis(triarylamine) based compounds, linked by a variety of heterocyclic units, as potential initiators for two-photon-microfabrication. Strategies to increase the 2PA and thus the efficiency of two-photon initiation of these quadrupolar cap-linker-cap type molecules are (i) increasing the electron density of the linker, as well as (ii) a planarization of the linker, (iii) and the caps. In order to adjust the solubility to the respective monomer formulation hexyl residues are introduced to the triarylamine building blocks. Structural incorporation of acceptors towards D- π -A- π -D type compounds based on 1,3,4-oxadiazole and 1,3,4-thiadiazole are investigated.



Scheme 6: Acceptor building blocks based on 1,3,4-oxadiazole (*left*) and 1,3,4-thiadiazole (*right*).

Besides the photophysical characterization of target molecules an evaluation of their efficiency as 2PA-PIs *via* speed-power screenings is matter of interest. Furthermore, within the scope of this thesis a reliable protocol to 5,11-substituted indolocarbazole (ICz) building blocks is developed.

B. General Part

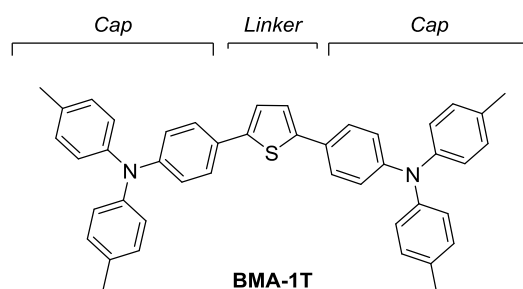


Scheme 7: Structural motif of quadrupolar target molecules.

C. Specific Part

C.1 Introduction

Cap-linker-cap type structures of D- π -D and A- π -A constitution have been investigated within our research group as potential OLED-Materials intensively.^[61-63] Although highly fluorescent (e.g. BMA-1T: fluorescence quantum yield = 44%; Scheme 8),^[61] several of these compounds were analyzed towards their applicability as 2PA-PIs showing promising results. However, the application was limited, due to low solubility in the respective monomer formulation.

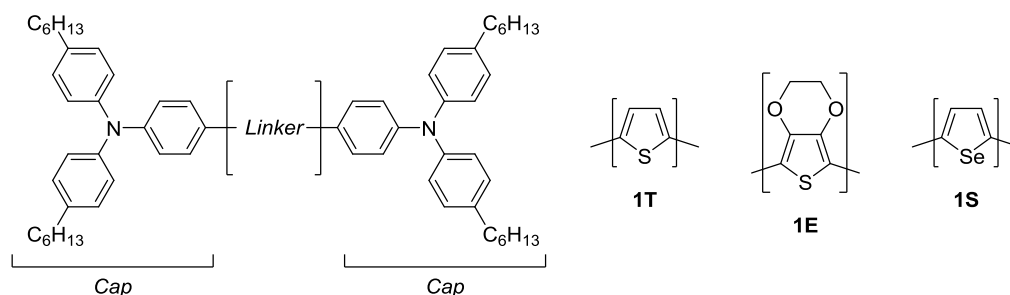


Scheme 8: Molecular structure of **BMA-1T**.^[61]

To overcome solubility issues, especially those of planarized structures, the introduction of *n*-hexyl residues to the cap moieties seems to be an approach worth pursuing. Additionally, other applications in the field of organic electronics (OE) could potentially benefit from increased solubility, since both characterization and processability of some of the already investigated compounds suffer from their insolubility.^[62]

One strategy towards highly efficient 2PA-PIs features the variation of electron rich π -linker functionalities in D- π -D quadrupoles. The enhancement of electron density in the delocalized π -system is expected to improve intermolecular electron transfer from excited 2PA-PIs to monomer molecules, thus promoting 2PIP.^[7] Therefore, starting from thiophene the aim of this thesis focusses on the incorporation of electron-rich moieties like EDOT and selenophene as linkers in the named cap-linker-cap systems (Scheme 9).

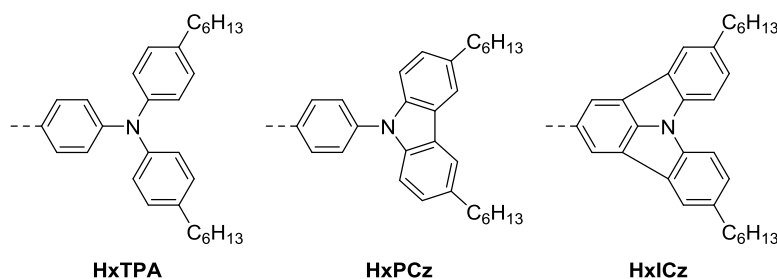
C. Specific Part



Scheme 9: left: Cap-linker-cap motif; right: electron rich π -center units with **T** = thiophene, **E** = EDOT, and **S** = selenophene

As reported in literature the degree of coplanarity is a critical factor for high 2PA and thus the efficiency of 2PA-PIs.^[3, 14] To compare the benefits induced by differing building blocks a variety of both planarized π -linkers and donors were introduced separately.

For this purpose several π -donors like *n*-hexyl substituted triphenylamine (**HxTPA**), phenylcarbazole (**HxPCz**), and indolocarbazole (**HxICz**) should serve as π -donors respectively (Scheme 10).

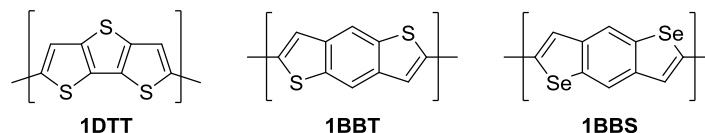


Scheme 10: Arylamine-caps used for the synthesis of 2PA-PIs

Previous works of our group demonstrated, that an increase of planarization from triphenylamine (**TPA**) to phenylcarbazole (**PCz**) and indolocarbazole (**ICz**) leads to significantly blue shifted absorption peak maxima $\lambda_{\text{abs.max}}$ of compound **ICz-T-ICz** (352 nm) compared to **TPA-T-TPA** (386 nm).^[62] It is proposed that these findings correlate with the decreasing donor strength of the triarylamine moiety (**ICz** < **PCz** < **TPA**) by planarization. The alteration in donor strength is attributed to the fact that the lone pair of the nitrogen increasingly contributes to the aromaticity (**PCz** and **ICz**).^[64] Since the laser device applied for structuring tests operates at 798 nm, only absorption bands above 399 nm can be excited by 2PA with the equipment used. Thus, bithiophene units causing red shifted absorption spectra are introduced as π -centers to adjust the spectral range to the excitation source.

C. Specific Part

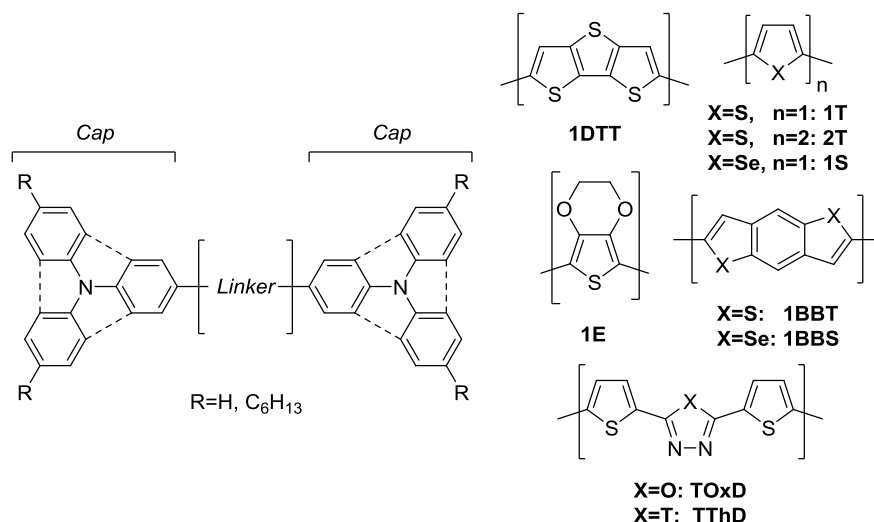
Dithienothiophene, benzobithiophene, and benzobiselenophene (Scheme 11) providing both coplanarity and increased electron density in their function as planarized π -linkers were hence subjects of investigation.



Scheme 11: Fused π -linkers: dithienothiophene (**DTT**), benzobithiophene (**BBT**), and benzobiselenophene (**BBS**)

While the effects of the 1,3,4-oxadiazole acceptor unit on 2PA properties have repeatedly been matter of research,^[13, 56, 65-67] investigations towards the structurally similar, yet synthetically analogically accessible 1,3,4-thiadiazole acceptor can rarely be found (Scheme 12).^[68] As a reliable synthetic protocol giving rise to both acceptor building blocks based on 2,5-bis(5-bromo-2-thienyl) functionality pattern was readily at hand, structural incorporation of these acceptors towards D- π -A- π -D type compounds are part of the investigation.

The linear target molecules (Scheme 12) based on D- π -D and D- π -A- π -D configurations can be synthesized from the respective precursors *via* Pd-catalyzed cross-coupling reactions. If not otherwise suggested in literature, Suzuki-Miyaura reaction^[69-78] was utilized preferentially, as a reliable Suzuki protocol was developed in our group, based on the application of pinacol boronic acid esters.^[61-63] Alternatively, Stille cross-coupling reaction,^[79-83] or C-H activation^[84] was applied, respectively.



Scheme 12: Structural motifs towards target molecules

The efficiency of these target molecules as 2PA-PIs is then probed by speed-power screenings. Hence, an array of woodpile structures with a lateral length of $50\ \mu\text{m}$ is written in a monomer solution of the 2PA-PI of interest at different laser powers and writing speeds aiming for broader processing windows than already established 2PA-PIs (Figure 10).

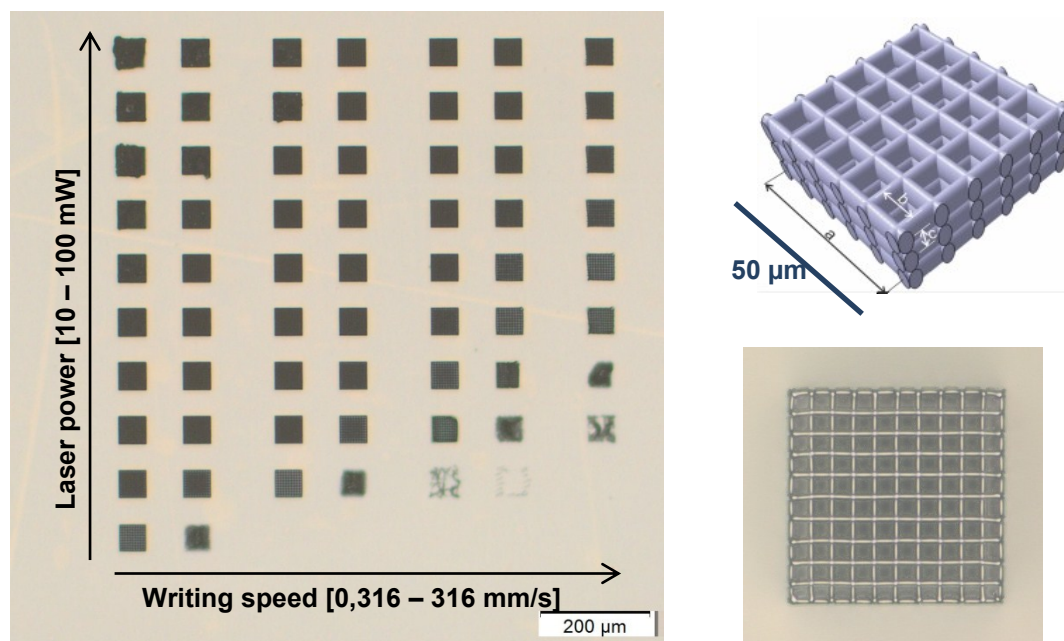


Figure 10: *left*: Typical speed-power screening by fabrication of woodpile structures; microscope image, magnification: 50x. *right above*: CAD drawing of woodpile structure with $a = 50\ \mu\text{m}$. *right below*: woodpile structure; microscope image, magnification: 1000x.

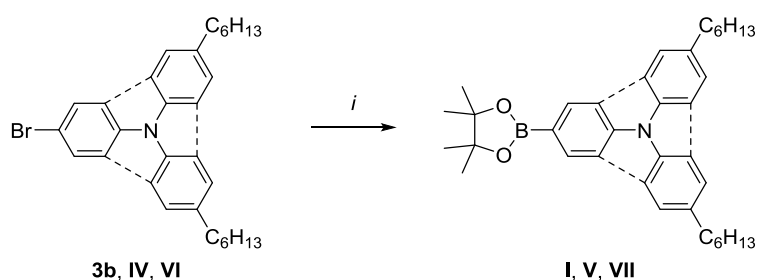
Broad processing windows allow for the fabrication of structures with excellent quality both at high laser intensities and low writing speeds (high damage threshold) as well as low laser intensities and high writing speeds (low polymerization threshold). The former characteristic facilitates robust polymerization in tolerating high energy input without loss of structural quality. This is of crucial importance for the applicability of 2PA-PIs, since the writing speed can vary dramatically when the focal ellipsoid changes its direction of movement. The latter parameter is of critical relevance for the progress of the 2P-microfabrication process, as the splitting of a single laser beam into an array of simultaneous moving focal points of accordingly lower intensity requires 2PA-PIs with low polymerization thresholds.^[28]

C.2 Synthesis

C.2.1 Synthesis of Cap-systems

C.2.1.1 Synthesis of Boronic Acid Esters

The brominated precursors of **HxTPA**, **HxICz** and **HxPCz** caps were converted into the corresponding pinacol boronic acid esters by lithiation *via* lithium-halogen exchange followed by quenching of the organometallic intermediates with Pinbop[®] (Scheme 13) according to Anemian,^[85] yielding **I** (77%), **V** (75%) and **VII** (58%).

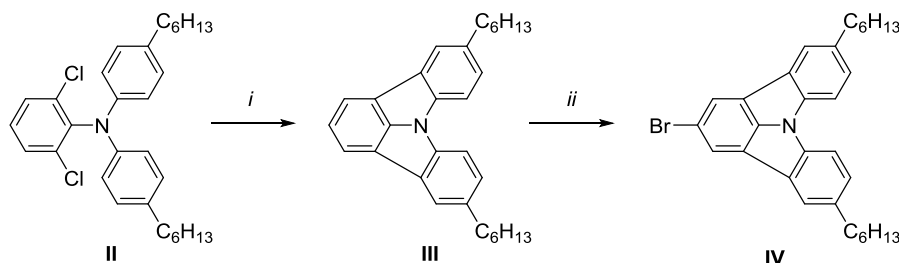


Scheme 13: Conversion of brominated precursors to pinacol boronic acid esters. *i*: THF, -78°C, 1) *n*-BuLi; 2) Pinbop[®].

The lower yield of the **VII** can be attributed to separation problems from impurities and may be improved by optimization of the purification process.

C.2.1.2 Synthesis of Brominated 5,11-Dihexylindolocarbazole

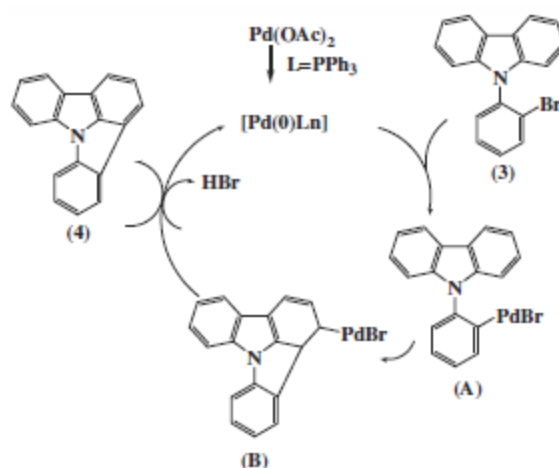
The synthesis towards brominated 5,11-dihexylindolocarbazole was conducted according to a protocol developed by Bintinger during his diploma thesis.^[62, 64, 86]



Scheme 14: Synthesis of precursor **II**. *i*: (NHC)Pd(allyl)Cl, K₂CO₃, DMAc, 130 °C. *ii*: NBS, CHCl₃/AcOH, 55 °C.

Hence, conversion of precursor **II** towards the corresponding indolocarbazole **III** (94%) was performed by double sided C-H-activation utilizing (NHC)Pd(allyl)Cl⁹ as catalyst.^[86] As previous experiments in our group indicate, a marginal water content of the reaction mixture was crucial for the efficiency of C-H activation of these systems. Thus, the water content of the dry solvent¹⁰ was adjusted to approximately 1000 pm by addition of deionized water. Subsequently, **III** was brominated with NBS giving **IV**, which was purified by recrystallization from ACN (85%).

Lv *et al.* proposed a plausible mechanism for the palladium-catalyzed cyclization of a substrate related to the intermediate in the cyclization of **II** towards **III**, that could also be applied to this reaction (Scheme 15). Herein, initially oxidative addition of (3) with palladium might form aryl-palladium intermediate (A), followed by addition to the double bond of carbazole to give intermediate (B). Finally, the β -hydrogen elimination is triggered by the attack of base to the aromatic proton to form compound (4).^[89]



Scheme 15: Proposed mechanism for the palladium-catalyzed cyclization of **ICz**.^[89]

C.2.1.3 Synthesis of Triphenylamine Cap-systems

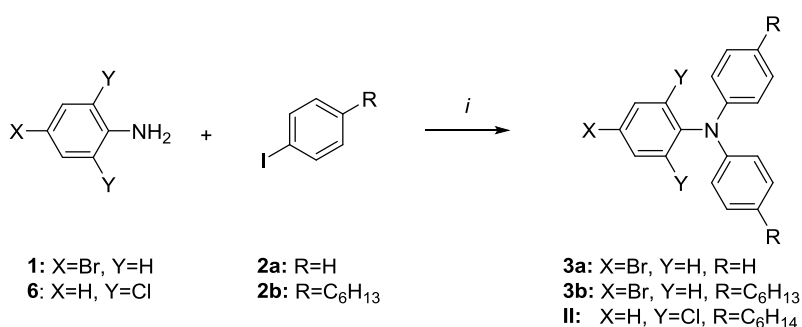
The precursors of the respective cap-systems were realized *via* by Ullmann condensation.^[90-91] The syntheses of substituted triphenylamines **3a**, **3b** and **II** were performed applying ligand accelerated catalysis as described by Goodbrand (Scheme 16).^[92] Starting from the properly substituted benzeneamines the corresponding bromides **3a**, **3b** and **II** were synthesized in 75%, 86%, and 35% yield,

⁹ 1,3-Bis[2,6-bis(1-methylethyl)phenyl]-1,3-dihydro-2H-imidazol-2-ylidene]chloro(η^3 -2-propen-1-yl) palladium^[87-88]

¹⁰ DMAc, Sigma-Adrich, H₂O \leq 100 pm according to specifications, store over molecular sieve.

C. Specific Part

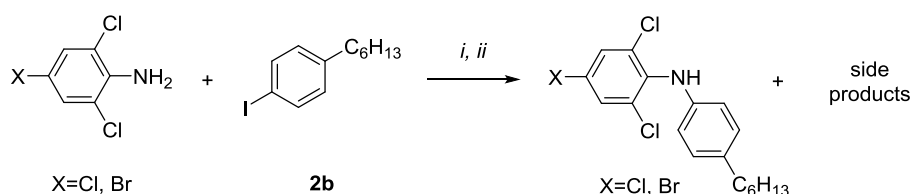
respectively. The purification procedures of **3b** and **II** deviated from the standard protocol reported earlier of in our group^[61-63] as the hexyl-substituted triphenylamines were isolated as liquids and therefore recrystallization could not be applied. Hence, the crude reaction mixtures were flashed over a pad of silica to separate the product from residues of the copper catalyst, before remaining contaminations were distilled off *via* Kugelrohr-distillation.



Scheme 16: Synthesis of cap-precursors by Ullmann condensation. *i*: CuCl, KOH, 1,10-phenanthroline, toluene, reflux.

The reactivity order Ar-I > Ar-Br > Ar-Cl >> Ar-F of aryl halogenides in Ullmann condensations was successfully exploited in the synthesis of precursor **II**,^[90, 92] as no formation of side products was observed. Nevertheless, the yield of precursor **II** was rather modest (35%) with a long reaction time (8d), presumably owing to the steric hindrance of the amino functionality. In the course of the reaction dehalogenation of unconverted 1-hexyl-4-iodobenzene **2b** was observed by GC-MS analysis. Therefore, a possible optimization parameter could be the stepwise addition of iodide **2b**.

A further synthetic strategy towards precursor **II** utilizing Buchwald-Hartwig reaction according to Marion^[93] proved to be unsuccessful. In a preliminary test reaction using iodobenzene **2a** instead of **2b**, (NHC)Pd(ally)Cl as catalyst, and KO^tBu as base no significant conversion after 24 hours of refluxing in toluene could be observed.

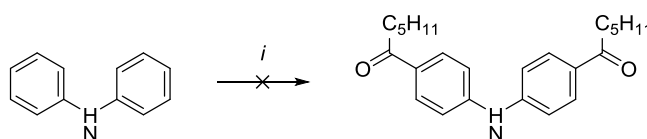


Scheme 17: Direct synthetic approach towards halogenated precursors. *i*: CuCl, KOH, 1,10-phenanthroline, toluene, reflux. *ii*: CuI, K₃PO₄, 1,2-DACH, toluene, reflux.

A direct synthetic approach towards halogenated derivatives of precursor **II** starting from 4-bromo-2,6-dichlorobenzeneamine and 2,4,6-trichlorobenzeneamine,

C. Specific Part

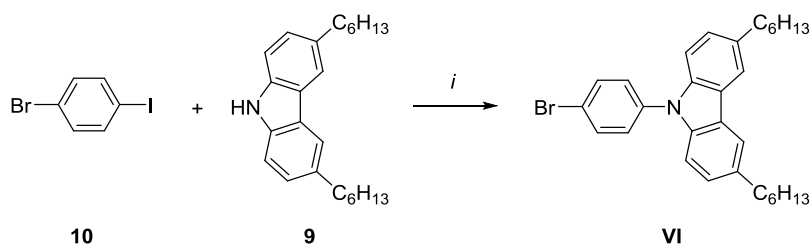
respectively, seemed to be more economic. However, this strategy failed due to a variety of side reactions in addition to almost only monocondensation taking place. The side reactions included dehalogenation and formation of carbazole derivatives under conditions (i), and Br-I-exchange under conditions (ii), with long reaction times up to eleven days. Additionally to the catalyst system developed by Goodbrand (i),^[92] another catalytic system based on CuI, K₃PO₄ and (±)-*trans*-1,2-diaminocyclohexane (DACH) adapted from Kim (ii)^[94] was tested without success (Scheme 17).



Scheme 18: Acylation of *N,N*-diphenylamine. *i*: hexanoyl chloride, AlCl₃, DCM.

An alternative reaction path towards hexyl-substituted triphenylamines starting with the twofold acylation of *N,N*-diphenylamine failed because of only single yet incomplete acylation – probably at the amino functionality – taking place (Scheme 18). The further hypothetical path would have been reduction of the diacylated phenylamine followed by nucleophilic aromatic substitution reaction with appropriate fluorobenzene derivatives.^[61-62, 95]

Previous experiments^[62-63] have demonstrated that the synthesis of the brominated precursor of phenylcarbazole *via* Ullmann condensation according to Goodbrand^[92] proceeds relatively slow, resulting in only low yields. Another approach based on the Ullmann condensation of dihexylcarbazole **9** and 1,4-dibromobenzene applying CuSO₄ and K₂CO₃ in the molten mass proved to be impractical due to sublimation of the dibromide. Thus, an effective methodology was adapted from Aizawa *et al.* to improve the synthetic accessibility of **VI** (Scheme 19).^[96]

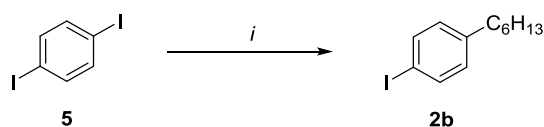


Scheme 19: Ullmann condensation towards **VI**. *i*: Cu(0), K₂CO₃, DMF, reflux.

Starting from dihexylcarbazole **9** and 1-bromo-4-iodobenzene **10**, this Ullmann reaction based on the application of Cu(0) and K₂CO₃ without the necessity of a ligand, yielded precursor **VI** in 90% yield after 20 h of refluxing in DMF. Besides, traces of the coupling product between **9** and **VI** could be isolated by column chromatography.

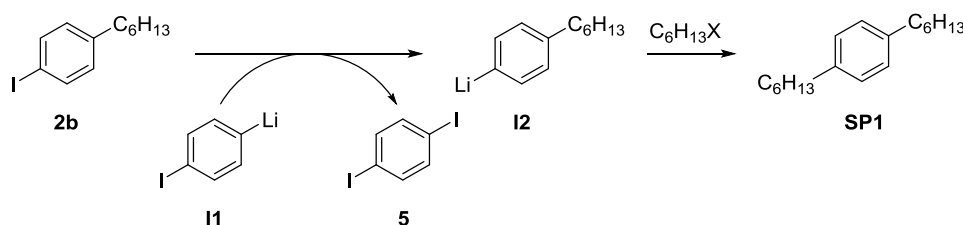
C.2.1.4 Synthesis of 1-Hexyl-4-iodo-benzene

Precursor **2b** was synthesized from available 1,4-diiodobenzene via Wurtz-Fittig-type coupling^[97-98] by one-sided lithiation of **5** with *n*-HexLi followed by subsequent addition of either A: 1-iodohexane or B: 1-bromohexane and stirring at room temperature overnight, giving **2b** in sufficient purity with yields of 67% and 55%, respectively (Scheme 20).



Scheme 20: Synthesis of p-hexyliodobenzene **2b**. *i*: Et₂O, -78 °C, Variant A: 1) *n*-HexLi; 2) 1-iodohexane; Variant B: 1) *n*-HexLi; 2) 1-bromohexane.

Due to an undesired lithium-halogen exchange between **2b** with intermediate **I1**, a minor amount of side product **SP1** and reactant **5** is formed in the cause of the reaction (Scheme 21). While **5** can be separated extensively by distillation, slight impurities of **SP1** remain in the product. However, because of the inert nature of **SP1** under subsequent reaction conditions its formation affects the yield of this one-pot reaction only, leaving the applicability of the product unimpaired.



Scheme 21: Side reaction towards **SP1** with X=Br, I.

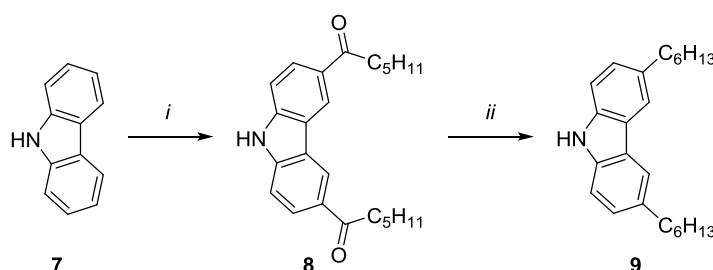
Besides, other synthetic attempts towards **2b** included direct iodination of available hexylbenzene using NIS mediated by trifluoroacetic acid in acetonitrile or acetic acid respectively,^[99] as well as utilizing I₂ and periodic acid.^[100] While in the former case

even after four days almost no conversion could be observed, the latter reactions lead to mixtures of the respective *ortho*- and *para*-isomers.

Another path aiming for the synthesis of **2b** *via* classical Sandmeyer reaction in three steps including nitration of hexylbenzene and subsequent reduction of *p*-hexylnitrobenzene to *p*-hexylbenzeneamine failed at the first step giving only a mixture of isomers, not separable to sufficient purity by distillation. A further strategy towards *p*-hexylbenzeneamine *via* Friedel-Crafts acylation of acetanilide proved to be unpractically, due to the necessity of hydrolyzation of the *N*-acetyl group followed by the reduction of the hexanoyl functionalities.

C.2.1.5 Synthesis of 3,6-Dihexyl-9*H*-carbazole

A protocol from Yasuda *et al.* describing the acylation and subsequent reduction of carbazole was adapted for the synthesis of the precursor dihexylcarbazole **9** (Scheme 22).^[101]



Scheme 22: Two step conversion of carbazole **7** to 3,6-dihexylcarbazole **8**. *i*: hexanoyl chloride, AlCl₃, DCM, T<5 °C. *ii*: LiAlH₄, AlCl₃, THF, 0 °C.

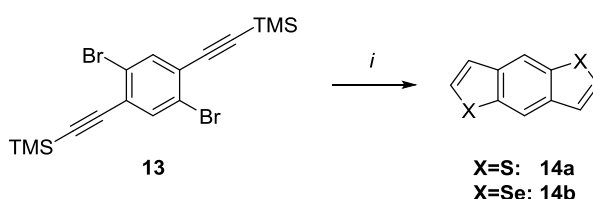
Hence, carbazole **7** was converted into diketone **8** (68%) by Friedel-Crafts acylation, using hexanoyl chlorid and aluminium chloride. In the subsequent reduction of **8** to the corresponding dihexylcarbazole **9** (97%) a solution of 4 eq LAH and 2 eq AlCl₃ in THF was used. It is very likely that this reaction proceeds *via* intermediately formed alane (AlH₃).^[102]

C.2.2 Synthesis of Linkers

As a result of previous studies in our group some of the required linkers or precursors were already available either from synthesis or purchase. All others were synthesized in the course of this thesis as described below.

C.2.2.1 Synthesis of BBT and BBS

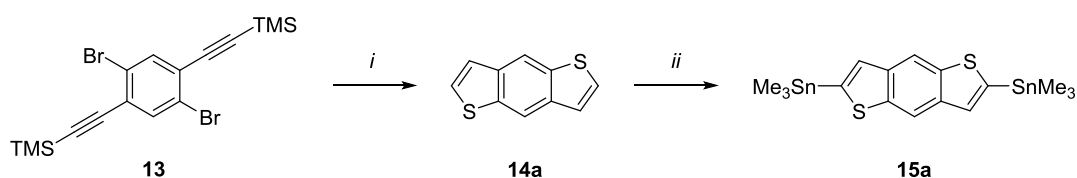
Recently, Kashiki *et al.* published a convenient one-pot procedure for the synthesis of benzodithiophenes and benzodiselenophenes from symmetrical *o*-halo-substituted diethynylbenzenes using sodium chalcogenides as reagents (Scheme 23).



Scheme 23: Ring closure of precursor **13** to benzodichalcogenophenes **14a** and **14b**. X=S: *i*: Na₂S nonahydrate, NMP, 180 °C. X=Se: *i*: 1) Se(0), NaBH₄, EtOH, 0 °C; 2) NMP, 180 °C.

The researchers proposed no entire reaction mechanism, however, they stated that the sodium chalcogenide acts as a nucleophile to nonactivated bromobenzenes and that the resulting phenylchalcogenolate intermediate attacks the adjacent acetylene moiety to form the corresponding chalcogenophene ring.^[103]

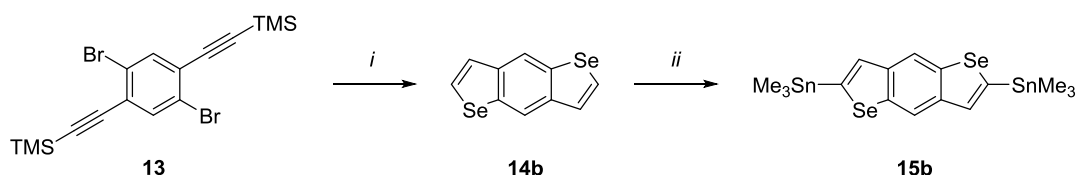
In the course of this reaction the trimethylsilyl (TMS) group is displaced, probably due to the high basicity of the reagent. To accelerate the S_NAr reactions between the chalcogen-based nucleophiles and the nonactivated substrate, the application of NMP as polar aprotic solvent and elevated reaction temperature (180 °C) were suggested.^[103] Related mechanisms towards fused molecules of this kind can be found in literature.^[104]



Scheme 24: Synthesis towards **15a**. i) Na₂S, NMP, 200 °C. ii) THF, -78 °C, 1) *n*-BuLi; 2) Me₃SnCl.

Benzodithiophene **14a** was synthesized according to the protocol from Kashiki *et al.*^[103] In deviation from literature anhydrous Na₂S was applied and the temperature

was increased to 200 °C. In this way starting from precursor **13** benzodithiophene **14a** was obtained as a white solid (37%) after column chromatography (Scheme 24). The fused heterocycle **14a** was further converted into the bisstannane **15a** by lithiation with *n*-BuLi and subsequent addition of with Me₃SnCl following a procedure from Søndergaard.^[105]

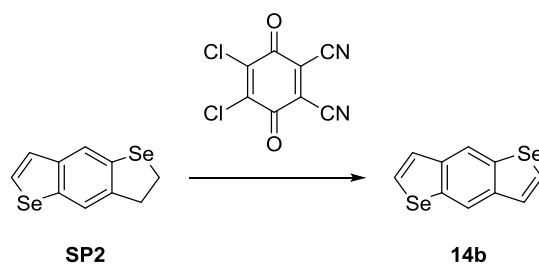


Scheme 25: Synthesis of **15b**. i) 1) Se(0), NaBH₄, EtOH, 0 °C; 2) **13**, NMP, 200 °C; 3) DDQ, DCM. ii) THF, -78 °C, 1) *t*-BuLi, TMEDA; 2) Me₃SnCl.

The synthetic approach towards the corresponding benzodiselenophene **14b** proceeds in a similar manner and includes the *in-situ* generation of sodium selenide reagents from sodium borohydride (NaBH₄) and selenium powder in ethanol. As reported in literature, selenium reacts with NaBH₄ in ethanol to form NaHSe, Na₂Se and, Na₂Se₂ depending on the molar equivalents used.^[106-107] Thus, due to the fourfold excess of NaBH₄ the reactive intermediate is NaHSe. In the course of the reaction the solvent was exchanged from ethanol to NMP, after addition of precursor **13** to the selenide intermediate, followed by stirring of the reaction mixture for 24 h at 190 °C, before proceeding according to the protocol.^[103] However, the crude products of repeated independent syntheses contained a major amount of a dihydro-side product, which was detected by GC-MS and NMR.

As the ¹H-NMR shows two doublets at 7.89 and 7.59 ppm with J = 5.9 Hz as well as two singlets at 7.76 and 7.70 ppm with the integrals of all signals being 1H, a molecular structure like **SP2** in Scheme 26 was suggested, but the singlet at 3.45 ppm with an integral of 4H disagrees with that assumption (Figure 11, center). On the contrary, the ¹³C-NMR reveals two CH₂ signals at 38.4 and 27.2 ppm, assigned from an APT-experiment not shown, accounting for structure **SP2** (Figure 11, below).

C. Specific Part



Scheme 26: Aromatization of the supposed side product **SP2** to **14b** applying DDQ.

The crude product was applied in a re-aromatization reaction *via* oxidative dehydrogenation by treatment with DDQ yielding only **14b** after column chromatography (45%; Figure 11, above).

The conversion of benzodiselenophen **14b** to bisstannane **15b** proceeds analogically to the synthesis of **15a** *via* lithiation and addition of trimethyltin chloride (Scheme 25). While Hwang *et al.* reported the use of 2.3 eq *n*-BuLi in this reaction, yielding a solid (36%),^[108] Leenen *et al.* stated the dose of 2.5 eq of *t*-BuLi, leading to an oil (61%).^[109]

However, in previous experiments by our group under both conditions no lithiation of **14a** could be observed, but quantitative Li-Se exchange was detected *via* GC-MS and NMR. Hence, we figured that the addition of a complexating donor ligand could activate the organolithium species towards deprotonation. Whereas the application of 2.5 eq *n*-BuLi and 0.3 eq TMEDA and steady warming to room temperature lead to no deprotonation, using 4.0 eq of *t*-BuLi and 0.3 eq of TMEDA resulted in two-sided lithiation after slowly warming to -40°C. Finally, **15b** could be obtained with the latter metalation method after quenching with trimethyltin chloride and recrystallization from ACN as light yellow crystals (73%).

C. Specific Part

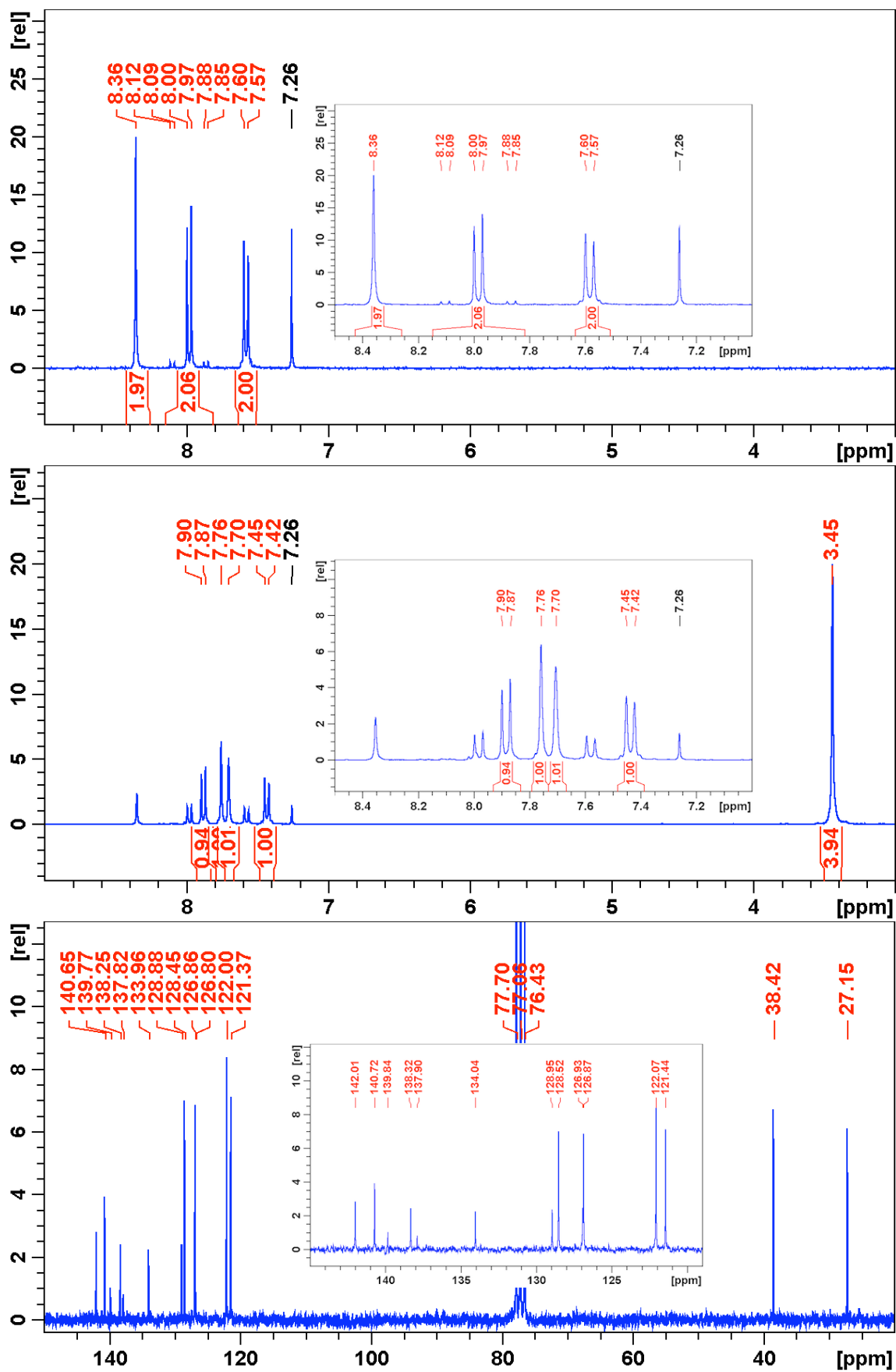
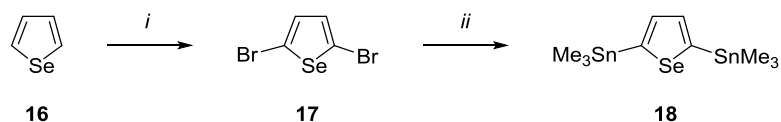


Figure 11: above: $^1\text{H-NMR}$ of **14b**; center: $^1\text{H-NMR}$ of crude product containing **14b** and **SP2**; below: $^{13}\text{C-NMR}$ of crude product containing **14b** and **SP2**.

C.2.2.2 Synthesis of the Selenophene Linker

The synthesis of linker **18** was accomplished according to literature (Scheme 27).

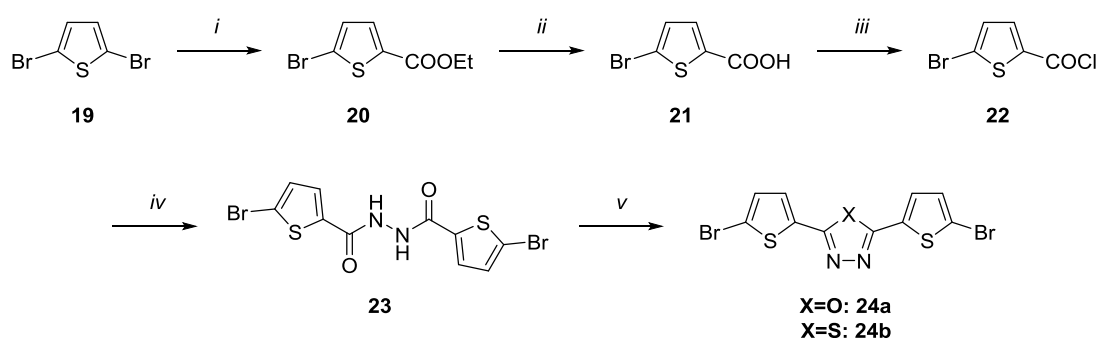


Scheme 27: Synthesis of linker **18**. *i*: Br₂, chloroform, 0°C. *ii*: Et₂O, -78 °C, 1) *n*-BuLi; 2) Me₃SnCl.

Selenophene **16** was brominated in 2- and 5-position *via* an electrophilic aromatic substitution with bromine, giving **17** in 61% yield after column chromatography.^[110] Dibromide **17** was further converted into bis(trimethylstannane) **18** (44%) by lithium-halogen exchange and subsequent quenching of the organometallic intermediate with trimethyltin chloride, following a protocol described by Haid.^[111] Purification of **18** was performed by washing with MeOH yielding **18** as a beige solid (44%).

C.2.2.3 Synthesis of Acceptors

The **TOxD** and **TThD** acceptor building blocks were synthesized following a procedure developed by Kautny in the course of his master thesis (Scheme 28).^[95]



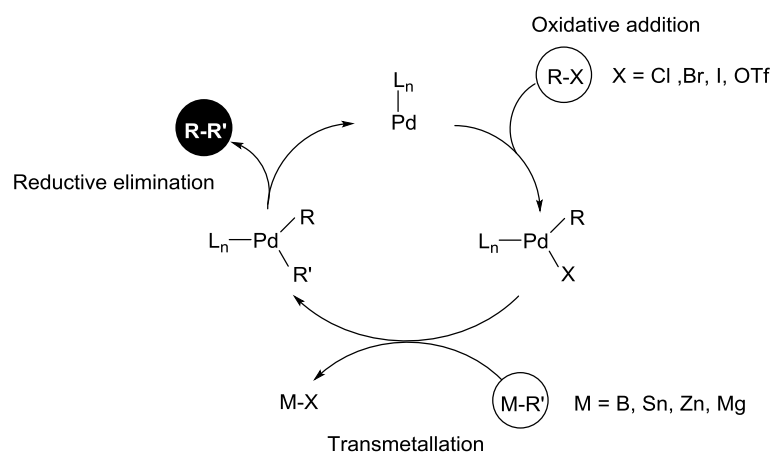
Scheme 28: Syntheses of **24a** and **24b**. *i*: Et₂O, -78°C, 1) *n*-BuLi; 2) ClCO₂CH₂CH₃. *ii*: 1) NaOH, H₂O, reflux; 2) HCl. *iii*: SOCl₂, catalytic DMF, reflux. *iv*: H₂NNH₂·XH₂O, Na₂CO₃, H₂O/THF. *v*: X=O: POCl₃, reflux; X=S: Lawesson's reagent, xylenes, reflux.

Dibromide **19** was converted to ester **20** by one-sided lithium-halogen exchange and subsequent slow addition of the lithium-thiophene intermediate to a precooled solution of ethyl chloroformate to avoid the formation of secondary products from the thus prepared ester. Subsequently, ester **20** was hydrolyzed to acid **21**, which was thereafter refluxed in thionyl chloride with catalytic amounts of DMF to form

carboxylic acid chloride **22**. The acid chloride was further reacted with hydrazine hydrate in a mixture of THF and water using Na_2CO_3 as base.^[112] Starting from hydrazide **23** Paal-Knorr type ring closing reactions towards 1,3,4-oxadiazole **24a** and 1,3,4-thiadiazole **24b** were accomplished by the use of POCl_3 ^[113] and Lawesson's reagent^[114], respectively. While oxadiazole **24a** (76%) was obtained after recrystallization from ACN, thiadiazole **24b** (89%) could be purified by repeated digestion in small amounts of MeOH.

C.2.3 Synthesis of 2PA-PIs

In the last decades Palladium catalyzed cross-coupling reactions have been established as standard reactions for the formation of $\text{C}_{\text{aryl}}\text{-C}_{\text{aryl}}$ bonds in organic chemistry, since necessary precursors are usually easily synthetically accessible and with growing impact also commercially available. The possibility of joining a variety of functional building blocks under rather mild reaction conditions has inspired whole research areas within the field of materials chemistry and beyond. However, the many parameters that allow for tuning of reaction conditions, from the choice of organo-metallic precursors over catalysts and bases to solvents, can be boon and bane of these methods.



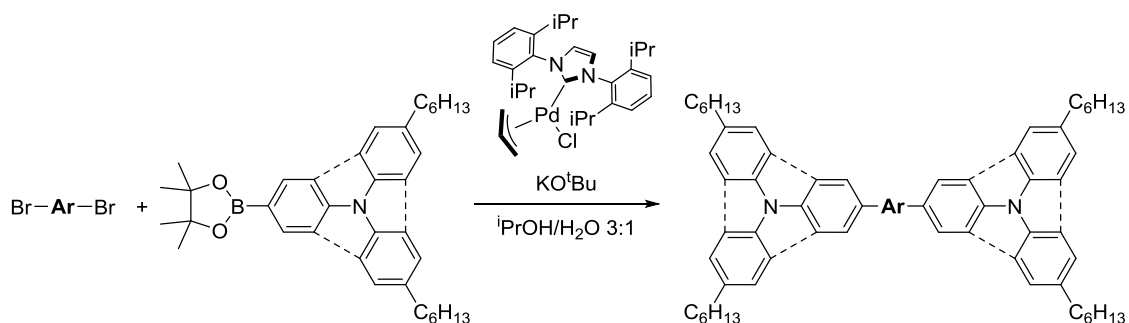
Scheme 29: General catalytic cycle for palladium-catalyzed cross-coupling reactions.^[115]

Among cross-coupling reactions the Suzuki-Miyaura methodology^[69-78] has proved to be favorable due to its practical handling and the stability of the organoboron reagents applied, which are inert towards water and oxygen, generally thermally stable, and tolerant toward various functional groups. Furthermore, both the boron-containing reagents as well as generated byproducts of the Suzuki-Miyaura reaction display low toxicity.^[78, 93]

Since a reliable protocol for Suzuki-Miyaura reaction was developed in our group^[61-63] and for the reasons mentioned above, this type of cross-coupling reaction was utilized preferentially for the synthesis of target molecules. Alternatively, for some compounds Stille reaction^[79-83] or C-H activation^[84] were suggested in literature and thus chosen.

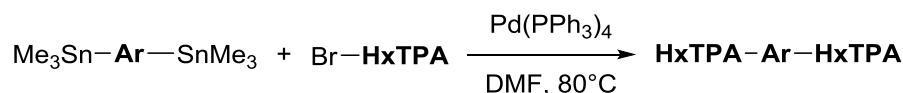
C.2.3.1 Synthesis of Linker-based 2PA-PIs

The methodology for Suzuki-Miyaura coupling of the respective pinacol boronic acid esters and dibromoaryls applying (NHC)Pd(allyl)Cl^[93] as catalyst (Scheme 30) and KO^tBu as base in a 1:1-mixture of water and isopropanol proved to be highly efficient.



Scheme 30: General reaction scheme of Suzuki-Miyaura coupling reactions of pinacol boronic acid esters and dibromoaryls applying (NHC)Pd(allyl)Cl as catalyst.

Halogeno selenophenes and their derivatives seem to be inappropriate substrates for Suzuki-Miyaura reactions, as prior experiments from our group indicate and the synthetic strategies used in literature underline. Hence, target molecules **XII**, **XIVb** and due to structural similarity also **XIVa** were synthesized *via* Stille cross-coupling with Pd(PPh₃)₄ as catalyst, following a procedure described by Haid.^[111] Adversely, in comparison to boronic esters organotin compounds are highly toxic.

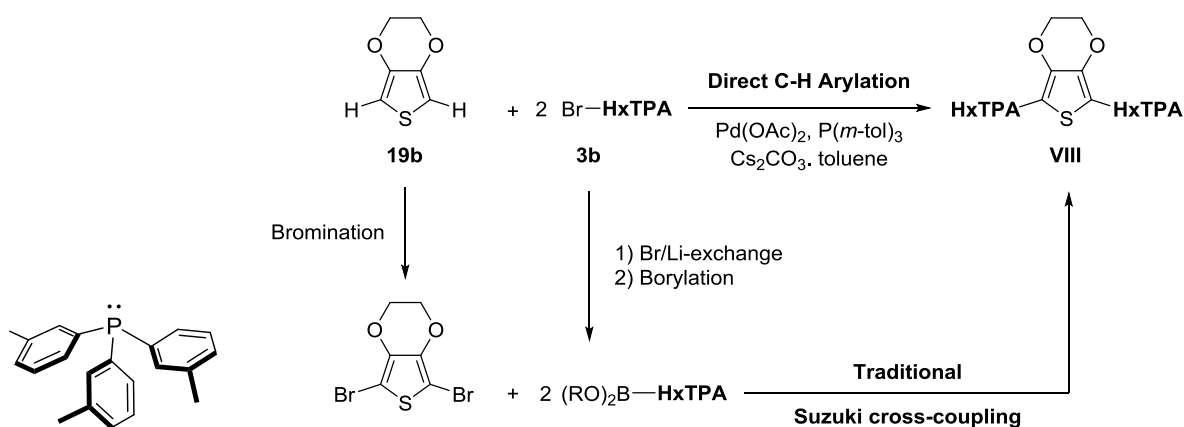


Scheme 31: General reaction scheme of Stille coupling reactions of bromoaryl **3b** and bisstannanes applying Pd(PPh₃)₄ as catalyst.

Recently Liu *et al.* demonstrated an effective synthesis for EDOT based π -conjugated molecules *via* direct C-H-activation.^[84] In contrast to traditional Suzuki-coupling this direct C-H-approach requires one modification step fewer for each precursor, making it significantly more attractive in terms of efficiency and atom-economy. Thus the

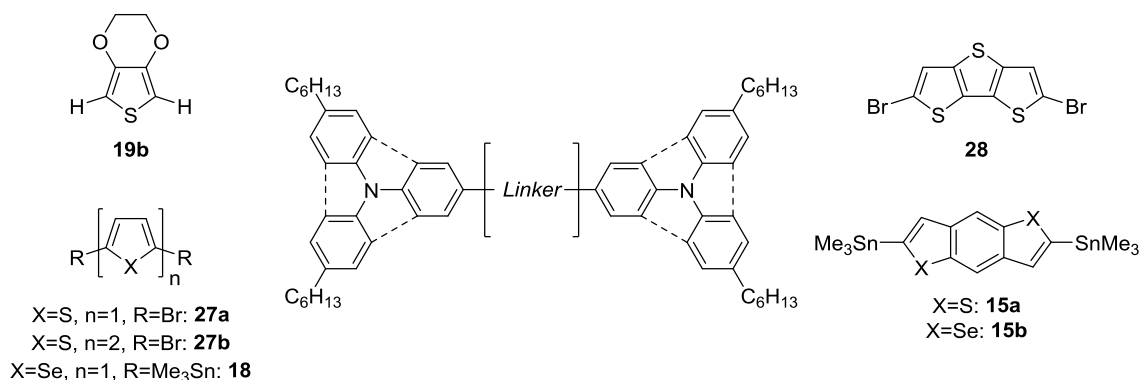
C. Specific Part

synthesis of **VIII** was performed according to Liu *et al.* applying Pd(OAc)₂ as catalyst, P(*m*-tol)₃ as ligand, and Cs₂CO₃ as base.



Scheme 32: Molecular structure of ligand P(*m*-tol)₃. *right*: Synthetic approach towards target molecule **VIII** via direct CH-arylation in comparison to traditional Suzuki-route.

Structural motifs of building blocks used for the synthesis of linker based 2PA-PIs are depicted in Scheme 33.



Scheme 33: Structural motifs of building blocks used for the synthesis of linker based 2PA-PIs.

All reaction mixtures were refluxed until TLC showed full conversion at 366 nm using UV-illumination. However, purification for some of the compounds proved to be difficult, since separation from impurities by column chromatography could not be realized. As some target molecules were sticky glasses rather than crystalline solids, recrystallization was not practical. Since attempts of recrystallization of some synthesized compounds utilizing BuOH as solvent failed, pure products were obtained after repeated column chromatography by varying eluents. Table 2 summarizes syntheses of linker based target molecules.

C. Specific Part

Table 2: Synthesis of linker based 2PA-PIs

	<i>Substrate</i>	<i>Product</i>	<i>Yield [%]</i>	<i>Method</i>
HxTPA-1E	19b + 3b	VIII	38	C-H
HxTPA-1T	27a + I	IXa	57	Suzuki
HxTPA-2T	27b + I	IXb	82	Suzuki
HxICz-2T	27b + V	X	65	Suzuki
HxPCz-2T	27b + VII	XI	84	Suzuki
HxTPA-1S	18 + 3b	XII	55	Stille
HxTPA-1DTT	28 + I	XIII	58	Suzuki
HxTPA-1BBT	15a + 3b	XIVa	40	Stille
HxTPA-1BBS	15b + 3b	XIVb	33	Stille

The linker based 2PA-PIs could be isolated in good to acceptable yields. While the Suzuki-methodology gave average yields certainly above 50 %, those of Stille-cross-coupling reaction and C-H-arylation were below. The Suzuki-reactions generally proceeded faster (~4h) than the other methodologies (> 24 h) giving higher yields.

Determination of full conversion was generally difficult, as usually many bright spots were observed on TLCs of reaction mixtures, of which some could neither be assigned to a reactant nor the product.

Low yields are attributed to purification difficulties as some of the target molecules had to be repeatedly purified by column chromatography. Certainly, purification could be optimized by screening of different eluents and stationary phases. However, in the cases of **HxTPA-1BBT** and **HxTPA-1BBS** low yields could be caused by partially crystallization of product on the column during the chromatographic run, which was finally not eluated. **HxTPA-1E** still contained impurities after repeated column chromatography, which was observed *via* TLC as NMR only showed broad multiplet in the aromatic range (see Appendix). Nevertheless, the integrals in the ¹H-NMR spectra of isolated product correlated with the structure of **HxTPA-1E**.

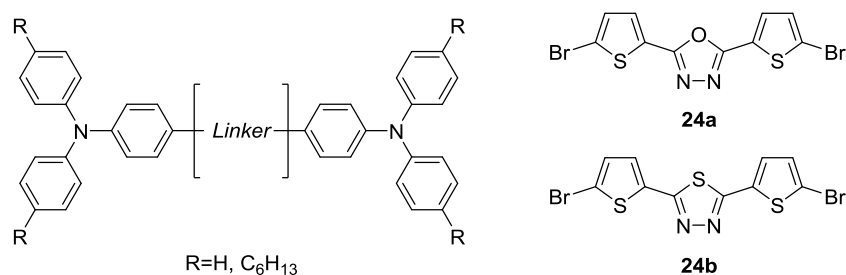
C.2.3.3 Synthesis of Acceptor-based 2PA-PIs

Compound **29** was first synthesized and characterized in a series of fluorescent 2PA dyes by Huang *et al.*^[67] Although easily synthetically accessible *via* a similar synthetic approach, the corresponding 1,3,4-thiadiazole based compound has not been investigated. Therefore, both **29** and **XV** were synthesized utilizing the Suzuki methodology discussed above and isolated by recrystallization from toluene as monosolvates, which were determined by NMR. Since both compounds were insufficiently soluble in the monomer formulation used for 2P-microfabrication structuring tests, hexyl-substituted derivatives proved to be more appropriate. Therefore synthesis of **XVIa** and **XVIb** was realized applying hexyl-substituted boronic acid ester **I**. The results are summarized in Table 3.

Table 3: Synthesis of acceptor-based 2PA-PIs. c: Yield corrected with regard to toluene.

	substrate	product	yield [%]
TPA-1TOxD	24a + 4	29	88 ^c
TPA-1TThD	24b + 4	XV	60 ^c
HxTPA-1TOxD	24a + I	XVIa	82
HxTPA-1TThD	24b + I	XVIb	48

Structural motifs of building blocks used for the synthesis of acceptor based 2PA-PIs are depicted in Scheme 34.



Scheme 34: Structural motifs of building blocks used for the synthesis of acceptor based 2PA-PIs.

C.3 Photophysical Characterization of Target Molecules

UV-VIS-Absorption and photoluminescence (PL) spectra of selected linker based 2PA-PIs and acceptor based 2PA-PIs have been measured and will be discussed in the following chapter. For experimental details see chapter **D.3 Analytical Methods**.

C.3.1 Absorption and PL-Emission Spectra of Linker Based 2PA-PIs

The Absorption and fluorescence spectra of thiophene based compound **HxTPA-1T** ($\lambda_{max}^{abs}=398$ nm, $\lambda_{max}^{em1}=465$ nm) and its selenophene analog **HxTPA-1S** ($\lambda_{max}^{abs}=408$ nm, $\lambda_{max}^{em1}=478$ nm) both show qualitatively similar band shapes (Figure 12; *left*), with absorption λ_{max}^{abs} and PL-emission maximum λ_{max}^{em1} of **HxTPA-1S** being red shifted for about 10 nm. The absorption maximum of dithienothiophene based **HxTPA-1DTT** (419 nm) is further red shifted for about 10 nm compared to **HxTPA-1S**, due to its more extended π -system. All three compounds feature an absorption band at 306 nm, which can be assigned to triphenylamine centered $n-\pi^*$ transition,^[116] whereas the broader absorption bands at higher wavelengths result from $\pi-\pi^*$ charge transfer transitions from electron donating triphenylamines to the linker units. Carbazole containing **HxPCz-2T** exhibits a relative sharp absorption band at 299 nm, which can be attributed to the $n-\pi^*$ transition of the carbazole moiety.^[117] Although **HxPCz-2T** features an enlarged π -center (bithiophene), its absorption maxima at higher wavelengths (395 nm) is slightly blue shifted compared to thiophene bridged **HxTPA-1T**.

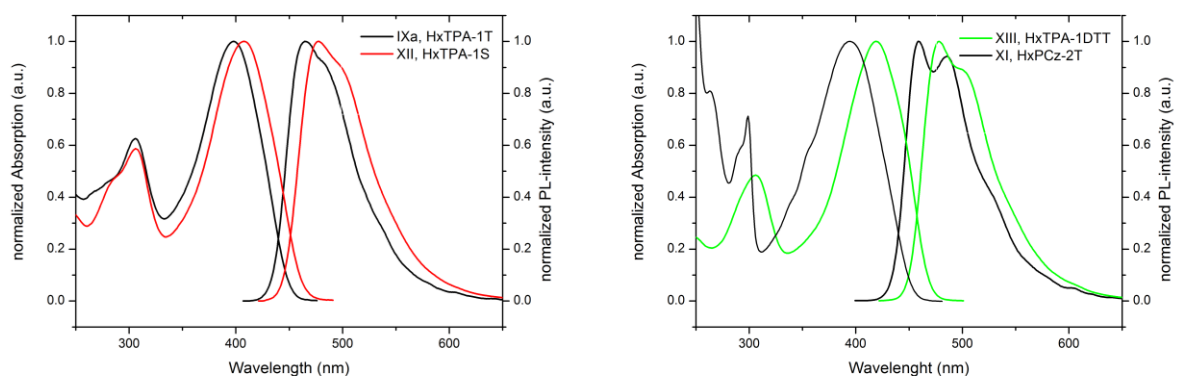


Figure 12: Comparison of absorption and fluorescence spectra of **HxTPA-1T** and **HxTPA-1S** (*left*) as well as **HxTPA-1DTT** and **HxPCz-2T** (*right*).

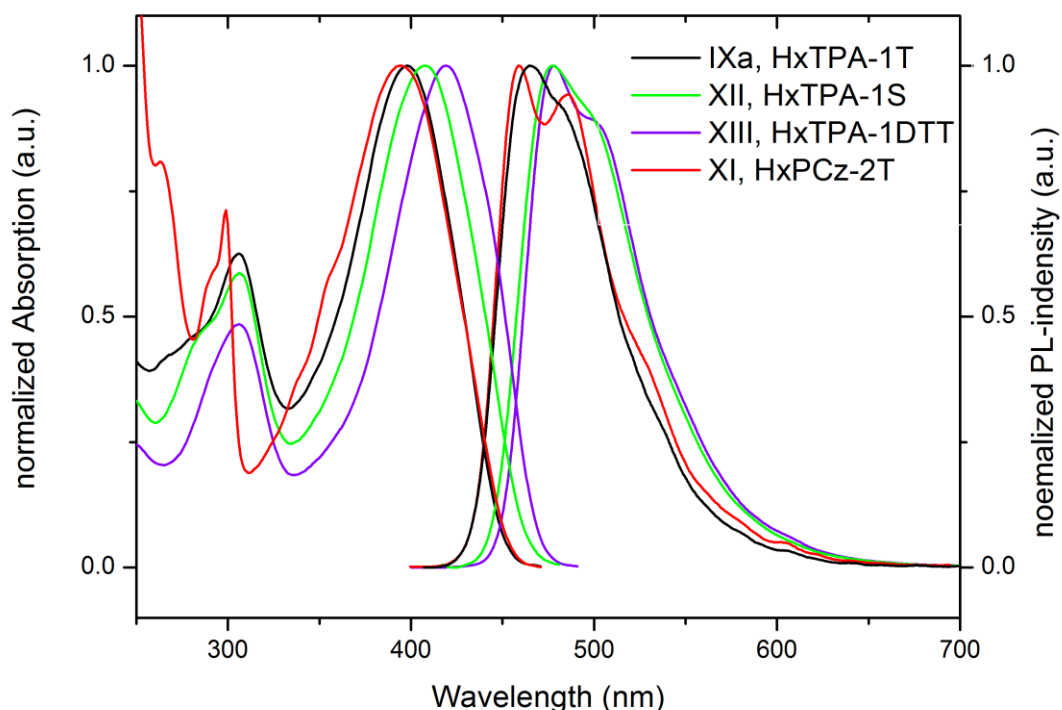


Figure 13: UV-VIS-Absorption and fluorescence spectra of **HxTPA-1T**, **HxTPA-1S**, **HxTPA-1DTT**, and **HxPCz-2T**. All spectra were recorded in DCM at a concentration of 5 nmol/ml.

It is worth noting that the emission spectra of **HxTPA-1DTT** almost resembles that of **HxTPA-1S**, only marginally red shifted. Whereas the PL spectra of **HxTPA-1T**, **HxTPA-1S** and **HxTPA-1DTT**, with emission maxima at 465 nm, 478 nm and 478 nm, exhibit only a slight shoulder at higher wavelengths, bithiophene based **HxPCz-2T** exhibits two distinct emission maxima at 459 nm and 489 nm, respectively. The general blue shift in emission of **HxPCz-2T** can be attributed to the decreased donor strength of carbazole compared to triphenylamine, as in carbazole the lone pair of the nitrogen contributes increasingly to the aromaticity.^[64]

Table 4: Comparison of longer wavelength absorption λ_{max}^{abs} , molar extinction coefficient ϵ at λ_{max}^{abs} , and emission maxima λ_{max}^{em} of linker based 2PA-PIs.

		λ_{max}^{abs} [nm]	ϵ [L/mol/cm]	λ_{max}^{em1} [nm]	λ_{max}^{em2} [nm]
HxTPA-1T	IXa	398	58280	465	-
HxTPA-1S	XII	408	57480	478	-
HxPCz-2T	XI	395	60140	459	489
HxTPA-1DTT	XIII	419	83480	478	-

C.3.2 Absorption and PL-Emission Spectra of Acceptor Based 2PA-PIs

Absorption and emission spectra of all acceptor based target molecules exhibit qualitatively equal band shapes (Figure 14). All absorption spectra feature a smaller absorption maximum between 302 nm and 306 nm and more intense absorption maxima at higher wavelengths. The former can be attributed to triphenylamine centered $n-\pi^*$ transmission as in the case of linker based target molecules. Despite these rather equally positioned absorption bands, both locations of absorption maxima at higher wavelength as well as PL-emission maxima obey a distinct order. Hence, oxathiazole containing compounds are more blue shifted than their thiadiazole based derivatives and hexyl substituted molecules are further red shifted than their non-substituted counterparts.

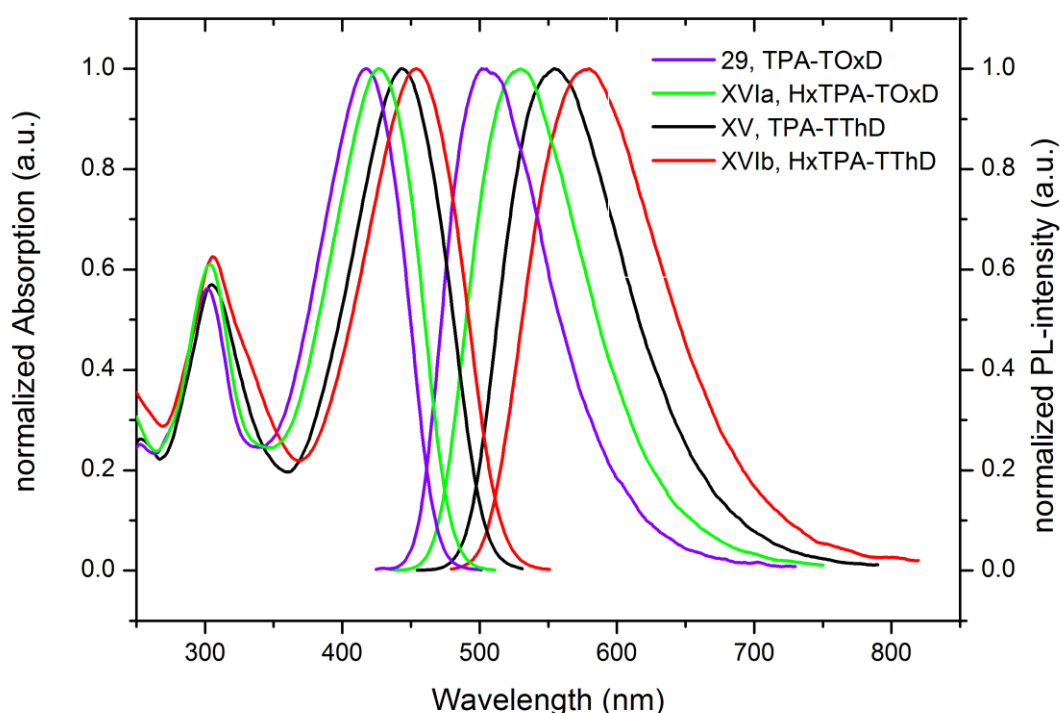


Figure 14: UV-VIS-Absorption and fluorescence spectra of acceptor based target molecules. All spectra recorded from DCM solutions.

The longer wavelength absorption bands originate from $\pi-\pi^*$ charge transfer transitions from electron-donating triphenylamines to electron-accepting oxadiazole and thiadiazole units, respectively. The influence of hexyl moieties on the donor

strength of triphenylamine caps and the consequently red shift in both absorption and emission maxima are obvious.

Table 5: Comparison of spectroscopic characteristics of acceptor based target molecules, with λ_{max}^{abs} being longer wavelength absorption maximum, ϵ molar extinction coefficient at λ_{max}^{abs} , and λ_{max}^{em} emission maximum.

		λ_{max}^{abs} [nm]	ϵ [L/mol/cm]	λ_{max}^{em} [nm]
TPA-TOxD	29	418	62323	502
TPA-TThD	XV	444	65949	555
HxTPA-TOxD	XVIa	427	76100	530
HxTPA-TThD	XVIb	454	80740	581

C.4 2PIP-Structuring Tests

The 2PIP performance of four target molecules was evaluated by writing of woodpile structures at different laser intensities and writing speeds in an acrylate formulation containing the respective compound of interest. Scanning electron microscopy (SEM) images of polymerized structures were evaluated according to visual aspects and rated in four different quality classes (Figure 15). In this manner processing windows for each formulation were determined, allowing for comparison of different 2PA-PIs.

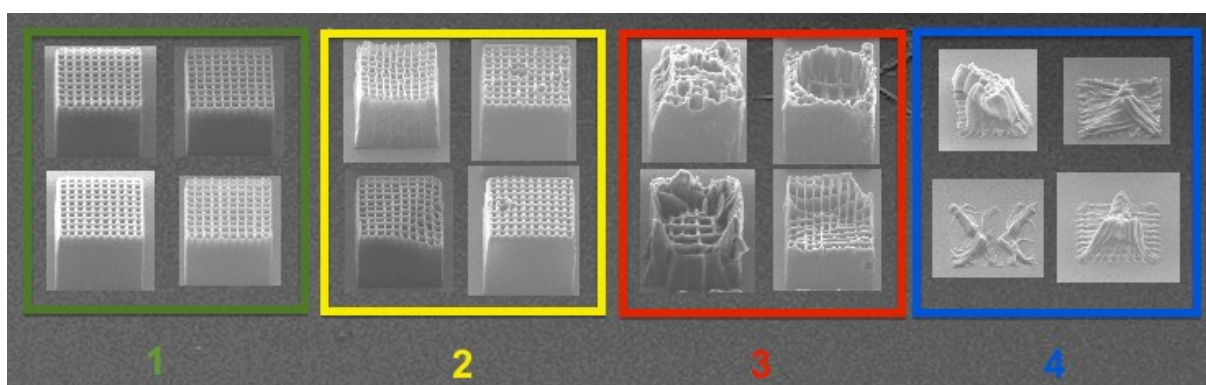


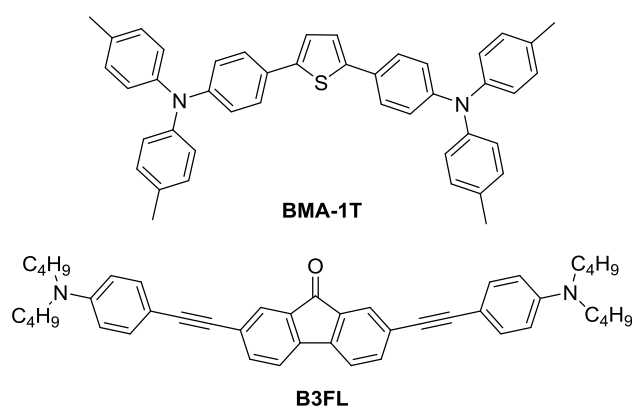
Figure 15: Examples for the four different quality categories and the associated color code.

The first category includes only perfect structures with straight lines, whereas category 2 contains good structures with wavy lines or slight marks. Class 3 consists of still identifiable structures with medium to severe errors. Within this category often structures with holes are found, originating from overexposure due to exceeding laser

C. Specific Part

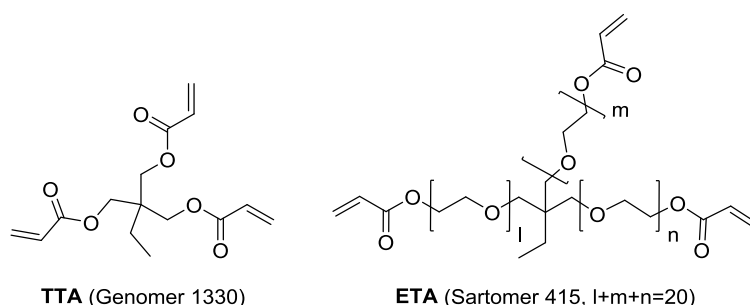
power. Objects from category 4 are not identifiable as lattices anymore. These structures are usually found at higher writing speed and low laser power and are a result of underexposure.

Two different reference compounds were used for the evaluation of 2PIP efficiencies of the target molecules. On the one hand the cap-linker-cap structure **BMA-1T** was chosen, which has a structural relationship to the target molecules and represents the starting point of this investigation (Scheme 35). On the other hand fluorenone based 2PA-PI **B3FL** was selected as reference for exhibiting a relative broad processing window and as it has been subject of several studies.^[43, 118-121]



Scheme 35: Molecular structures of reference compounds **BMA-1T**^[61] and **B3FL**^[118].

To formulate the test resins an exact amount of the respective 2PA-PI was dissolved in a defined quantity of acrylate mixture to give a concentration of 8.8 $\mu\text{mol/g}$ (Scheme 36).¹¹ Acetone was added as solubilizer and subsequently removed by rotary evaporation. Thus, kinetically stable solutions for the time period of the measurement were obtained.



Scheme 36: Molecular structures of triacrylates **TTA** and **ETA**.

The resins were deposited on acrylate coated microscope slides and structured with the *2PP Micro Processing system Mipro*^[43] at the *Institute of Materials Science and*

¹¹ 1:1 mixture of trimethylolpropane triacrylate **TTA** and ethoxylated-(20/3)-trimethylolpropane triacrylate **ETA**

C. Specific Part

Technology, VUT. The manufacturing parameters included average laser powers from 10-100 mW and writing speeds from 0.316-316 mm/s. The target molecules analyzed in this preliminary test series include **HxTPA-1T**, **HxTPA-1E**, **HxTPA-1S**, and **HxTPA-1DTT**. Acceptor based **TPA-TOxD** could not be investigated due to insufficient solubility in the test resin.

In the following the results of the 2PIP structuring tests are presented in tabular form. The corresponding SEM-images are displayed in Appendix F.2.

Table 6: Processing window of reference compound **B3FL** (8.8 $\mu\text{mol/g}$ TTA:ETA = 1:1).

		B3FL						
		Writing speed [mm/s]						
Laser intensity [mW]		316	100	31.6	10	3.16	1	0.316
	100	1	1	1	1	3	3	3
	90	1	1	1	1	1	3	3
	80	1	1	1	1	1	2	3
	70	1	1	1	1	1	1	3
	60	1	1	1	1	1	1	1
	50	2	1	1	1	1	1	1
	40	3	2	1	1	1	1	1
	30	4	4	1	1	1	1	1
	20	-	-	4	4	1	1	1
10	-	-	-	-	-	-	1	

Both reference compounds exhibited relative broad processing windows, with **B3FL** (Table 6) showing superior performance at low energy and low writing speed and **BMA-1T** (Table 7) behaving slightly better at high intensity but low writing speed.

Table 7: Processing window of reference compound **BMA-1T** (8.8 $\mu\text{mol/g}$ TTA:ETA = 1:1).

		BMA-1T						
		Writing speed [mm/s]						
Laser intensity [mW]		316	100	31.6	10	3.16	1	0.316
	100	1	1	1	1	1	3	3
	90	1	1	1	1	1	3	3
	80	1	1	1	1	1	1	3
	70	1	1	1	1	1	1	3
	60	1	1	1	1	1	1	1
	50	3	2	1	1	1	1	1
	40	4	4	1	1	1	1	1
	30	-	4	4	1	1	1	1
	20	-	-	-	4	4	1	1
10	-	-	-	-	-	4	4	

C. Specific Part

Compound **HxTPA-1T** (Table 8) though structurally closely related to **BMA-1T** showed inferior results at high energy and low writing speeds with more lattices being damaged due to overexposure. However, the hexyl-substituted derivative of **BMA-1T** performed almost similar as its counterpart at lower laser powers.

Table 8: Processing window of **HxTPA-1T** (8.8 $\mu\text{mol/g}$ TTA:ETA = 1:1).

IXa, HxTPA-1T		Writing speed [mm/s]						
		316	100	31.6	10	3.16	1	0.316
Laser intensity [mW]	100	1	1	1	1	3	3	3
	90	1	1	1	1	3	3	3
	80	1	1	1	1	1	3	3
	70	1	1	1	1	1	1	3
	60	2	1	1	1	1	1	2
	50	3	2	1	1	1	1	1
	40	4	3	1	1	1	1	1
	30	4	4	3	1	1	1	1
	20	-	-	4	4	1	1	1
	10	-	-	-	-	-	4	1

EDOT based compound **HxTPA-1E** (Table 9) behaved even slightly worse than **HxTPA-1T** at high laser intensities and low writing speeds. However, performance at lower laser intensities was slightly better than that of **BMA-1T**. The yellow area in Table 9 presumably can be attributed to artefacts from the manufacturing process (see SEM-image).

Table 9: Processing window of **HxTPA-1E** (8.8 $\mu\text{mol/g}$ TTA:ETA = 1:1).

VIII, HxTPA-1E		Writing speed [mm/s]						
		316	100	31.6	10	3.16	1	0.316
Laser intensity [mW]	100	1	1	1	1	3	3	3
	90	1	1	1	1	3	3	3
	80	1	1	1	1	1	3	3
	70	1	1	1	1	1	3	3
	60	1	1	1	1	1	1	3
	50	3	1	1	1	2	1	3
	40	4	3	1	1	2	1	1
	30	4	4	4	1	1	1	1
	20	-	-	-	4	1	1	1
	10	-	-	-	-	-	4	4

C. Specific Part

HxTPA-1S represents the highlight of this series with the broadest processing window of all investigated compounds, succeeding both at low and high laser intensities (Table 10). Accordingly, **HxTPA-1S** features the lowest polymerization threshold and yet the highest damage threshold.

Table 10: Processing window of **HxTPA-1S** (8.8 $\mu\text{mol/g}$ TTA:ETA = 1:1).

		XII, HxTPA-1S						
		Writing speed [mm/s]						
		316	100	31.6	10	3.16	1	0.316
Laser intensity [mW]	100	1	1	1	1	1	3	3
	90	1	1	1	1	1	2	3
	80	1	1	1	1	1	1	3
	70	1	1	1	1	1	1	2
	60	1	1	1	1	1	1	1
	50	1	1	1	1	1	1	1
	40	3	2	1	1	1	1	1
	30	4	4	1	1	1	1	1
	20	-	4	4	1	1	1	1
	10	-	-	-	-	4	2	1

HxPTA-1DTT exhibited a slightly lower polymerization threshold than its selenophene derivative. Nevertheless, the behavior at low writing speed and high energies was inferior to that of the reference compounds (Table 11).

Table 11: Processing window of **HxTPA-1DTT** (8.8 $\mu\text{mol/g}$ TTA:ETA = 1:1).

		XIII, HxTPA-1DTT						
		Writing speed [mm/s]						
		316	100	31.6	10	3.16	1	0.316
Laser intensity [mW]	100	1	1	1	1	1	3	3
	90	1	1	1	1	1	3	3
	80	1	1	1	1	1	3	3
	70	1	1	1	1	1	2	3
	60	1	1	1	1	1	1	2
	50	1	1	1	1	1	1	2
	40	2	2	1	1	1	1	1
	30	4	4	1	1	1	1	1
	20	-	4	4	1	1	1	1
	10	-	-	-	-	4	1	1

From a general viewpoint all characterized compounds show useful performance though exhibiting extensive photoluminescence and could be applied in a 2P-manufacturing process as their behavior at average parameters is satisfactory.

C. Specific Part

Nevertheless, the result of a fabrication processes depends on a variety of factors and thus the most efficient 2PA-PIs should be utilized.

As the power density is maximal at the lowest writing speed, a comparison of lattice qualities at 0.316 mm/s can be used to rate the high energy performance of the formulations and thus the corresponding damage threshold (Table 12). Within this rating selenophene based **HxTPA-1S** exhibits the best behavior at high energies, slightly superior to **B3FL**, with both compounds reaching optimal structural quality up to 60 mW at 0.316 mm/s. The lattice generated by **HxTPA-1S** at 70 mW still shows only minor imperfections.

Table 12: Comparison of lattice qualities at a writing speed of 0.316 mm/s.

		0.316 mm/s				
mW	B3FL	BMA-1T	HxTPA-1T	HxTPA-1E	HxTPA-1S	HxTPA-1DTT
100	3	3	3	3	3	3
90	3	3	3	3	3	3
80	3	3	3	3	3	3
70	3	3	3	3	2	3
60	1	1	2	3	1	2
50	1	1	1	3	1	2
40	1	1	1	1	1	1
30	1	1	1	1	1	1
20	1	1	1	1	1	1
10	1	4	1	4	1	1

To efficiently evaluate the full performance of 2PA-PIs structuring tests are designed to cover relatively wide processing windows. For economic reasons and with regards to commercialization 2PA-PIs should exhibit good performance at low to medium average laser intensities. Hence, the areas between 20 mW and 40 mW of input power are compared in Table 13. **HxTPA-1DTT** shows the widest processing window in this area, closely followed by **HxTPA-1S** and **B3FL** in this order. The other compounds exhibit quite similar and overall good behavior under these working conditions.

C. Specific Part

Table 13: Performance of tested 2PA-PIs at average laser powers of 20-40 mW.

		0.316 mm/s							
		mW	316	100	31.6	10	3.16	1	0.316
B3FL	50	3	2	1	1	1	1	1	1
	30	4	4	1	1	1	1	1	1
	30	-	-	4	4	1	1	1	1
BMA-1T	50	4	4	1	1	1	1	1	1
		-	4	4	1	1	1	1	1
	30	-	-	-	4	4	1	1	1
HxTPA-1T	50	4	3	1	1	1	1	1	1
	40	4	4	3	1	1	1	1	1
	30	-	-	4	4	1	1	1	1
HxTPA-1E	50	4	3	1	1	2	1	1	1
	40	4	4	4	1	1	1	1	1
	30	-	-	-	4	1	1	1	1
HxTPA-1S	50	3	2	1	1	1	1	1	1
	40	4	4	1	1	1	1	1	1
	30	-	4	4	1	1	1	1	1
HxTPA-1DTT	50	2	2	1	1	1	1	1	1
	40	4	4	1	1	1	1	1	1
	30	-	4	4	1	1	1	1	1

For a rough quantification of 2PIP-performances the tested 2PA-PIs were ordered according to their number of green lattices. Hence, **HxTPA-1S** and **HxTPA-1DTT** both exhibit broader processing windows than the reference compounds (Table 14).

C. Specific Part

Table 14: List of tested 2PA-PIs ordered according to their number of green rated lattices.

	HxTPA-1S	HxTPA-1DTT	B3FL	BMA-1T	HxTPA-1T	HxTPA-1E
1	51	48	47	45	42	39

To finally challenge the performance of **HxTPA-1S** a high resolution 3D-model with structural features in the sub-micrometer range and complex geometries was successfully manufactured utilizing the resin from the structuring test (Figure 16). As one can see from a 45° tilt the polymerized lines do not have a round cross-section, which is due to the shape of the focal ellipsoid.

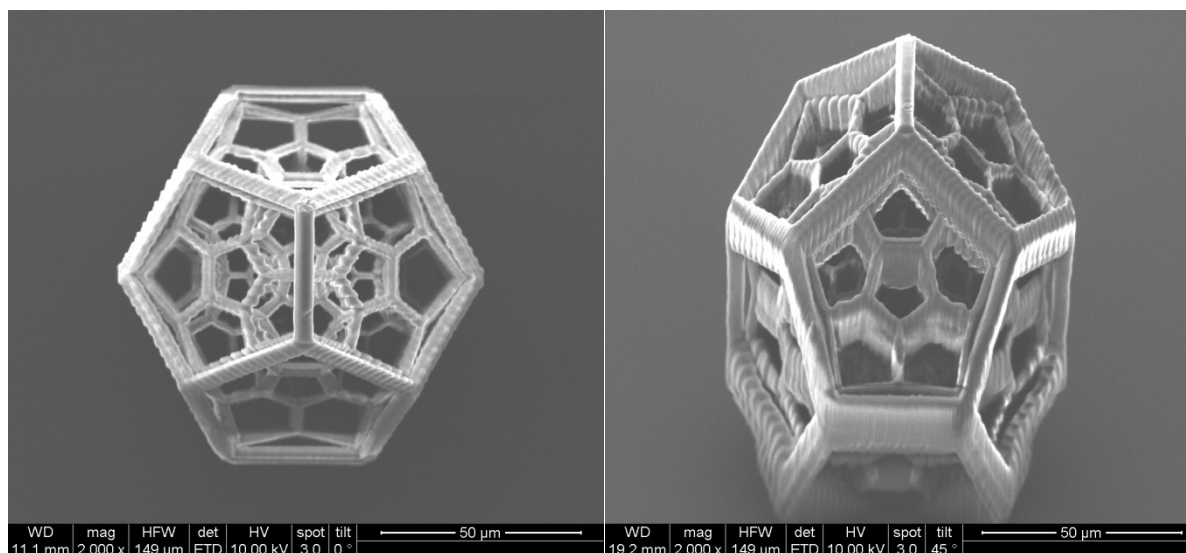


Figure 16: SEM images of complex object written with as HxTPA-1S formulation; magnification: 2000x; *left*: top view; *right*: 45° tilt.

As the mechanism of 2PA photoinitiation is undetermined yet and presumably only a minor quantity of 2PA-PIs per volume are consumed in the polymerization process, intact 2PA-PIs are incorporated into the transparent polymer structures and can be excited to fluorescence. This fact can be illustrated by dark field mode microscope images of polymerized structures illuminated by UV-light (Figure 17).

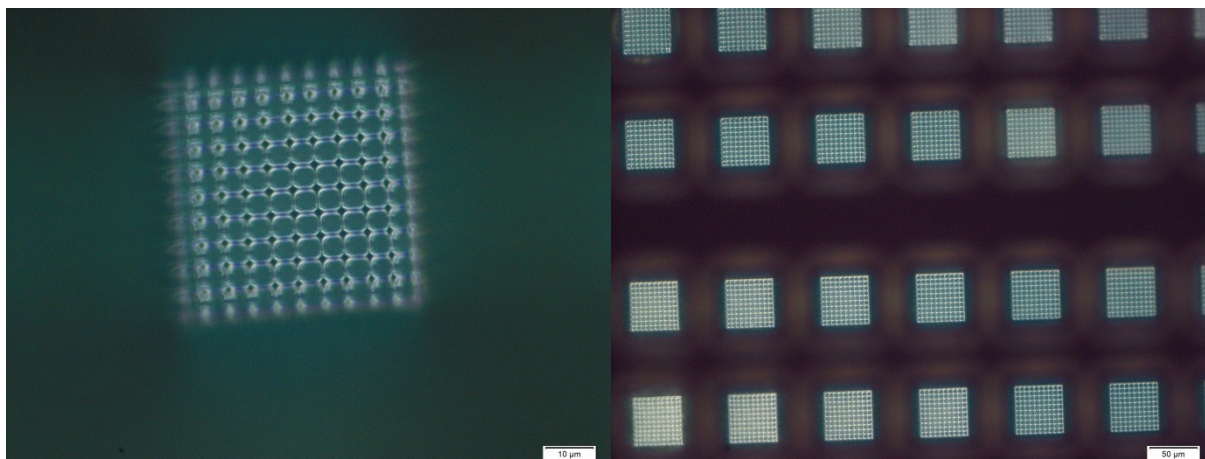


Figure 17: Microscope images of fluorescing lattices produced during structuring test of **HxTPA-1DTT**. The samples were illuminated with UV-light of 366 nm and recorded in dark field mode; *left*: magnification: 1000x; *right*: magnification: 200x.

Photoluminescence can be considered as a distinctive feature of this class of 2PA-PIs, although it is usually regarded as undesired characteristic attenuating the 2PIP efficiency.

C.5 Conclusion and Outlook

A series of symmetrical hexyl-substituted α,ω -bis(triarylamine) based compounds has been synthesized. In order to increase the 2PA and thus the efficiency of these D- π -D type target molecules as potential initiators for two-photon-microfabrication structural motifs have been optimized, including the introduction of electron rich linkers as well as the separated incorporation of both planarized linkers and caps.

In the course of this work a reliable protocol towards 5,11-disubstituted indolocarbazole (ICz) building blocks was developed. Furthermore, D- π -A- π -D type compounds based on 1,3,4-oxadiazole and 1,3,4-thiadiazole have been synthesized. Selected substances of all three classes of D- π -D type compounds as well as all D- π -A- π -D based target molecules have been characterized photophysically.

In the case of D- π -A- π -D type compounds a strict order of absorption maxima towards higher wavelength as well as PL-emission maxima has been observed. Thus, oxathiazole containing compounds are more blue shifted than their thiadiazole based derivatives and hexyl substituted molecules are further red shifted than their non-substituted counterparts.

Furthermore, an evaluation of 2P-microstructuring efficiency of an assortment of D- π -D type target molecules *via* speed-power screenings has been realized. All

characterized compounds showed good performance at average process settings. Among the investigated 2PA-PIs in this preliminary test selenophene based **HxTPA-1S** exhibited the broadest processing window. Besides, dithienothiophene based **HxTPA-1DTT** also performed above average succeeding both investigated reference compounds under the experimental settings.

Finally, a high resolution 3D-model with complex geometries and structural features in the sub-micrometer range was manufactured utilizing **HxTPA-1S**. As intact photoluminescent 2PA-PIs are incorporated into the transparent polyacrylate structures, photoluminescence upon illumination of the polymerized objects with UV-light can still be observed.

Further investigations will be focused on the full photophysical characterization of all synthesized target molecules. Furthermore, measurements of 2P cross-sections δ_{2PA} *via* z-scan method are of particular interest, as this value allows for comparison with other 2PA active materials.

Beyond that, 2PIP structuring tests need to be expanded to include all synthesized compounds as well as additional reference materials to further benchmark the 2PIP efficiency of target molecules. As 2PIP-structuring tests will reveal the results of synthetic modification strategies further specific combinations of adequate building blocks towards maximized 2PA-PI performance are matter of interest.

D. Experimental Part

D.1 General Remarks

Unless explicitly mentioned otherwise, all reagents from commercial suppliers were used without further purification. Anhydrous solvents like toluene, diethyl ether, dichloromethane and tetrahydrofuran were absolutized by a *PURESOLV*-system from *it-innovative technology inc.* Other anhydrous solvents were purchased from commercial suppliers or dried as stated in the experimental procedures. Lithiation reagents were purchased from Sigma-Aldrich® and used without additional quantitative analyses, using the declared values given below.

- *n*-BuLi (2.5 M solution in hexanes)
- *t*-BuLi (1.7 M solution in pentane)
- *n*-HexLi (2.3 M solution in hexane)

All coupling reactions were performed using HPLC-grade isopropanol.

D.2 Chromatographic Methods

D.2.1 Thin Layer Chromatography

Thin layer chromatography (TLC) was performed using TLC-aluminum foil (Merck, silica gel 60 F₂₅₄ and Macherey-Nagel ALUGRAM® aluminium oxide N/UV₂₅₄)

D.2.2 Column Chromatography

Preparative column chromatography was performed using a *Büchi Sepacore™ Flash system* which was equipped with the following components:

- Pump-system: 2 *Büchi* pump modules C-605
Büchi pump manager C-615
- Detector: *Büchi* UV photometer C-635
- Fraction collector: *Büchi* fraction collector C-660

The appropriate PP-cartridges or glass-columns were packed with silica gel (Merck, 40-63 µm). Further details (eluent (distilled solvents), amount of stationary phase) are given in the respective experimental procedures.

D.3 Analytical Methods

D.3.1 GC-MS Measurements

GC-MS measurements were conducted via a GC-MS interface from *Thermo Finnigan*:

- Gas chromatograph: *Focus GC* with a BGB5 column ($l = 30$ m, $\varnothing = 0.25$ mm, 0.25 μ m film, achiral).
- Mass spectrometer: *DSQ II* Quadrupol (electron ionization EI).

D.3.2 NMR-Spectroscopy

NMR spectra were recorded using a *Bruker DPX-200* (200 MHz for ^1H ; 50 MHz for ^{13}C) or an *Avance DRX-400* (400 MHz for ^1H ; 100 MHz for ^{13}C) fourier transform spectrometer. ^1H - and ^{13}C -spectra are given as stated: chemical shift in parts per million (ppm) referenced to the according solvent (^1H : CDCl_3 $\delta = 7.26$ ppm, CD_2Cl_2 $\delta = 5.32$, DMSO-d_6 $\delta = 2.50$ ppm; ^{13}C : CDCl_3 $\delta = 77.0$ ppm, CD_2Cl_2 $\delta = 54.0$, DMSO-d_6 $\delta = 39.5$) with tetramethylsilane (TMS) at $\delta = 0$ ppm. Multiplicities of the signals are given as: ^1H : s = singlet, bs = broad singlet, d = doublet, dd = doublet of doublets, t = triplet, q = quartet, quin = quintet, sept = septet, m = multiplet, and bm = broad multiplet. Assignments from the attached proton test (APT) experiments are: ^{13}C : s = quaternary C, d = CH, t = CH_2 , q = CH_3 .

D.3.3 Absorption Spectroscopy

Absorption spectra were recorded using a Perkin Elmer Lambda 750 spectrometer. Selected compounds were measured as solutions in DCM (5 nmol/ml)¹² in fused quartz cuvettes under standard laboratory conditions.

D.3.4 Fluorecence Spectroscopy

Fluorescence spectra were recorded using an Edinburgh FLS920 fluorometer. Selected compounds were measured as solutions DCM (5nmol/ml)¹³ in fused quartz cuvettes under standard laboratory conditions. Emission spectra of all absorption maxima of each measured compound were investigated. For all compounds different excitation wavelengths resulted in identical emission spectra.

¹² **29**, **TPA-TOxT** and **XV**, **TPA-TThT** were measured in DCM solutions of 4.4 nmol/ml containing 1 eq toluene.

¹³ **29**, **TPA-TOxT** and **XV**, **TPA-TThT** were measured in DCM solutions of 4.4 nmol/ml containing 1 eq toluene.

D.4. 2PIP-Structuring Tests

D.4.1 Laser Device

2PIP-structuring tests were performed with the *2PP Micro Processing system Mipro* designed by Torgersen as part of his PhD thesis (Figure 18).^[43]

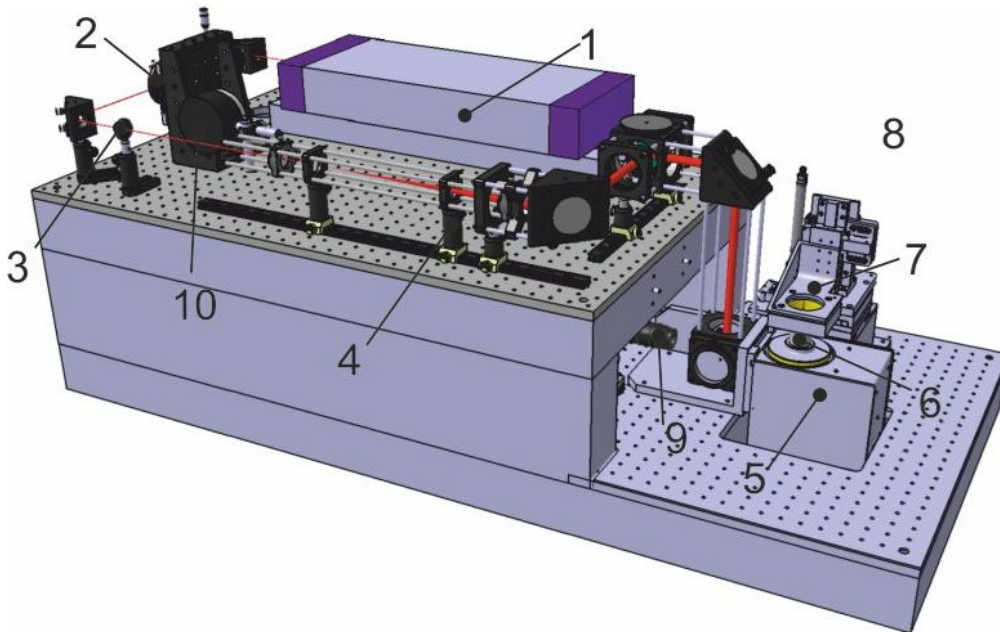


Figure 18: CAD drawing of 2PP Mipro setup; 1) Laser, 2) AOM, 3) Pinhole, 4) Beamexpander, 5) Galvanoscanner, 6) Microscope objective, 7) Specimen clamp, 8) XYZ translation axes, 9) CCD camera, 10) Laser power meter.^[43]

For the direct laser writing of 3D structures, a Ti:sapphire laser from *High Q Lasers* providing NIR pulses at 797.5 nm with a pulse duration of 72 fs is used. The system operates at a repetition rate of 73 MHz and a maximum output power of 428 mW. Direct laser writing with this system was carried out at laser powers between 10-100 mW (measured after passing the microscope objective). The laser is focused by a 20x microscope objective (NA = 0.8), and the sample is mounted on a high-precision piezoelectric XYZ scanning stage.

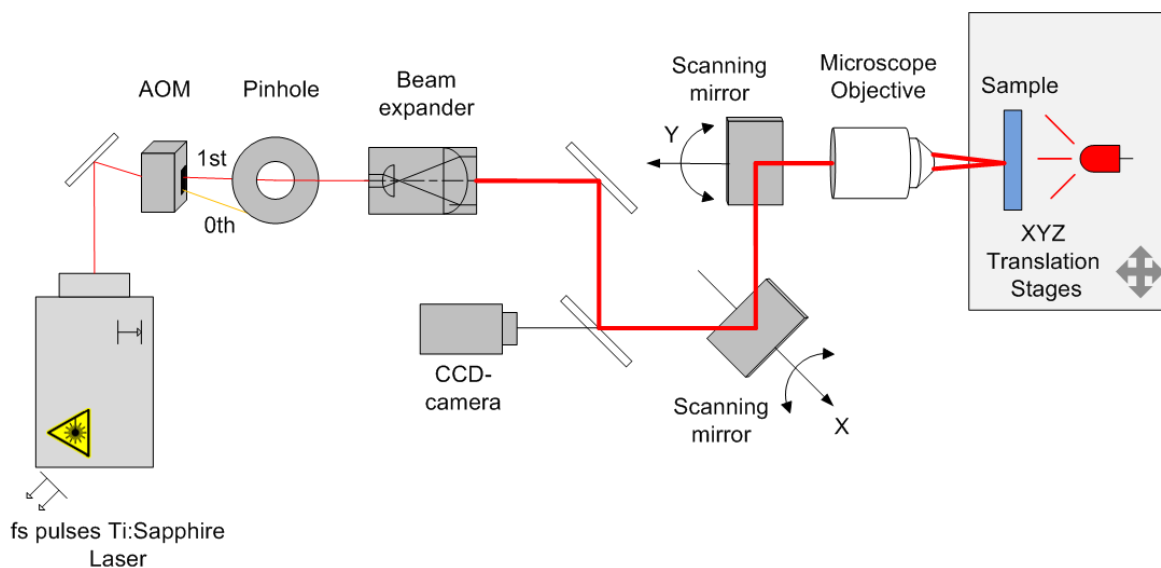


Figure 19: Scheme of the 2PP Mipro setup^[43]

Further detailed information can be found in Torgersen's PhD thesis^[43].

D.4.2 2PIP-sample Preparation

All samples were prepared by drop-casting a liquid formulation on methacrylate functionalized microscope slide as depicted in Figure 20.

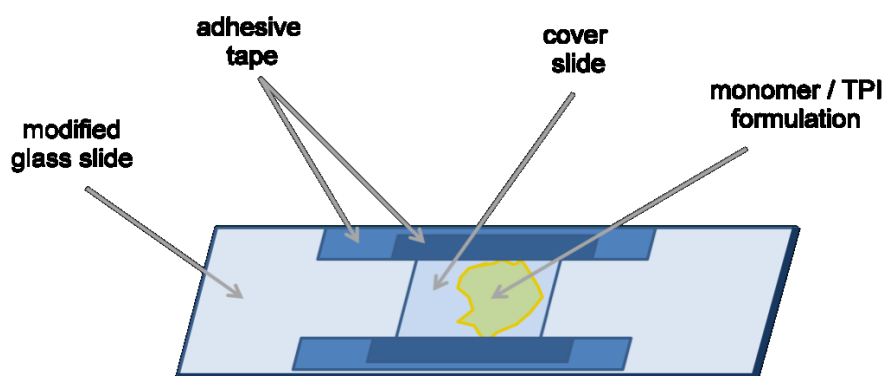


Figure 20: Scheme of a sample prepared on a glass slide^[28]

A $18 \times 18 \times 0.17 \text{ mm}^3$ coverslip was placed on a glass slide containing two pieces of parallel adhesive strip with specified thickness of about $120 \text{ }\mu\text{m}$. Then the coverslip was fastened with another two pieces of adhesive strip. About $30 \text{ }\mu\text{L}$ of formulation (2PI dissolved in a 1:1 mixture of trimethylolpropane triacrylate (**TTA**, Genomer 1330) and ethoxylated-(20/3)-trimethylolpropane triacrylate (**ETA**, Sartomer 415)) were applied between the modified glass slide and the coverslip, making use of the capillary forces.^[28]

The prepared samples were loaded into the designated clamp on the XYZ translation stages and exposed to the laser beam. The focus was scanned across the photosensitive material, which leads to an embedded 3D structure inside the material volume. After laser writing, the unexposed material was removed by development of the structures in isopropanol or acetone. The resulting structures, particularly their structural dimensions, integrity and surface quality, were imaged by means of scanning electron microscopy (SEM).^[28]

D.4.3 Functionalization of Glass Substrates

To improve adherence of the polymerized structures, conventional microscope glass slides were functionalized with methacrylate groups by first cleaning them with a 4:1 mixture of conc. H₂SO₄ and H₂O₂ (30% in water), then drying the slides at 100 °C, followed by applying a formulation of 3-(trimethoxysilyl)propyl methacrylate according to Garoff^[122].^[28] In the latter step exposition times of more than 20 min are recommended.

D.5 Synthesis and Characterization of the Compounds

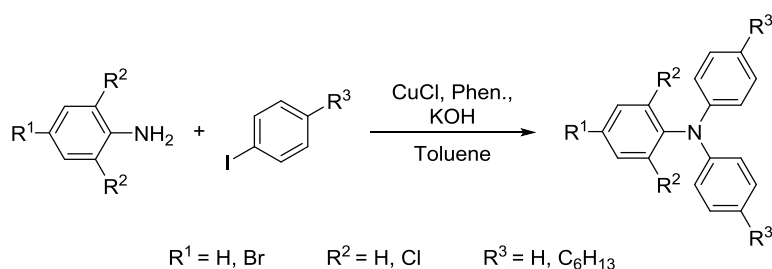
Detailed experimental procedures for the synthesis of each compound as well as their characterization are presented in the following chapter.

D.5.1. General Reaction Procedures

General reaction procedures used for the synthesis of more than one compound are described.

GP1: Ligand-accelerated Catalyzed Ullmann Condensation

The Ligand-accelerated catalyzed Ullmann condensation reactions were conducted according to Goodbrand.^[92]

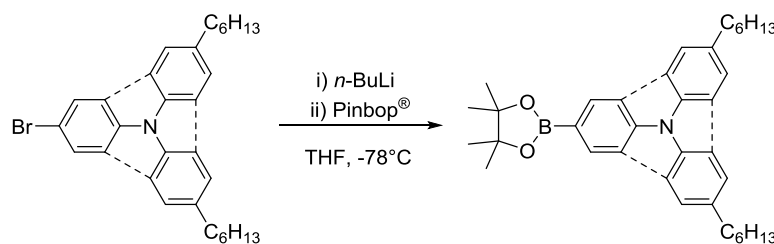


D. Experimental Part

The proper substituted aniline (1.0 eq), iodobenzene (2.2 eq), KOH (7.8 eq), Cu(I)Cl (0.04 eq) and 1,10-phenanthroline monohydrate (0.04 eq) were suspended in dry toluene in a round-bottomed flask equipped with a Dean-Stark trap under a reflux condenser and an argon-balloon. The reaction mixture was stirred magnetically refluxing until GC-MS showed full conversion. After cooling the dark reaction mixture to room temperature deionized water was added to the stirred suspension until the solid KOH residue was dissolved. The aqueous phase was extracted with toluene three times. The combined organic layers were washed with brine, dried over Na₂SO₄ and filtered before the toluene was removed by rotary evaporation. Purification was performed as stated in the detailed descriptions.

GP2: Synthesis of the Boronic Acid Esters

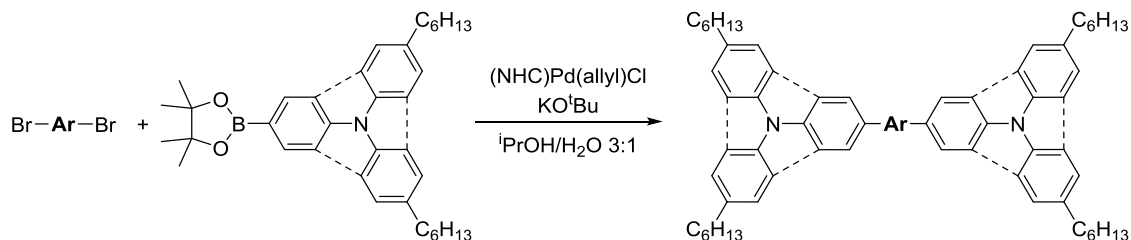
The boronic acid esters were synthesized following a protocol by Anémian.^[85]



The brominated precursor (1.0 eq) was dissolved in anhydrous THF (~0.2 M) under argon atmosphere and cooled below -78 °C. To the stirred solution *n*-BuLi (1.2 eq) was added dropwise and the reaction mixture was stirred below -65 °C for at least 1.5 h before Pinbop[®] (1.2 eq) was added. After warming the solution to room temperature slowly it was stirred overnight. THF was removed *in vacuo* before the residue was partitioned between DCM and water. The aqueous phase was extracted with DCM. The combined organic layers were dried over Na₂SO₄ followed by evaporation of the solvent *in vacuo*. Purification was performed as stated in the detailed descriptions.

GP3: Suzuki Cross-coupling Reaction Using (NHC)Pd(allyl)Cl as Catalyst

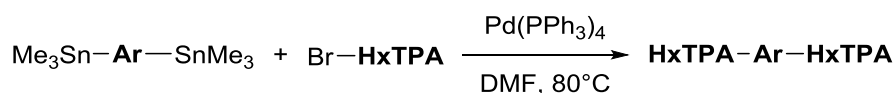
Suzuki cross-coupling reactions utilizing (NHC)Pd(allyl)Cl^[87] as catalyst were performed according to Marion.^[93]



To a suspension of the dihalogenide (1 eq), the boronic ester (~ 3 eq)¹⁴ and KO^tBu (3 eq) in a mixture of ⁱPrOH/H₂O (3:1) under argon atmosphere (NHC)Pd(allyl)Cl (20 μmol, 2 mol%) was added. The reaction mixture was refluxed until TLC showed full conversion (2-4 h). After cooling of the reaction mixture it was poured onto water and repeatedly extracted with DCM. The combined organic layers were dried over Na₂SO₄ and concentrated under reduced pressure. Purification was performed as stated in the detailed descriptions.

GP4: Stille Cross-coupling Reactions Using Pd(PPh₃)₄ as Catalyst

Stille cross-coupling reactions applying Pd(PPh₃)₄ as catalyst were realized following a procedure described by Haid.^[111]



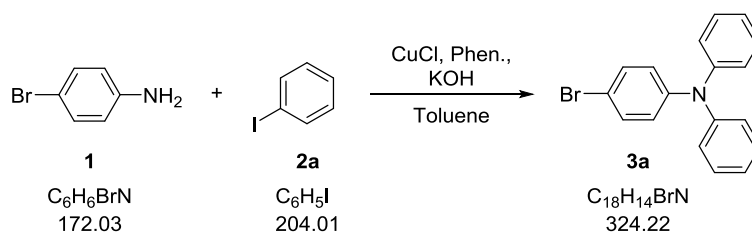
Organodistannane (1.0 eq), bromide (2.1 eq) and Pd(PPh₃)₄ (5 mol%) were dissolved in degassed dry DMF under argon atmosphere. The solution was degassed again before it was stirred at 80 °C until TLC showed full conversion. After cooling of the solution it was poured onto water and repeatedly extracted with DCM. The combined organic layers were dried over Na₂SO₄ and concentrated *in vacuo*. Purification was performed as stated in the detailed descriptions.

¹⁴ Due to difficult handling of these sticky liquids, amounts of the boronic esters used can slightly vary.

D.5.2 Synthesis of Cap-systems

D.5.2.1 Synthesis of Triphenylamine Cap-system

4-Bromo-*N,N*-diphenylbenzeneamine (**3a**)



The synthesis of **3a** followed the general procedure GP1.

4-Bromoaniline **1** (28.74 g, 167 mmol, 1.0 eq), iodobenzene **2a** (75.00 g, 367 mmol, 2.2 eq), KOH (73.13 g, 1303 mmol, 7.8 eq), Cu(I)Cl (660 mg, 6.7 mmol, 0.04 eq) and 1,10-phenanthroline monohydrate (1.32 g, 6.7 mmol, 0.04 eq) were refluxed in dry toluene (525 ml) until GC-MS showed full conversion (22 h). **3a** was isolated by Kugelrohr-distillation (160-220 °C, 0.08-0,06 mbar) as bright orange solid followed by recrystallization from ACN (ca. 200 ml) yielding white crystals (40.62 g, 125 mmol, 75%).

^1H NMR (200 MHz, CDCl_3 , FID LUM077/40): δ = 7.36-7.21 (m, 6H), 7.10-6.98 (m, 6H), 6.97-6.91 (m, 2H) ppm.

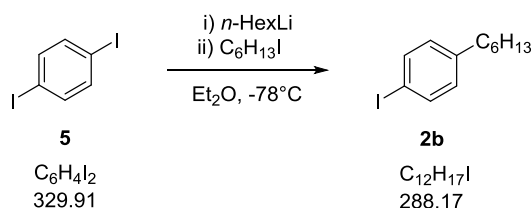
^{13}C NMR (50 MHz, CD_2Cl_2 , FID BHO035/33): δ = 148.0 (s), 147.7 (s), 132.6 (d), 129.9 (d), 125.5 (d), 125.0 (d), 123.8 (d), 115.0 (s) ppm.

D.5.2.1 Synthesis of Hexyl-substituted Cap-systems

4-Iodo-1-hexylbenzene (2b)

The syntheses of **2b** were adapted from a procedure described by Doszczak.^[123]

Variant A:



1,4-Diiodobenzene **5** (49.49 g, 150.0 mmol, 1.00 eq) was suspended in dry Et_2O (150 ml) under argon atmosphere and cooled below $-78^\circ C$ in a $N_{2(l)}$ /acetone cooling bath. Subsequently n -HexLi (66 ml, 151.5 mmol, 1.01 eq) was added dropwise (2 h) to the reaction mixture. After complete addition the suspension was stirred for 15 min below $-78^\circ C$ and then warmed to $-20^\circ C$. Thereafter it was cooled to $-70^\circ C$ and 1-iodohexane (39.76 g, 187.5 mmol, 1.25 eq) was slowly added before the $N_{2(l)}$ /acetone cooling bath was replaced by an ice-bath and the suspension was stirred overnight. Thereupon the reaction mixture was quenched with H_2O (100 ml) and extracted three times with Et_2O . The combined organic layers were dried over Na_2SO_4 , filtered and dried *in vacuo*. Remains of 1-iodohexane were removed on a high-vacuum rotary evaporator before the crude product was fractionated by high-vacuum distillation (88 - $98^\circ C$, 0.0018 mbar)¹⁵. In this way **2b** was obtained in sufficient purity as a pinkish liquid (28.88 g, 100.2 mmol, 67%).

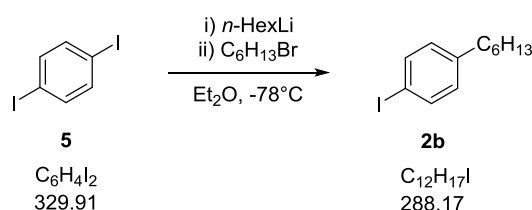
1H NMR (200 MHz, $CDCl_3$, FID LUM022/30): δ = 7.62-7.55 (m, 2H), 6.93 (m, 2H), 2.54 (t, J = 7.6 Hz, 2H), 1.61-1.50 (m, 2H), 1.42-1.18 (m, 6H), 0.88 (t, J = 7.7, 3H) ppm.

^{13}C NMR (50 MHz, CD_2Cl_2 , FID LUM022/71): δ = 142.4, 137.2, 130.5, 90.5, 35.4, 31.6, 31.2, 28.8, 22.5, 14.1 ppm.

¹⁵ After last remains of 1-iodohexane are evaporated 1,4-diiodobenzene follows in the distillation process, which solidifies in the condenser and can be melted using a heat-gun with the cooling water turned off.

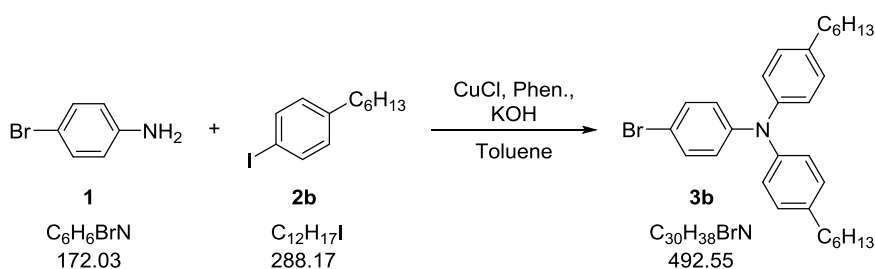
D. Experimental Part

Variant B:



1,4-Diodobenzene **5** (36.29 g, 110 mmol, 1.0 eq) was dissolved in dry Et₂O (730 ml) under argon atmosphere and cooled below -78 °C in a N_{2(l)}/acetone cooling bath. Subsequently *n*-HexLi (47.8 ml, 110 mmol, 1.0 eq) was added dropwise (45 min) to the reaction mixture and it was stirred for an hour without addition of N_{2(l)} to the cooling bath. Then the temperature was adjusted to -60 °C followed by the slow addition of 1-bromohexane (18.16 g, 110 mmol, 1.0 eq). Thereafter the cooling-bath was removed and the reaction mixture was stirred overnight before it was quenched with H₂O (40 ml) and washed with sat. sodium pyrosulfite solution (200 ml). The organic phase was then washed with brine and further handled according to variant A. Following this procedure **2b** was obtained in sufficient purity as a pinkish liquid (17.33 g, 60 mmol, 55%).

4-Bromo-*N,N*-bis(4-hexylphenyl)benzeneamine (**3b**)



The synthesis of **3b** followed the general procedure GP1.

4-Bromoaniline **1** (9.77 g, 57 mmol, 1.0 eq), 4-iodo-1-hexylbenzene **2b** (36.00 g, 125 mmol, 2.2 eq), KOH (24.87 g, 443 mmol, 7.8 eq), Cu(I)Cl (230 mg, 2.3 mmol, 0.04 eq) and 1,10-phenanthroline monohydrate (450 mg, 2.3 mmol, 0.04 eq) were refluxed in 120 ml of dry toluene until TLC showed full conversion (4 d). The raw product was flashed over a pad of silica and the crude fractions were purified by distilling the impurities off (120 °C, 0.24 mbar) by Kugelrohr-distillation. In this way **3b** was obtained as a yellowish oil (24.17 g, 49 mmol, 86%).

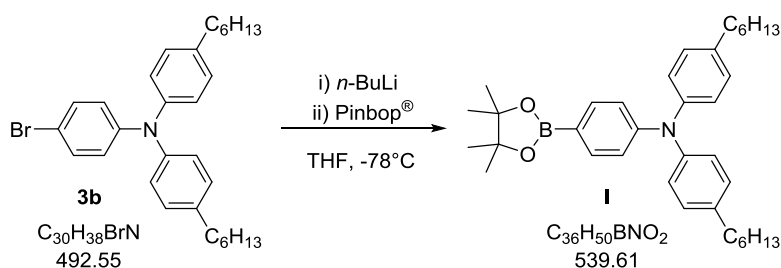
D. Experimental Part

$R_f = 0.44$ (PE)

^1H NMR (200 MHz, CH_2Cl_2 , FID LUM043/90): $\delta = 7.31\text{--}7.24$ (m, 2H), 7.11–7.06 (m, 4H), 6.98–6.94 (m, 4H), 6.90–6.83 (m, 2H), 2.56 (t, $J = 7.9$ Hz, 4H), 1.63–1.52 (m, 4H), 1.42–1.31 (m, 12H), 0.89 (t, $J = 6.6$, 6H) ppm.

^{13}C NMR (50 MHz, CDCl_3 , FID LUM043/121): $\delta = 147.4$ (s), 145.0 (s), 138.0 (s), 131.9 (d), 129.2 (d), 124.5 (d), 124.0 (d), 113.6 (s), 35.4 (t), 31.7 (t), 31.5 (t), 29.1 (t), 22.6 (t), 14.1 (q) ppm.

***N,N*-Bis(4-hexylphenyl)-4-(4,4,5,5-tetramethyl-1,3,2-dioxaborolan-2-yl)-benzeneamine (I)**



The synthesis of **I** followed the general procedure GP2. Differing from GP1 only 1.1 eq of *n*-BuLi and 1.1 eq of Pinbop[®] have been applied.

Starting from bromide **3b** (13.21 g, 26.8 mmol, 1.0 eq), *n*-BuLi (11.8 ml, 29.4 mmol, 1.1 eq) and Pinbop[®] (5.47 g, 29.4 mmol, 1.1 eq) in 120 ml of anhydrous THF **I** (11.11 g, 20.5 mmol, 77%) was isolated as a pale yellowish oil by column chromatography (350 g SiO_2 , PE:Et₂O = 2–3%) and drying using high vacuum.

$R_f = 0.26$ (PE:DCM = 15%)

^1H NMR (400 MHz, CDCl_3 , FID LUM050#F/100): $\delta = 7.66\text{--}7.60$ (m, 2H), 7.10–6.93 (m, 10H), 2.57 (t, $J = 7.8$ Hz, 4H), 1.68–1.54 (m, 4H), 1.39–1.25 (m, 24H), 0.90 (t, $J = 6.5$ Hz, 6H) ppm.

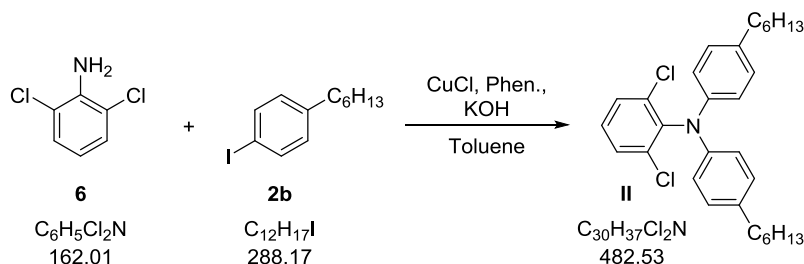
^{13}C NMR (100 MHz, CDCl_3 , FID LUM050#F/103): $\delta = 151.0$ (s), 145.0 (s), 138.2 (s), 135.7 (d), 129.2 (d), 125.1 (d), 120.7 (d), 83.4 (s), 35.4 (t), 31.7 (t), 31.4 (t), 29.1 (t), 24.8 (q), 22.6 (t), 14.1 (q) ppm.¹⁶

¹⁶ C-(B) could not be detected. Assignments adopted from incomplete APT LUM050/63.

D. Experimental Part

^{13}C NMR (50 MHz, CDCl_3 , FID LUM050/63): δ = 145.0 (s), 138.2 (s), 135.7 (d), 129.2 (d), 125.1 (d), 120.7 (d), 83.5 (s), 35.4 (t), 31.7 (t), 31.4 (t), 29.1 (t), 24.8 (q), 22.6 (t), 14.1 (q) ppm.

2,6-Dichloro-*N,N*-bis(4-hexylphenyl)benzeneamine (II)



The synthesis of **II** followed the general procedure GP1. Differing from GP1 only 2.06 eq of 1-hexyl-4-iodobenzene **2a** have been applied.

2,6-Dichlorobenzeneamine **6** (4.86 g, 30 mmol, 1.0 eq), 1-hexyl-4-iodobenzene **2a** (17.79 g, 61.7 mmol, 2.06 eq), KOH (13.13 g, 23 mmol, 7.8 eq), Cu(I)Cl (120 mg, 1.2 mmol, 0.04 eq) and 1,10-phenanthroline monohydrate (240 mg, 1.2 mmol, 0.04 eq) were refluxed in 43 ml of dry toluene until GC-MS showed full conversion of **2a** (8 d). After work-up according to GP1 the sticky black raw product (15.94 g) was flashed over SiO_2 (420 g) with PE. Impure fractions were further purified by distilling impurities off *via* Kugelrohr-distillation (140 °C, 0.014 mbar). In this manner **II** was obtained as a yellowish oil (5.09 g, 10.5 mmol, 35%).

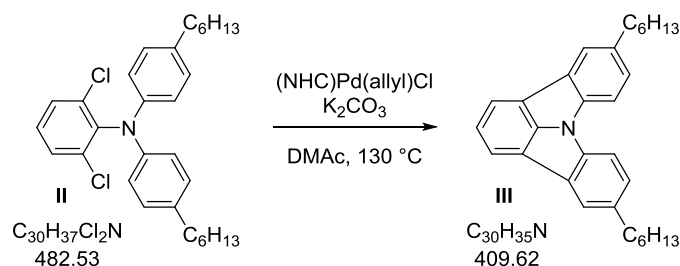
R_f = 0.47 (PE)

^1H NMR (200 MHz, CDCl_3 , FID LUM074/60): δ = 7.44-7.39 (m, 2H), 7.24-7.16 (m, 1H), 7.06 (m, 4H), 6.95-6.88 (m, 4H), 2.57 (t, J = 7.6 Hz, 4H), 1.69-1.53 (m, 4H), 1.39-1.28 (m, 12H), 0.91 (t, 6.6 Hz, 6H) ppm.

^{13}C NMR (100 MHz, CDCl_3 , FID LUM074#F/113): δ = 143.1 (s), 140.6 (s), 137.2 (s), 136.4 (s), 129.5 (d), 128.8 (d), 128.1 (d), 120.3 (d), 35.3 (t), 31.7 (t), 31.5 (t), 29.1 (t), 22.6 (t), 14.1 (q) ppm.¹⁷

^{13}C NMR (50 MHz, CDCl_3 , FID LUM074/63): δ = 143.1 (s), 137.2 (s), 136.4 (s), 129.5 (d), 128.9 (d), 128.1 (d), 120.3 (d), 35.3 (t), 31.7 (t), 31.5 (t), 29.1 (t), 22.6 (t), 14.1 (q) ppm

¹⁷ Assignments adopted from incomplete APT LUM074/63.

5,11-Dihexylindolo[3,2,1-*jk*]carbazole (III)

The synthesis of **III** followed an adapted protocol by Campeau.^[64, 86]

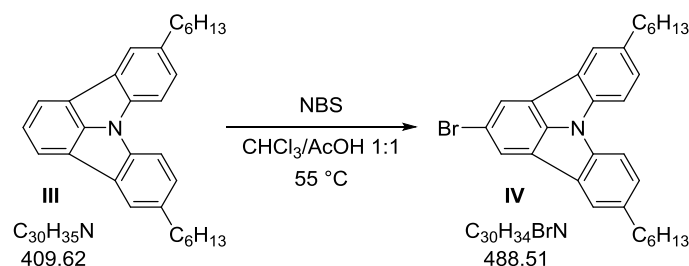
In order to adjust the water content of the solvent to 1000 ppm deionized water (22 mg) was added to dry DMAc (24.42 g, Sigma-Aldrich, $H_2O \leq 0.01\%$ according to specifications, stored over molecular sieve). The solvent was then degassed with argon in an ultrasonic bath. **II** (4.66 g, 9.6 mmol, 1.0 eq) and K_2CO_3 (2.68 g, 19.3 mmol, 2.0 eq) were suspended in degassed moistened DMAc before $(NHC)Pd(allyl)Cl$ (276 mg, 0.5 mmol, 5 mol%) was added in a countercurrent flow of argon and the reaction mixture was heated to $130\text{ }^\circ\text{C}$. The reaction progress was monitored by GC-MS. After 3 days of heating no further conversion of **II** could be observed and therefore more catalyst (276 mg, 0.5 mmol, 0.05 eq) was added and the temperature was raised to $160\text{ }^\circ\text{C}$. After 4 hours the reaction was complete.¹⁸ The reaction mixture was poured onto water and extracted with DCM. The combined organic layers were dried over Na_2SO_4 , filtered and dried under reduced pressure. The sticky black raw product (7.52 g) was flashed over SiO_2 (60 g) with PE:DCM (2:1). Following this procedure **III** (3.70 g, 9.0 mmol, 94%) was obtained as an off-white powder.

$R_f = 0.52$ (PE)

1H NMR (400 MHz, $CDCl_3$, FID LUM080#F/40): $\delta = 8.02$ (d, $J = 7.4$ Hz, 2H), 7.95 (m, 2H), 7.77 (m, 2H), 7.56 (t, $J = 8.1$ Hz, 1H), 7.36 (m, 2H), 2.82 (t, 7.6 Hz, 4H), 1.76 (quin, $J = 7.6$ Hz, 4H), 1.45-1.35 (m, 12H), 0.93 (t, 7.0 Hz, 6H) ppm.

^{13}C NMR (100 MHz, $CDCl_3$, FID LUM080#F/43): $\delta = 144.3$ (s), 137.0 (s), 136.2 (s), 130.0 (s), 127.0 (d), 122.8 (d), 122.4 (d), 119.1 (d), 118.5 (s), 111.5 (d), 36.1 (t), 32.1 (t), 31.8 (t), 29.0 (t), 22.7 (t), 14.1 (q) ppm.

¹⁸ By initial heating to $160\text{ }^\circ\text{C}$ a shorter reaction time could have been achieved.

2-Bromo-5,11-dihexylindolo[3,2,1-*jk*]carbazole (IV)

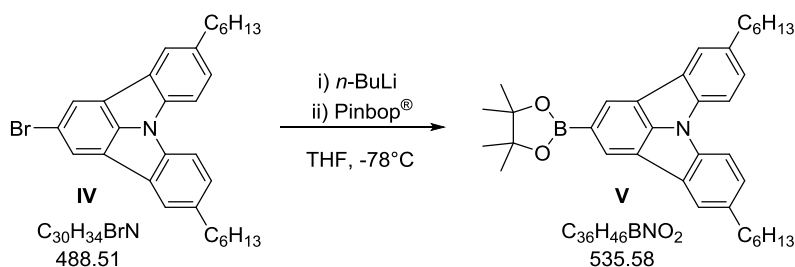
The bromination of **III** was performed according to Bintinger.^[62]

Dihexylindolocarbazole **III** (3.50 g, 8.5 mmol, 1.0 eq) was suspended in an equal mixture of CHCl₃ and AcOH (42 ml) under argon atmosphere and heated to 55 °C. To this suspension NBS (1.52 g, 8.5 mmol, 1.0 eq) was added in small portions over a period of 2.5 hours. During the addition a white precipitate formed. The mixture was further stirred for 30 min before it was carefully poured onto aqueous NaOH solution (2N, 300 ml) and extracted with DCM. **IV** was purified by recrystallization from ACN and obtained as fine yellowish needles (3.54 g, 7.2 mmol, 85%).

R_f = 0.58 (PE)

¹H NMR (400 MHz, CDCl₃, FID LUM081#F/40): δ = 8.06 (s, 2H), 7.82 (m, 2H), 7.69 (m, 2H), 7.34 (m, 2H), 2.78 (t, J = 7.8, 4H), 1.73 (quin, J = 7.1 Hz, 4H), 1.42-1.33 (m, 12H), 0.91 (t, J = 6.7 Hz, 6H) ppm.

¹³C NMR (100 MHz, CDCl₃, FID LUM081#F/43): δ = 142.4 (s), 137.3 (s), 136.6 (s), 129.1 (s), 127.7 (d), 122.9 (d), 122.0 (d), 119.6 (s), 115.3 (s), 111.7 (d), 36.0 (t), 32.0 (t), 31.8 (t), 29.0 (t), 22.6 (t), 14.1 (q) ppm.

5,11-Dihexyl-2-(4,4,5,5-tetramethyl-1,3,2-dioxaborolan-2-yl)indolo[3,2,1-*jk*]carbazole (V)

The synthesis of **V** followed the general procedure GP2.

D. Experimental Part

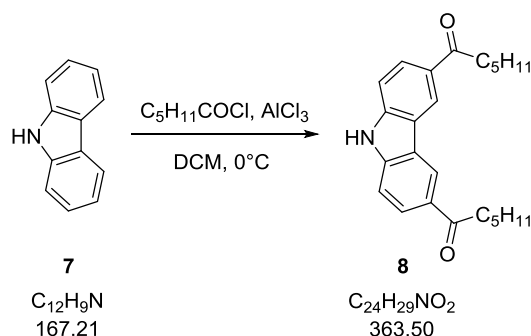
Starting from bromide **IV** (3.17 g, 6.5 mmol, 1.0 eq), *n*-BuLi (3.1 ml, 7.8 mmol, 1.2 eq) and Pinbop[®] (1.45 g, 7.8 mmol, 1.2 eq) in anhydrous THF (110 ml) **I** was isolated by recrystallization from ACN and subsequent flash chromatography (34 g SiO₂, PE:EA = 0-7%)¹⁹ as a grayish solid (2.02 g, 3.8 mmol, 58%).

R_f = 0.53 (PE:DCM = 30%)

¹H NMR (400 MHz, CD₂Cl₂, FID LUM082#F/10): δ = 8.51 (s, 2H), 7.98 (m, 2H), 7.79 (m, 2H), 7.38 (m, 2H), 2.82 (t, 7.8 Hz, 4H), 1.74 (quin, 7.6 Hz, 4H), 1.44-1.34 (m, 24H), 0.92 (t, 6.8 Hz, 6H) ppm.

¹³C NMR (100 MHz, CD₂Cl₂, FID LUM082#F/13): δ = 146.9 (s), 137.7 (s), 137.3 (s), 130.4 (s), 127.8 (d), 126.5 (d), 123.4 (d), 118.8 (s), 112.2 (d), 84.4 (s), 36.6 (t), 32.6 (t), 32.4 (t), 29.6 (t), 25.4 (q), 23.3 (t), 14.5 (q) ppm.²⁰

1,1'-(9*H*-Carbazole-3,6-diyl)bishexan-1-one (**8**)



The synthesis of **8** was performed according to Yasuda.^[101]

A suspension of carbazole **7** (18.40 g, 110 mmol, 1 eq) and AlCl₃ (44.02 g, 330 mmol, 3.0 eq) in anhydrous DCM (360 ml) was cooled below 5 °C under argon atmosphere. Hexanoyl chloride (44.44 g, 330 mmol, 3 eq) was added steady to the stirred reaction mixture keeping the temperature below 5 °C. Subsequently the suspension was allowed to warm to room temperature over night and was stirred until GC-MS and TLC (PE:DCM = 2:1) showed full conversion (2d). The reaction mixture was hydrolyzed by pouring it on ice (800 ml) and allowed to stand overnight. The formed precipitation was filtered, washed first with water and subsequently with

¹⁹ Recrystallization could have been avoided by direct execution of flash chromatography.

²⁰ C-(B) could not be detected.

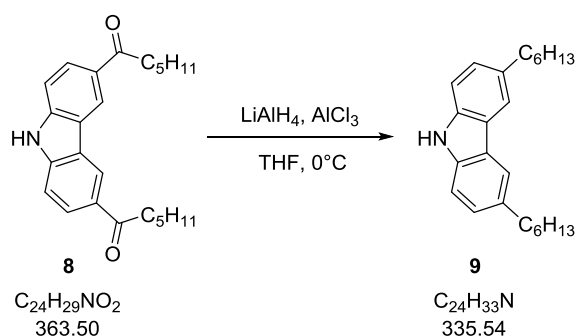
D. Experimental Part

MeOH before it was dried in a desiccator. **8** (27.04 g, 74 mmol, 68%) was obtained as a grey-pinkish powder and no further purification was necessary.

$R_f = 0.42$ (PE:EA = 30%)

^1H NMR (200 MHz, CDCl_3 , FID LUM018/20): $\delta = 8.79$ (m, 2H), 8.55 (bs, 1H), 8.15 (dd, $J = 8.6, 1.6$ Hz, 2H), 7.49 (m, 2H), 3.11 (t, 7.4 Hz, 4H), 1.86-1.75 (m, 4H), 1.46-1.39 (m, 8H), 0.94 (t, $J = 6.9$ Hz, 6H) ppm.

3,6-Dihexyl-9H-carbazole (**9**)



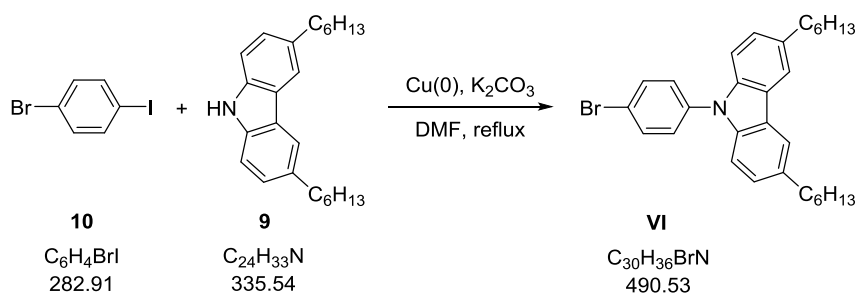
The synthesis of **9** followed a procedure described by Yasuda.^[101]

To a suspension of LAH (1.04 g, 27.52 mmol, 4 eq) in anhydrous THF (35 ml) which was cooled below 5°C AlCl_3 (1.84 g, 13.76 mmol, 2 eq) was added in small portions in a countercurrent flow of argon. After 15 min of stirring carbazole **8** (2.50 g, 6.88 mmol, 1.0 eq) was added in the same manner before the reaction mixture was allowed to warm to room temperature overnight. Reaction control was performed by TLC (PE: $\text{CHCl}_3 = 1:2$). The cooled suspension was quenched with EA (50 ml) followed by 2N HCl (2 ml) and subsequently filtered through a batch of celite (washed with EA) and concentrated *in vacuo*. **9** (2.24 g, 6.67 mmol, 97%) was obtained as a grey-brownish powder. No further purification was necessary.

$R_f = 0.26$ (PE:DCM = 15%)

^1H NMR (200 MHz, CD_2Cl_2 , FID LUM025/70): $\delta = 7.98$ (bs, 1H), 7.85 (m, 2H), 7.34 (m, 2H), 7.23 (dd, $J = 8.3, 1.6$ Hz, 2H), 2.77 (t, 7.6 Hz, 4H), 1.77-1.63 (m, 4H), 1.46-1.35 (m, 12H), 0.90 (t, $J = 6.9$ Hz, 6H) ppm.

^{13}C NMR (50 MHz, CDCl_3 , FID LUM025/51): $\delta = 138.2, 133.8, 126.4, 123.4, 119.5, 110.2, 36.1, 32.3, 31.8, 29.1, 22.6, 14.1$ ppm.

9-(4-Bromophenyl)-3,6-dihexyl-9H-carbazole (VI)

The synthesis of **VI** was realized according to Aizawa.^[96]

3,6-Dihexyl-9H-carbazole **9** (4.64 g, 13.8 mmol, 1.0 eq) and with 1-bromo-4-iodobenzene **10** (4.30 g, 15.2 mmol, 1.1 eq), Cu(0) powder (2.73 g, 42.9 mmol, 3.1 eq) and K₂CO₃ (5.93 g, 42.9 mmol, 3.1 eq) was refluxed in dry DMF (29 ml) under argon atmosphere until TLC (PE) showed full conversion (20 h). After cooling to room temperature the reaction mixture was suspended in DCM and filtered over Celite. The solution was washed with water, dried over Na₂SO₄ and filtered before it was concentrated under high vacuum. **VI** was isolated by column chromatography (200 g SiO₂, PE) as a white solid (6.08 g, 12.4 mmol, 90%).²¹

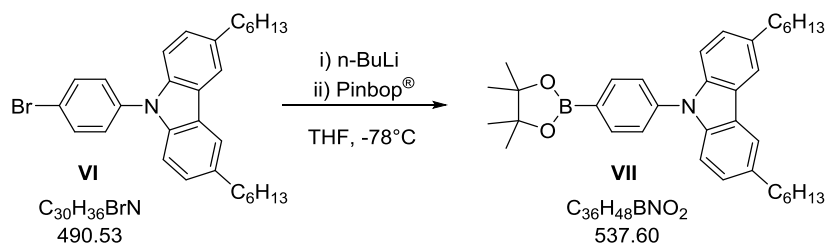
R_f = 0.51 (PE)

¹H NMR (200 MHz, CDCl₃, FID LUM045/50): δ = 7.86 (m, 2H), 7.68-7.61 (m, 2H), 7.47-7.35 (m, 2H), 7.24-7.14 (m, 4H), 2.74 (t, J = 7.5 Hz, 4H), 1.67 (quin, J = 7.5, 4H), 1.42-1.23 (m, 12H), 0.85 (t, J = 6.9 Hz, 6H) ppm.

¹³C NMR (50 MHz, CDCl₃, FID LUM045/53): δ = 139.2 (s), 137.3 (s), 134.8 (s), 133.0 (d), 128.4 (d), 126.6 (d), 123.6 (s), 120.3 (s), 119.6 (d), 109.2 (d), 36.0 (t), 32.3 (t), 31.8 (t), 29.0 (t), 22.7 (t), 14.1 (q) ppm.

²¹ As a side product the coupling product of **9** and **VI** (238 mg, 0.3 mmol) was eluted using PE:DC (9:1). ¹H NMR (200 MHz, CD₂Cl₂, FID LUM045/30): δ = 7.96-7.95 (m, 4H), 7.80 (s, 4H), 7.48 (d, J = 8.5 Hz, 4H), 7.29 (dd, J = 8.5 Hz, 1.6 Hz, 4H), 2.86-2.78 (m, 8H), 1.77-1.70 (m, 8H), 1.46-1.27 (m, 24H), 0.94-0.88 (m, 12H) ppm.

3,6-Dihexyl-9-(4-(4,4,5,5-tetramethyl-1,3,2-dioxaborolan-2-yl)phenyl)-9H-carbazole (VII)



The synthesis of **VII** followed the general protocol GP2.

Starting from bromide **VI** (2.55 g, 5.2 mmol, 1.0 eq), *n*-BuLi (2.5 ml, 6.2 mmol, 1.2 eq) and Pinbop[®] (1.16 g, 6.2 mmol, 1.2 eq) in 26 ml of anhydrous THF **VII** was isolated as a white solid (2.09 g, 3.9 mmol, 75%) by passing through a pad of silica (15 g SiO₂, PE:DCM).

R_f = 0.20 (PE:DCM = 15%)

¹H NMR (200 MHz, CD₂Cl₂, FID LUM048/60): δ = 8.02 (d, J = 8.3 Hz, 2H), 7.94 (s, 2H), 7.61 (d, 8.3 Hz, 2H), 7.39 (d, J = 8.5 Hz, 2H), 7.25 (dd, J = 8.5, 1.6 Hz, 2H), 2.81 (t, J = 7.5 Hz, 4H), 1.81-1.67 (m, 4H), 1.49-1.30 (m, 24H), 0.93 (t, J = 6.9 Hz, 6H) ppm.

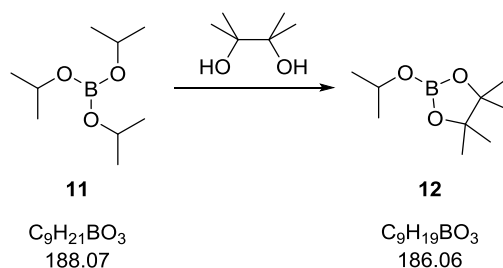
¹³C NMR (100 MHz, CDCl₃, FID LUM048#F/103): δ = 140.9 (s), 139.1 (s), 136.3 (d), 134.6 (s), 126.5 (d), 125.7 (d), 123.6 (s), 119.5 (d), 109.5 (d), 84.0 (s), 36.0 (t), 32.3 (t), 31.8 (t), 29.1 (t), 24.9 (q), 22.7 (t), 14.1 (q) ppm.²²

¹³C NMR (50 MHz, CD₂Cl₂, FID LUM048/63): δ = 141.4 (s), 139.7 (s), 136.8 (d), 135.4 (s), 127.2 (d), 126.2 (d), 124.2 (s), 120.0 (d), 110.1 (d), 84.6 (s), 36.5 (t), 33.0 (t), 32.5 (t), 29.7 (t), 25.3 (q), 23.3 (t), 14.5 (q) ppm.

²² C-(B) could not be detected. Assignments adopted from APT LUM048/63.

D.5.3. Synthesis of Pinbop[®]

4,4,5,5-Tetramethyl-2-(1-methylethoxy)-1,3,2-dioxaborolane (Pinbop[®]) (**12**)



Pinbop[®] was synthesized according to Andersen.^[124]

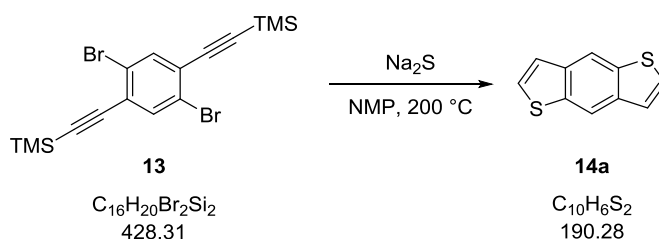
Pinacol (100.00 g) was dried by dissolving in toluene (450 ml) and evaporation of the azeotrope on a rotary evaporator. Subsequently the dried pinacol (86.80 g, 734.5 mmol, 1.0 eq) and triisopropyl borate **11** (138.14 g, 734.5 mmol, 1.0 eq) were refluxed in 500 ml of dry *n*-hexane under argon atmosphere and thereby a mixture of *n*-hexane and 2-propanol was distilled off via a vigreux-column. The crude product was purified by fractional distillation under reduced pressure (77-79 °C, 25 mbar). Following this procedure **12** was obtained as a colorless liquid (119.20 g, 640.7 mmol, 87%).

¹H NMR (200 MHz, CDCl₃, FID LUM002/20): δ = 4.32 (sept, J = 6.2 Hz, 1H), 1.24 (s, 12H), 1.19 (d, J = 6.2 Hz, 6H) ppm. CDCl₃ was dried over molecular sieve.

¹³C NMR (50 MHz, CDCl₃, FID BHO003/23): = 82.4 (s), 67.3 (d), 24.5 (q), 24.3 (q) ppm. CDCl₃ was dried over molecular sieve.

D.5.4 Synthesis of Linkers

1,1'-Benzo[1,2-*b*:4,5-*b'*]dithiophene (**14a**)

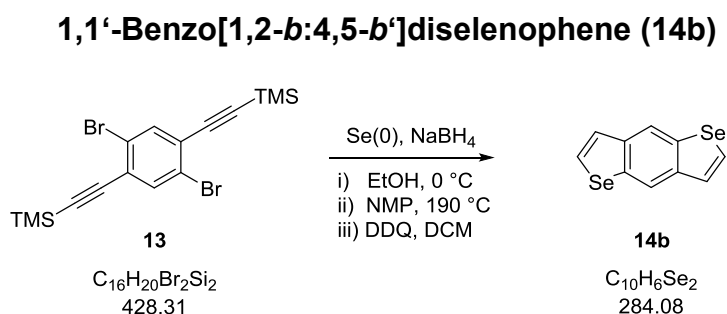


The synthesis of **14a** followed a protocol by Kashiki.^[103]

D. Experimental Part

Dialkyne **13** (4.28 g, 10.0 mmol, 1.0 eq) and anhydrous Na₂S (1.64, 2.1 mmol, 2.1 eq) were dissolved in 135 ml of NMP under argon atmosphere and heated to 200 °C until TLC (PE) showed full conversion (17 h). After cooling of the reaction mixture to room temperature it was poured onto saturated aqueous NH₄Cl solution (700 ml) and the formed precipitate was filtered off. Subsequently the brown solid was dissolved in CHCl₃ and the solution was washed with brine, dried over Na₂SO₄ and concentrated under reduced pressure. **14a** was isolated by column chromatography (90 g SiO₂, PE:EA (1-2%)) as a white solid (695 mg, 3.7 mmol, 37%).

¹H NMR (200 MHz, CDCl₃, FID LUM071/30): δ = 8.32 (s, 2H), 7.47 (d, J = 5.6 Hz, 2H), 7.37 (d, J = 5.6 Hz, 2H) ppm.



The synthesis of **14b** was performed according to Kashiki.^[103]

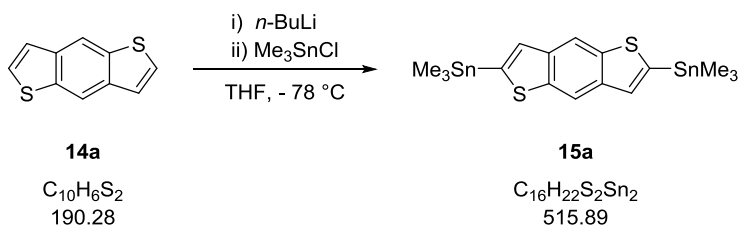
NMP was dried by azeotropic distillation with toluene. Selenium (2.84 g, 36.0 mmol, 1.0 eq) was suspended in anhydrous degassed EtOH under argon atmosphere at 0 °C. In a countercurrent flow of argon NaBH₄ (1.51 g, 40 mmol, 4.0 eq) was added in portions. After stirring for 1 hour **13** (4.28 g, 10 mmol, 1.0 eq) and NMP (250 ml) were added and EtOH was removed by distillation. After the mixture was stirred for 24 h at 190 °C, NMP was partly removed by distillation under reduced pressure and the cooled mixture was poured onto saturated aqueous NH₄Cl solution (750 ml). Subsequently The formed precipitate was filtered off and dissolved in CHCl₃. Subsequently the solution was washed with brine, dried over Na₂SO₄ and concentrated *in vacuo*. The crude product was dissolved in DCM and stirred with DDQ (1.59 g, 7.0 mmol, 0.7 eq) at room temperature overnight. **14b** was isolated by column chromatography (100 g SiO₂, PE) as a yellow solid (1.28 g, 4.5 mmol, 45%).

D. Experimental Part

^1H NMR (200 MHz, CDCl_3 , FID LUM066/30): δ = 8.36 (s, 2H), 7.98 (d, J = 5.9 Hz, 2H), 7.59 (m, 2H) ppm.

^{13}C NMR (100 MHz, CD_2Cl_2 , FID ALA038#F/51): δ = 139.8, 137.8, 128.9, 126.8, 122.0 ppm.

1,1'-Benzo[1,2-*b*:4,5-*b'*]dithiophene-2,6-diylbis(1,1,1-trimethylstannane) (**15a**)



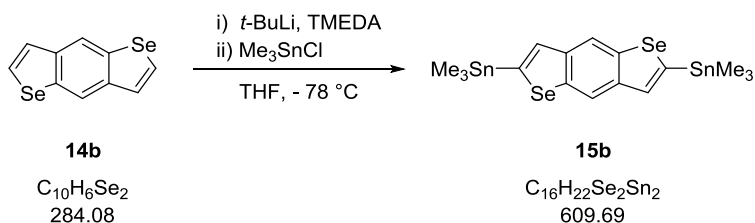
The synthesis of **15a** followed a protocol by Søndergaard.^[105]

Benzodithiophen **14a** (388 mg, 2.0 mmol, 1.0 eq) was dissolved in anhydrous THF (19 ml) under argon atmosphere and cooled below $-78\text{ }^\circ\text{C}$. *n*-BuLi (3.3 ml, 8.2 mmol, 4.0 eq) was added dropwise to the solution which was subsequently warmed to room temperature and stirred for one hour before it was cooled again below $-78\text{ }^\circ\text{C}$. Me_3SnCl (2476 mg, 12.4 mmol, 6.1 eq, dissolved in 4 ml anhydrous THF) was added dropwise to the cooled solution. Then the reaction mixture was warmed to room temperature before it was stirred overnight and consecutively quenched with deionized water (60 ml). The crude product was isolated by extraction with Et_2O . The combined organic layers were dried over Na_2SO_4 and concentrated under reduced pressure. Purification was performed by flash chromatography (basic aluminium oxide²³, toluene: Et_3N (2%)) yielding **15a** as a white solid (983 mg, 1.9 mmol, 93%).

^1H NMR (200 MHz, CDCl_3 , FID LUM076/10): δ = 8.28 (s, 2H), 7.42 (s, 2H), 0.44 (s, 18H) ppm.

²³ Merck, aluminium oxide 150, basic, 63-200 μm , type T

1,1'-Benzo[1,2-*b*:4,5-*b'*]diselenophene-2,6-diylbis(1,1,1-trimethylstannane)
(15b)



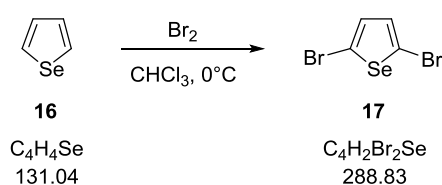
The synthesis of **15b** was adapted from a protocol by Leenen.^[109]

To a solution of benzodiselenophene **14b** (625 mg, 2.2 mmol, 1.0 eq) and TMEDA (77 mg, 0.7 mmol, 0.3 eq) in anhydrous THF (45 ml) under argon atmosphere *t*-BuLi (6.5 ml, 11.0 mmol, 5.0 eq) was added dropwise below -90 °C. The stirred solution was subsequently slowly warmed to -40 °C (1.5 h) before it was cooled again below -65 °C and Me₃SnCl (2192 mg, 11.0 mmol, 5.0 eq, dissolved in 3.5 ml anhydrous THF) was added dropwise. It was then warmed to room temperature and stirring was continued overnight. The reaction mixture was poured onto saturated aqueous NaHCO₃ solution (100 ml) and extracted with DCM. The combined organic layers were dried over Na₂SO₄ and the solvent was removed by evaporation. The crude product (1339 mg, 2.2 mmol, 100%) was recrystallized from ACN (40 ml) to yield **15b** as light yellow crystals (975 mg, 1.6 mmol, 73%).

¹H NMR (200 MHz, CDCl₃, FID LUM069/50): δ = 8.34 (s, 2H), 7.71 (s, 2H), 0.44 (s, 18H) ppm.

¹³C NMR (50 MHz, CDCl₃, FID LUM069/51): δ = 145.5, 141.5, 141.4, 141.0, 135.1, 120.6, -8.1 ppm.

2,5-Dibromoselenophene (17)



The synthesis of **17** was adapted from Purushothaman.^[110]

Selenophene **16** (2.00 g, 15.3 mmol, 1.0 eq) was dissolved in CHCl₃ (50 ml), cooled to 0 °C and bromine (4.88 g, 30.5 mmol, 2.0 eq) was added dropwise. Subsequently

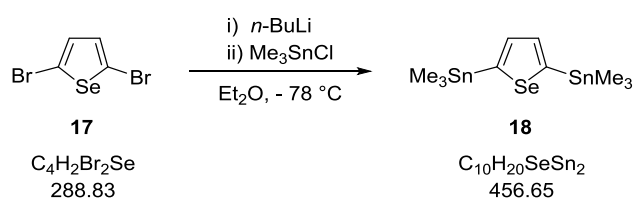
D. Experimental Part

the reaction mixture was warmed to room temperature and stirred until GC-MS showed full conversion (50 min). The reaction mixture was washed with deionized water, saturated aqueous NaHCO₃ solution and saturated aqueous thiosulfate solution in the given order before it was dried over Na₂SO₄ and concentrated *in vacuo*. Purification was performed by column chromatography (90 g SiO₂, PE) yielding **17** as a colorless liquid (2.70 g, 9.4 mmol, 61%).

¹H NMR (200 MHz, CDCl₃, FID LUM053/30): δ = 7.0 (s, 2H) ppm.

¹³C NMR (50 MHz, CDCl₃, FID LUM053/33): δ = 132.9 (d), 115.6 (s) ppm.

1,1'-(2,5-Selenophenediyl)bis(1,1,1-trimethylstannane) (**18**)

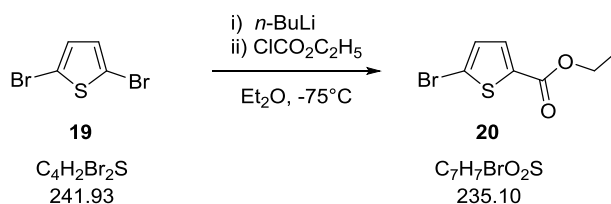


The synthesis of **18** followed a protocol described in literature.^[111]

17 (588 mg, 2.0 mmol, 1.0 eq) was dissolved in anhydrous Et₂O under argon atmosphere and cooled below -70 °C before *n*-BuLi (1.7 ml, 4.2 mmol, 2.1 eq) was added dropwise and the reaction mixture was stirred for 90 min. Subsequently Me₃SnCl (917 mg, 4.6 mmol, 2.3 eq, dissolved in 1.4 ml anhydrous Et₂O) was added dropwise and the reaction mixture was slowly warmed to room temperature and stirred overnight. The crude product was poured onto sat. aqueous NaHCO₃ solution (20 ml) and extracted with Et₂O. The combined organic layers were dried over Na₂SO₄ and concentrated *in vacuo* yielding an orange solid which was washed with MeOH and dried under reduced pressure. **18** was isolated as a beige solid (405 mg, 0.9 mmol, 44%).

¹H NMR (200 MHz, CDCl₃, FID LUM054/10): δ = 7.68 (s, 2H), 0.37 (s, 18 H) ppm.

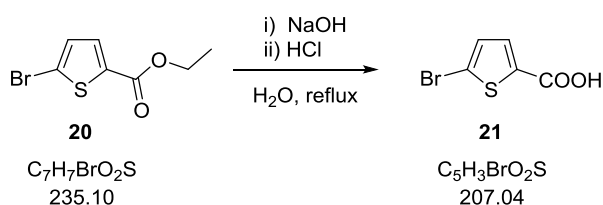
D.5.5 Synthesis of acceptors

5-Bromo-2-thiophenecarboxylic acid ethyl ester (**20**)

The synthesis of **20** followed a protocol described by Kautny.^[95]

To a solution of 2,5-dibromothiophene **19** (15.00 g, 62.0 mmol, 1 eq) in anhydrous Et_2O (100 ml), cooled to $-80^\circ C$ in an acetone cooling bath under argon atmosphere, *n*-BuLi (25.3 ml, 63.2 mmol, 1.02 eq) was added slowly, keeping the temperature below $-75^\circ C$. After the reaction mixture was stirred for further 45 min, it was slowly added to a precooled solution ($-80^\circ C$) of ethyl chloroformate (10.09 g, 93 mmol, 1.5 eq) in anhydrous Et_2O (100 ml) *via* a syringe keeping the temperature below $-75^\circ C$. The remaining white solid was dissolved in anhydrous Et_2O (50 ml) and transferred to the second reaction vessel as well. The reaction mixture was slowly warmed to room temperature before aqueous HCl (1N, 100 ml) was added and stirring was continued for 30 min. Then the aqueous phase was extracted with Et_2O and the combined organic layers were washed with saturated aqueous $NaHCO_3$ solution, dried over Na_2SO_4 and concentrated under reduced pressure. Purification was done by Kugelrohr-distillation ($120^\circ C$, 8 mbar) yielding **20** as a yellowish oil (12.42 g, 52.8 mmol, 85%).

1H NMR (200 MHz, $CDCl_3$, FID LUM012/10): δ = 7.54 (d, J = 4.0 Hz, 1H), 7.06 (d, J = 4.0 Hz, 1H), 4.33 (q, J = 7.2 Hz, 2H), 1.36 (t, J = 7.2 Hz, 3H) ppm.

5-Bromo-2-thiophenecarboxylic acid (**21**)

The synthesis of **21** followed a procedure described by Kautny.^[95]

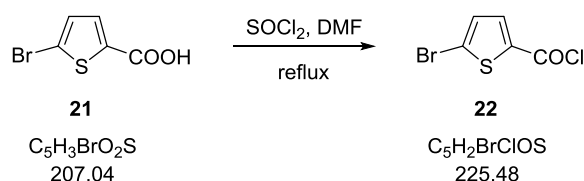
D. Experimental Part

Ester **20** (12.34 g, 52.5 mmol, 1 eq) was suspended in aqueous NaOH (2N, 300 ml) and refluxed for 6.5 h. After cooling the clear solution was washed with CHCl_3 and the organic layer was extracted with water. Subsequently the combined aqueous layers were filtered, acidified with HCl (conc.) giving a white precipitate and filtered again. The solid residue was dissolved in CHCl_3 , the resulting solution dried over anhydrous Na_2SO_4 and concentrated under reduced pressure yielding **21** (8.50 g, 41.0 mmol, 78%) as an off-white solid.

^1H NMR (200 MHz, CDCl_3 , FID LUM014/10): δ = 9.01 (bs, 1H), 7.64 (d, J = 4.0 Hz, 1H), 7.12 (d, J = 4.0 Hz, 1H) ppm.

^{13}C NMR (50 MHz, DMSO-d_6 , FID KAP112/13): δ = 161.8 (s), 136.1 (s), 133.9 (d), 131.9 (d), 118.9 (s) ppm.

5-Bromo-2-thiophenecarbonyl chloride (**22**)

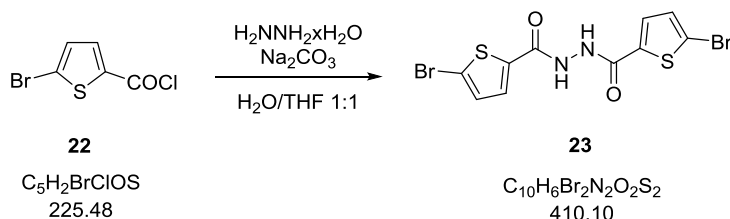


The synthesis of **22** was performed according to Kautny.^[95]

The acid **21** (8.50 g, 41.1 mmol, 1.0 eq) was dissolved in thionyl chloride (100 ml) and 3 drops of DMF were added. The reaction mixture was refluxed under exclusion of water overnight before SOCl_2 was removed under reduced pressure. **22** was obtained as a yellowish solid (8.71 g, 38.6 mmol, 94%) after Kugelrohr-distillation (130 °C, 23 mbar).

^1H NMR (200 MHz, CDCl_3 , FID LUM017/10): δ = 7.74 (d, J = 4.2 Hz, 1H), 7.18 (d, J = 4.2 Hz, 1H) ppm.

5-Bromo-2-thiophenecarboxylic acid, 2-(5-bromo-2-thienylcarbonyl)hydrazide (23)

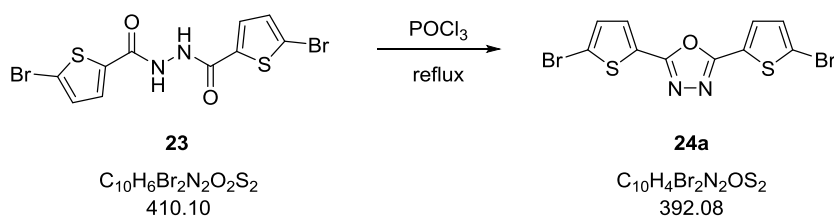


Hydrazide **23** was synthesized following a procedure described by Hua.^[112]

Hydrazine monohydrate (0.88 g, 17.5 mmol, 1.0 eq) and Na_2CO_3 (3.70 g, 35.0 mmol, 2 eq) were dissolved in a mixture of water and THF (1:1, 175 ml, 1 M), stirred mechanically and cooled to 0 °C. The acid chloride **22** (8.70 g, 38.5 mmol, 2.2 eq), dissolved in anhydrous THF, was added dropwise to the cooled mixture. During the addition of the acid chloride a white precipitate formed. The suspension was slowly warmed to room temperature and stirred overnight before it was diluted with water (150 ml), filtered and washed with cold water. **23** was obtained as a white solid (6.77 g, 16.5 mmol, 94%) and no further purification was necessary.

1H NMR (200 MHz, $DMSO-d_6$, FID LUM019/20): δ = 10.7 (s, 2H), 7.70 (d, J = 4.0 Hz, 2H), 7.36 (d, J = 4.0 Hz, 2H) ppm.

2,5-Bis(5-bromo-2-thienyl)-1,3,4-oxadiazole (24a)



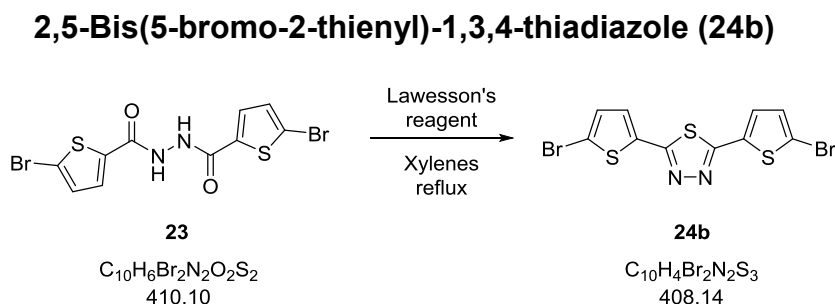
The reaction towards **24a** was performed according to Hayes.^[113]

Hydrazide **23** (3.25 g, 7.9 mmol, 1.0 eq) was dissolved in $POCl_3$ and refluxed overnight under exclusion of water. $POCl_3$ was removed under reduced pressure before the solid residue was dissolved in DCM and washed with saturated aqueous $NaHCO_3$ solution. The aqueous phase was extracted with DCM and the combined organic layers were dried over Na_2SO_4 and concentrated *in vacuo*. **24a** was isolated as a sandy solid (2.36 g, 6.0 mmol, 76%) after recrystallization from ACN.

D. Experimental Part

^1H NMR (200 MHz, CDCl_3 , FID LUM023/40): δ = 7.54 (d, J = 4.0 Hz, 2H), 7.15 (d, J = 4.0 Hz, 2H) ppm.

^{13}C NMR (50 MHz, CDCl_3 , FID KAP124/23): δ = 159.2 (s), 131.2 (d), 130.1 (d), 126.0 (s), 118.4 (s) ppm.



The synthesis towards **24b** followed a procedure described by Kiryanov.^[114]

Hydrazide **22** (3.25 g, 7.9 mmol, 1.0 eq) together with Lawesson's reagent (3.53 g, 8.7 mmol, 1.1 eq) was suspended in xylene (125 ml) and refluxed for 24 h. Xylene was removed under reduced pressure. The solid residue was digested several times in small amounts of MeOH. Following this procedure **24b** was obtained as a golden solid (2.89 g, 7.1 mmol, 89%).

^1H NMR (200 MHz, CDCl_3 , FID LUM024/50): δ = 7.28 (d, J = 4.0 Hz, 2H), 7.10 (d, J = 4.0 Hz, 2H) ppm.

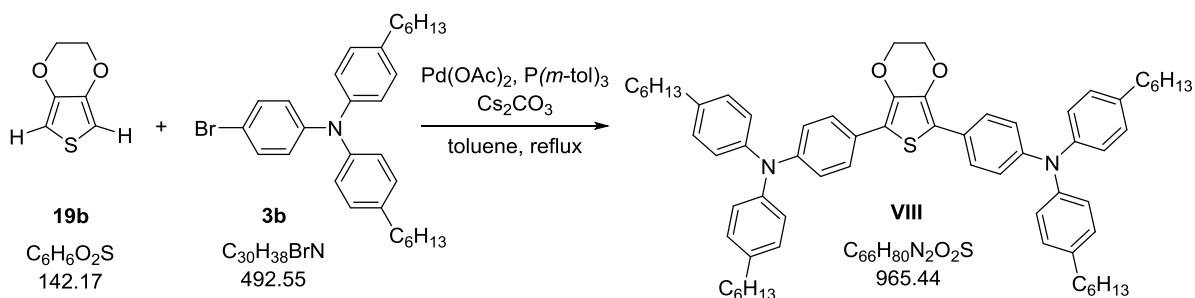
^{13}C NMR (50 MHz, CDCl_3 , FID KAP032/43): δ = 133.4 (s), 130.9 (d), 129.7 (d), 117.7 (s) ppm.²⁴

²⁴ Due to the low solubility of **24b** remaining carbon was not detected.

D.5.6 Synthesis of 2PA-PIs

D.5.6.1 Synthesis of linker-based 2PA-PIs

**4,4'-(2,3-Dihydrothieno[3,4-*b*]-1,4-dioxine-5,7-diyl)bis
[*N,N*-bis(4-hexylphenyl)benzeneamine] (VIII, HxTPA-1E)**



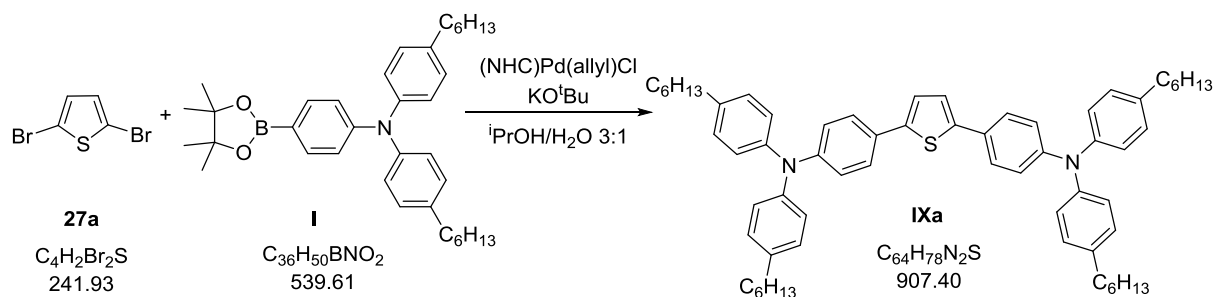
HxTPA-1E was synthesized analogously to literature.^[84]

To a solution of bromide **3b** (1034 mg, 2.1 mmol, 2.1 eq) and Cs_2CO_3 (782 mg, 2.4 mmol, 2.4 eq) in anhydrous degassed toluene (5 ml) were added Pd(OAc)_2 (11 mg, 50 μmol , 5 mol%), $\text{P}(m\text{-tol})_3$ (30 mg, 0.1 mmol, 0.10 eq) and EDOT **25b** (142 mg, 1.0 mmol, 1.0 eq) under argon atmosphere. The reaction mixture was refluxed for 40 h before it was diluted with DCM and washed with water. The organic phase was dried over Na_2CO_3 and concentrated *in vacuo*. Purification of **VIII** was performed by column chromatography (90 g SiO_2 , PE:DCM = 15%), recrystallization from *n*-BuOH and column chromatography (90 g SiO_2 , PE:toluene = 20%) yielding **VIII** as green sticky mass (361 mg, 3.7 mmol, 37%).²⁵

^1H NMR (400 MHz, CD_2Cl_2 , FID MOE006#F/10): δ = 7.56 (bm, 4H), 7.10-7.08 (bm, 8H), 7.01-6.97 (bm, 12H), 4.31 (bm, 4H), 2.57 (t, J = 7.5 Hz, 8H), 1.65-1.58 (m, 8H), 1.41-1.28 (m, 24H), 0.91 (t, J = 6.4 Hz, 12H) ppm.

²⁵ **VII** seems to be unstable in solution (DCM).

4,4'-(2,5-Thiophenediyl)bis[*N,N*-bis(4-hexylphenyl)benzeneamine]
(IXa, HxTPA-1T)



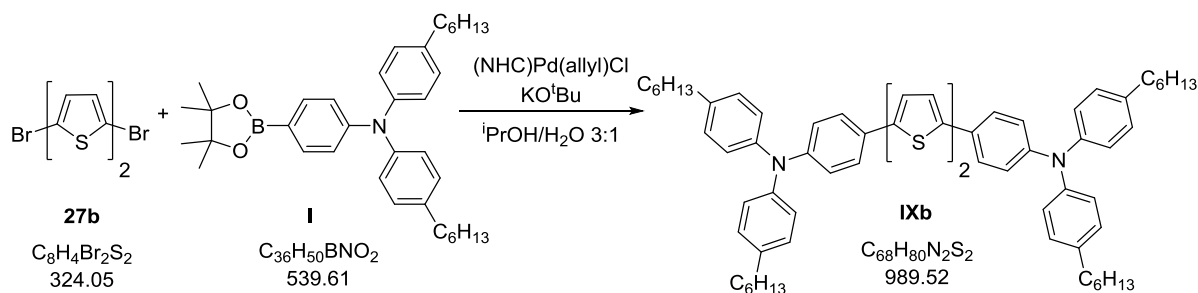
The synthesis of **IXa** followed the general protocol GP3.

To a suspension of boronic ester **I** (1715 mg, 3.2 mmol 3.2 eq), bromide **27a** (242 mg, 1.0 mmol, 1.0 eq) and KO^tBu (337 mg, 3.0 mmol, 3.0 eq) in an mixture of ⁱPrOH/H₂O (3:1, 16 ml) under argon atmosphere (NHC)Pd(allyl)Cl (11 mg, 20 μmol, 2 mol%) was added. The reaction mixture was refluxed until TLC showed full conversion of **27a** (2 h). After standard workup procedure purification of **IXa** was performed by column chromatography (90 g SiO₂, PE:DCM = 10%), recrystallization from *n*-BuOH and column chromatography (90 g SiO₂, PE:toluene = 20%). Following this protocol **IXa** could be obtained as a green sticky mass (518 mg, 0.57 mmol, 57%).

¹H NMR (400 MHz, CD₂Cl₂, FID LUM044#F/100): δ = 7.45 (m, 4H), 7.17 (s, 2H), 7.10 (m, 8H), 7.02-6.98 (m, 12H), 2.57 (t, J = 7.9 Hz, 8H), 1.65-1.57 (m, 8H), 1.40-1.32 (m, 24H), 0.90 (t, J = 6.7 Hz, 12H) ppm.

¹³C NMR (100 MHz, CD₂Cl₂, FID LUM044#F/103): δ = 148.2 (s), 145.7 (s), 143.1 (s), 138.7 (s), 129.8 (d), 128.0 (s), 126.6 (d), 125.2 (d), 123.4 (d), 122.9 (d), 35.9 (t), 32.3 (t), 32.1 (t), 29.6 (t), 23.2 (t), 14.4 (q) ppm.

4,4'-(2,2'-Bithiophene-5,5'-diyl)bis[*N,N*-bis(4-hexylphenyl)benzeneamine]
(IXb, HxTPA-2T)



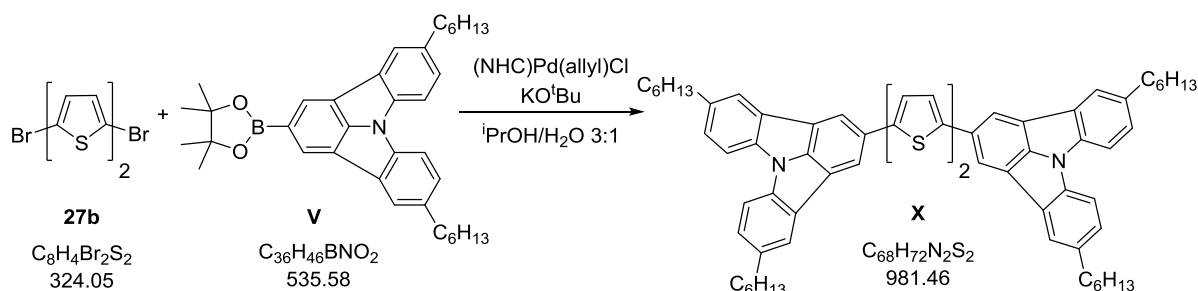
The synthesis of **IXb** followed the general protocol GP3.

To a suspension of boronic ester **I** (1680 mg, 3.1 mmol 3.1 eq), bromine **27b** (324 mg, 1.0 mmol, 1.0 eq) and KO^tBu (337 mg, 3.0 mmol, 3.0 eq) in an mixture of ⁱPrOH/H₂O (3:1, 20 ml) in argon atmosphere (NHC)Pd(allyl)Cl (11 mg, 20 μmol, 2 mol%) was added. The reaction mixture was refluxed until TLC showed full conversion of **27b** (1.5 h). After standard workup procedure purification of **IXb** was performed by column chromatography (90 g SiO₂, PE:DCM) followed by recrystallization from *n*-BuOH yielding **IXb** as a red sticky mass (809 mg, 0.8 mmol, 82%).

¹H NMR (400 MHz, CD₂Cl₂, FID LUM049#F/20): δ = 7.43 (m, 4H), 7.11-7.09 (m, 12H), 7.02-6.67 (m, 12H), 2.58 (t, J = 7.7 Hz, 8H), 1.63-1.58 (m, 8H), 1.41-1.34 (m, 24H), 0.92-0.89 (m, 12H) ppm.

¹³C NMR (100 MHz, CD₂Cl₂, FID LUM049#F/23): δ = 148.5 (s), 145.6 (s), 143.6 (s), 138.9 (s), 136.2 (s), 129.8 (d), 127.5 (s), 126.7 (d), 125.4 (d), 124.8 (d), 123.2 (d), 122.7 (d), 35.9 (t), 32.2 (t), 32.1 (t), 29.7 (t), 23.2 (t), 14.5 (q) ppm.

2,2'-(2,2'-Bithiophene-5,5'-diyl)bis(5,11-dihexylindolo[3,2,1-*jk*]carbazole)
(X, HxICz-2T)

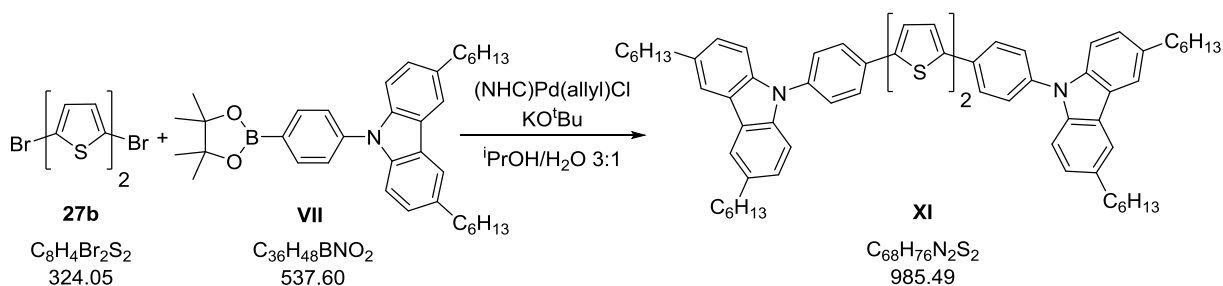


The synthesis of **X** followed the general protocol GP3.

Boronic ester **V** (1607 mg, 3.0 mmol, 3 eq), bithiophene **27b** (324 mg, 1.0 mmol, 1 eq), KO^tBu (337 mg, 3.0 mmol, 3 eq) and $(NHC)Pd(allyl)Cl$ (11 mg, 20 μ mol, 2 mol%) were refluxed in a mixture of $iPrOH/H_2O$ (3:1, 20 ml) for 4 h. **X** was isolated as an orange solid (642 mg, 0.7 mmol, 65%) after column chromatography (90 g SiO_2 , PE:DCM = 10% - 100%) and subsequent digesting in acetone.²⁶

1H NMR (400 MHz, CD_2Cl_2 , FID LUM083#F/40): δ = 8.34 (s, 4H), 8.02 (s, 4H), 7.82 (d, J = 8.2 Hz, 4H), 7.44-7.42 (m, 6H), 7.33 (d, J = 3.7 Hz, 2H), 2.84 (t, J = 7.6 Hz, 8H), 1.80-1.73 (m, 8H), 1.44-1.35 (m, 24H), 0.91 (t, J = 7.1 Hz, 12H) ppm.

9,9'-(2,2'-Bithiophene-5,5'-diyl)di-4,1-phenylene)bis-3,6-dihexyl-9H-carbazole
(XI, HxPCz-2T)



The synthesis of **XI** followed the general protocol GP3.

Boronic ester **VII** (1619 mg, 3.0 mmol, 3 eq), bithiophene **27b** (324 mg, 1.0 mmol, 1 eq), KO^tBu (337 mg, 3.0 mmol, 3 eq) and $(NHC)Pd(allyl)Cl$ (11 mg, 20 μ mol, 2 mol%) were refluxed in a mixture of $iPrOH/H_2O$ (3:1, 20 ml) for 2 h. Purification was

²⁶ Due to the low solubility of **X** ^{13}C NMR could not be measured with sufficient intensity.

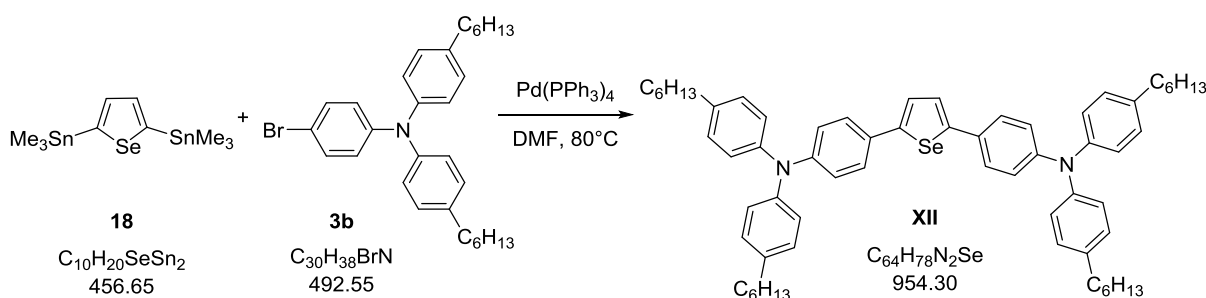
D. Experimental Part

performed by column chromatography (90 g SiO₂, PE:DCM = 10%) followed by recrystallization from *n*-heptane yielding **XI** as a yellow solid (827 mg, 0.8 mmol, 84%).

¹H NMR (400 MHz, CD₂Cl₂, FID LUM051#F/40): δ = 7.93 (s, 4H), 7.85 (m, 4H), 7.61 (m, 4H), 7.40-7.38 (m, 6H), 7.29-7.24 (m, 6H), 2.80 (t, J = 7.8 Hz, 8H), 1.76-1.69 (m, 8H), 1.41-1.34 (m, 24H), 0.91 (t, J = 6.9 Hz, 12H) ppm.

¹³C NMR (100 MHz, CD₂Cl₂, FID LUM051#F/43): δ = 142.9 (s), 139.8 (s), 138.1 (s), 137.4 (s), 135.4 (s), 133.1 (s), 127.6 (d), 127.4 (d), 127.2 (d), 125.4 (d), 124.9 (d), 124.1 (s), 120.1 (d), 110.0 (d), 36.5 (t), 32.9 (t), 32.4 (t), 29.7 (t), 23.3 (t), 14.5 (q) ppm.

4,4'-(2,5-Selenophenediyl)bis[N,N-bis(4-hexylphenyl)benzeneamine] (**XII**, HxTPA-1S)



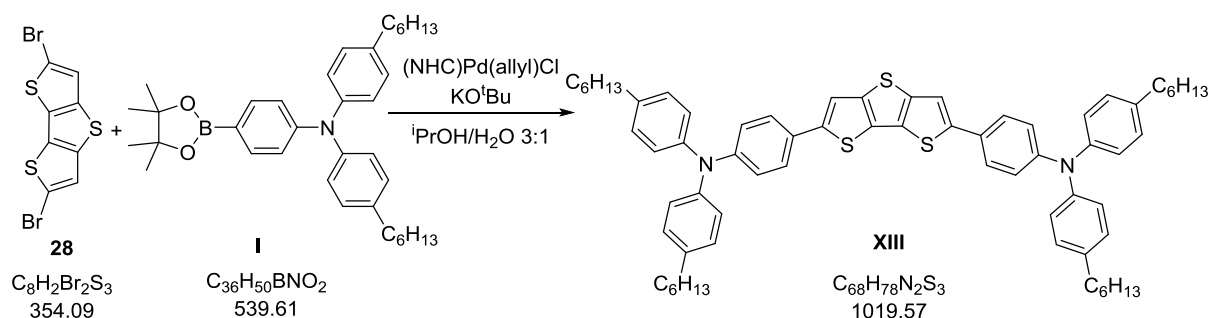
The synthesis of **XII** followed the general protocol GP4.

Bromide **3b** (940 mg, 1.91 mmol, 2.2 eq), organodistannane **18** (400 mg, 0.88 mmol, 1 eq) and Pd(PPh₃)₄ (51 mg, 44 μmol, 5 mol%) were heated to 80 °C in dry degassed DMF (20 ml) under argon atmosphere for 4 h. **XI** was obtained as a green glass (460 mg, 0.5 mmol, 55%) after column chromatography (90 g SiO₂, PE:DCM = 10%; 90 g SiO₂, PE:toluene = 9-14%).

¹H NMR (400 MHz, CD₂Cl₂, FID LUM056#F/90): δ = 7.39 (m, 4H), 7.32 (s, 2H), 7.10 (m, 8H), 7.01 (m, 8H), 6.97 (m, 4H), 2.57 (t, J = 7.8 Hz, 8H), 1.65-1.57 (m, 8H), 1.40-1.28 (m, 24H), 0.90 (t, J = 7.0 Hz, 12H) ppm.

¹³C NMR (100 MHz, CD₂Cl₂, FID LUM056#F/93): δ = 149.0 (s), 148.4 (s), 145.6 (s), 138.8 (s), 130.0 (s), 129.8 (d), 127.0 (d), 125.5 (d), 125.3 (d), 122.8 (d), 35.9 (t), 32.3 (t), 32.1 (t), 29.6 (t), 23.2 (t), 14.5 (q) ppm.

**4,4'-(Dithieno[3,2-b:2',3'-d]thiophene-2,6-diyl)bis
[N,N-bis(4-hexylphenyl)benzeneamine] (XIII, HxTPA-1DTT)**



The synthesis of **XIII** followed the general protocol GP3.

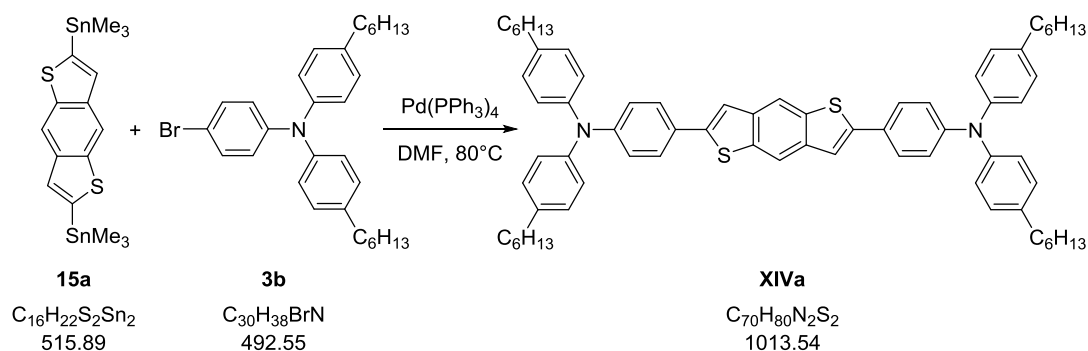
Boronic ester **I** (1619 mg, 3.0 mmol, 3 eq), dithienothiophene **28** (354 mg, 1.0 mmol, 1 eq), KO^tBu (337 mg, 3.0 mmol, 3 eq) and $(NHC)Pd(allyl)Cl$ (11 mg, 20 μmol , 2 mol%) were refluxed in a mixture of $iPrOH/H_2O$ (3:1, 20 ml) for 2 h. Purification was performed by column chromatography (90 g SiO_2 , PE:DCM = 10%, 830 mg, 83%; 90 g SiO_2 , PE:DCM = 10%, 703 mg, 69%²⁷; 90 g SiO_2 , PE:toluene = 9-14%) yielding **XIII** as a yellow glass (590 mg, 0.6 mmol, 58%).

1H NMR (400 MHz, CD_2Cl_2 , FID LUM057#F/70): δ = 7.47 (m, 4H), 7.40 (s, 2H), 7.11 (m, 8H), 7.04-6.98 (m, 12H), 2.58 (t, J = 7.7 Hz, 8H), 1.65-1.58 (m, 8H), 1.40-1.30 (m, 24H), 0.90 (t, J = 6.9 Hz, 12H) ppm.

^{13}C NMR (100 MHz, CD_2Cl_2 , FID LUM057#F/73): δ = 148.7 (s), 145.6 (s), 145.5 (s), 142.1 (s), 139.0 (s), 129.9 (s), 129.8 (d), 127.8 (s), 126.8 (d), 125.4 (d), 122.6 (d), 115.8 (d), 35.9 (t), 32.3 (t), 32.1 (t), 29.6 (t), 23.2 (t), 14.5 (q) ppm.

²⁷ An attempt was made to pre-dry the silica by conditioning with a mixture of PE (575 ml), 2,2-dimethoxypropane (13 ml) and glacial acetic acid (13ml) followed by a washing step with PE (500 ml).^[125] However, the product was eluted without retention.

**4,4'-(1,1'-Benzo[1,2-*b*:4,5-*b'*]dithiophene-2,6-diyl)bis
[*N,N*-bis(4-hexylphenyl) benzeneamine] (XIVa, HxTPA-1BBT)**



The synthesis of **XIVa** followed the general protocol GP4.

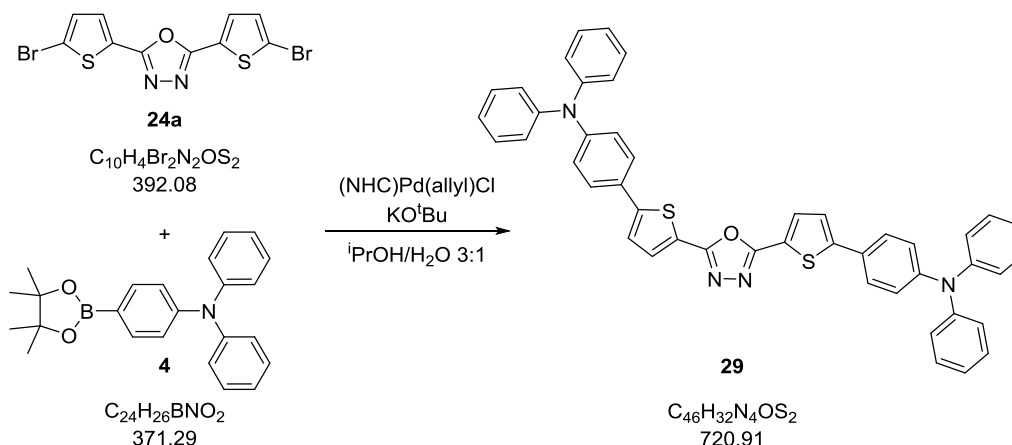
Bromide **3b** (1034 mg, 2.1 mmol, 2.1 eq), organodistannane **15b** (516 mg, 1.0 mmol, 1 eq) and $Pd(PPh_3)_4$ (58 mg, 50 μ mol, 5 mol%) were heated to 80 °C in dry degassed DMF (25 ml) under argon atmosphere for 44 h.²⁸ Purification was performed by column chromatography (110 g SiO_2 , PE:toluene = 9-22%, 585 mg, 58%; 90 g SiO_2 , PE:DCM ~ 10%, 489 mg, 48%) followed by selective dissolving of the product in PE yielding **XIVa** an orange glass (405 mg, 0.4 mmol, 40%).

1H NMR (400 MHz, CD_2Cl_2 , FID LUM079#F/20): δ = 8.09 (s, 2H), 7.54 (m, 4H), 7.43 (s, 2H), 7.11 (m, 8H), 7.04-7.00 (m, 12H), 2.58 (t, J = 7.7 Hz, 8H), 1.64-1.58 (m, 8H), 1.43-1.34 (m, 24H), 0.91 (t, J = 6.7 Hz, 12H) ppm.

^{13}C NMR (100 MHz, CD_2Cl_2 , FID LUM079#F/23): δ = 149.2 (s), 145.5 (s), 144.8 (s), 139.2 (s), 139.1 (s), 137.3 (s), 129.9 (d), 127.5 (d), 127.4 (s), 125.6 (d), 122.3 (d), 117.5 (d), 116.5 (d), 35.9 (t), 32.3 (t), 32.1 (t), 29.7 (t), 23.2 (t), 14.5 (q) ppm.

²⁸ TLC showed full conversion of **15a** after 20 h but due to a blue spot next to the product spot the reaction mixture was heated for further 16 h to 90 °C before more catalyst (29 mg, 25 μ mol, 3 mol%) was added to verify full conversion to **XIVa**.

D.5.6.2 Synthesis of acceptor-based 2PA-PIs

4,4'-(1,3,4-Oxadiazole-2,5-diyl)bis[*N,N*-diphenylbenzeneamine]
(**29**, TPA-TOxD)

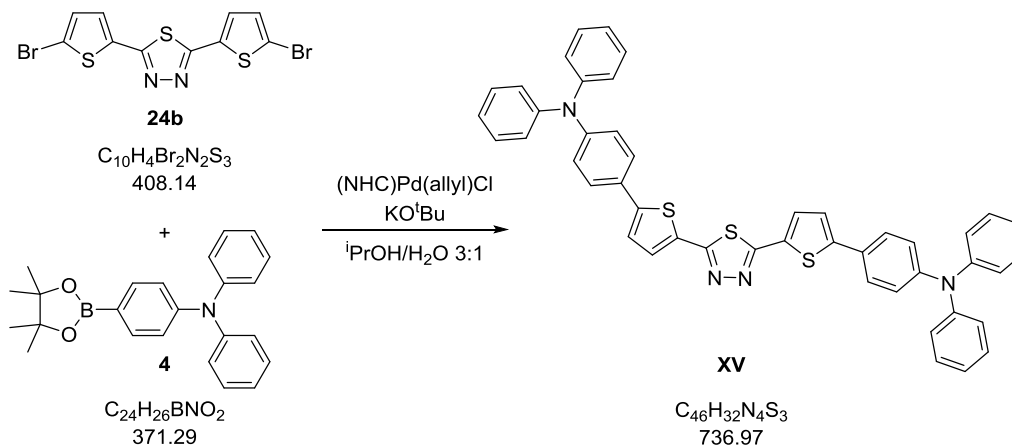
The synthesis of **29** followed the general protocol GP3.

Boronic ester **4** (1114 mg, 3.0 mmol, 3 eq), oxadiazole **24a** (393 mg, 1.0 mmol, 1 eq), KO^tBu (337 mg, 3.0 mmol, 3 eq) and (NHC)Pd(allyl)Cl (11 mg, 20 μmol, 2 mol%) were refluxed in a mixture of ⁱPrOH/H₂O (3:1, 16 ml) for 4 h³⁰. Purification was performed by column chromatography (90 g SiO₂, PE:DCM = 75-100%, DCM:MeOH ~ 4%, 770 mg, 107%) followed by recrystallization from toluene yielding **XV** as yellow crystals (toluene solvate, 712 mg x toluene = 631 mg pure, 0.9 mmol, 88%).

¹H NMR (200 MHz, CD₂Cl₂, FID LUM041#F/100): δ = 7.75 (d, J = 3.8 Hz, 2H), 7.55 (m, 4H), 7.32-7.29 (m, 10H), 7.14-7.06 (m, 16H) ppm.

³⁰ TLC monitored conversion was constant after 45 min.

4,4'-(1,3,4-Thiadiazole-2,5-diyl-di-2,5-thiophenediyl)bis[*N,N*-diphenylbenzeneamine]
(XV, TPA-TThD)



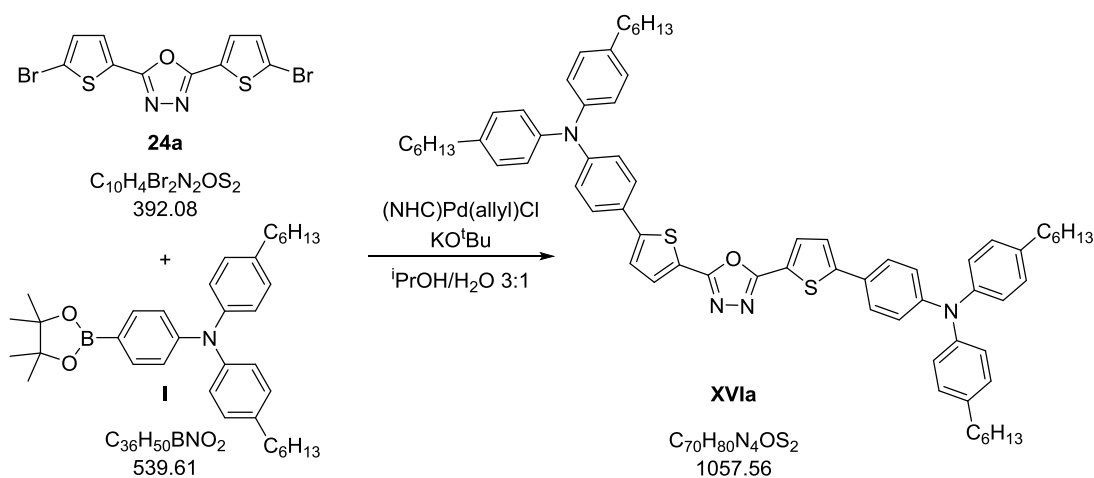
The synthesis of **XV** followed the general protocol GP3.

Boronic ester **4** (1114 mg, 3.0 mmol, 3 eq), thiadiazole **24b** (408 mg, 1.0 mmol, 1 eq), KO^tBu (337 mg, 3.0 mmol, 3 eq) and (NHC)Pd(allyl)Cl (11 mg, 20 μmol, 2 mol%) were refluxed in a mixture of ⁱPrOH/H₂O (3:1, 14 ml) for 2.5 h. Purification was performed by column chromatography (90 g SiO₂, PE:DCM ~ 80-90%, 470 mg, 64%) followed by recrystallization from toluene yielding **XV** as orange crystals (toluene solvate, 494 mg x toluene = 439 mg pure, 0.6 mmol, 60%).

¹H NMR (400 MHz, CD₂Cl₂, FID LUM039#F/60): δ = 7.54 (m, 4H), 7.50 (d, J = 3.9 Hz, 2H), 7.32-7.26 (m, 10H), 7.14-7.05 (m, 16H) ppm.

¹³C NMR (100 MHz, CD₂Cl₂, FID LUM039#F/63): δ = 161.4 (s), 149.0 (s), 148.8 (s), 147.8 (s), 131.3 (d), 130.6 (s), 130.0 (d), 127.2 (d), 127.3(s), 125.5 (d) 124.2 (d), 123.4 (d), 123.4 (d) ppm.

**4,4'-(1,3,4-Oxadiazole-2,5-diyl)di-2,5-thiophenediyl)bis
[N,N-bis(4-hexylphenyl)benzeneamine] (XVIa, HxTPA-TOxD)**



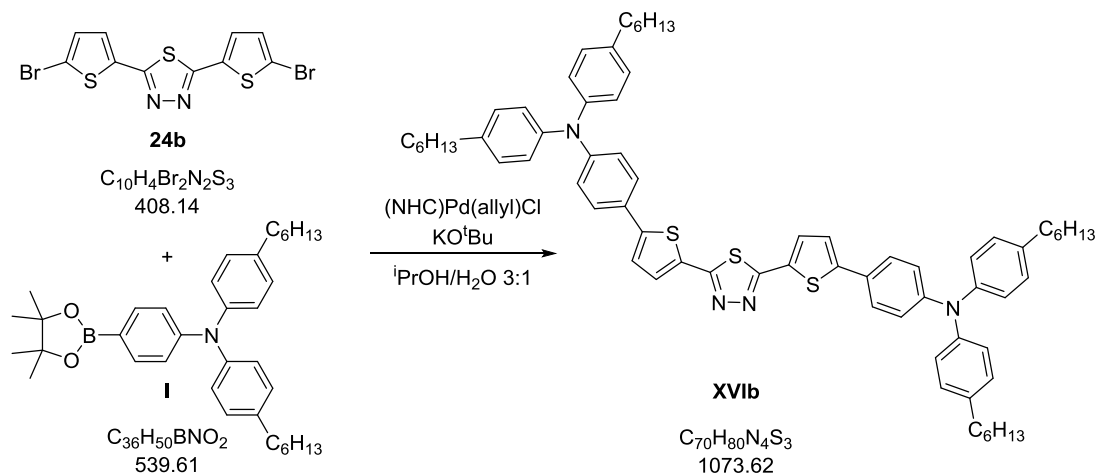
The synthesis of **XVIa** followed the general protocol GP3.

Boronic ester **I** (1619 mg, 3.0 mmol, 3 eq), oxadiazole **24a** (392 mg, 1.0 mmol, 1 eq), KO^tBu (337 mg, 3.0 mmol, 3 eq) and $(NHC)Pd(allyl)Cl$ (11 mg, 20 μ mol, 2 mol%) were refluxed in a mixture of $iPrOH/H_2O$ (3:1, 20 ml) for 4 h. Purification was performed by column chromatography (90 g SiO_2 , PE:DCM ~ 50%) yielding **XVIa** as a yellow solid (869 mg, 0.8 mmol, 82%).

1H NMR (400 MHz, CD_2Cl_2 , FID LUM064#F/10): δ = 7.71 (d, J = 3.9 Hz, 2H), 7.48 (m, 4H), 7.26 (d, J = 3.9 Hz, 2H), 7.12 (m, 8H), 7.04-6.98 (m, 12H), 2.59 (t, J = 7.8 Hz, 8H), 1.64-1.58 (m, 8H), 1.39-1.33 (m, 24H), 0.91 (t, J = 6.7 Hz, 12H) ppm.

^{13}C NMR (100 MHz, CD_2Cl_2 , FID LUM064#F/13): δ = 160.7 (s), 150.0 (s), 149.6 (s), 145.3 (s), 139.3 (s), 131.2 (d), 129.9 (d), 127.3 (d), 126.0 (s), 125.8 (d), 123.2 (d), 122.8 (s), 121.9 (d), 35.9 (t), 32.3 (t), 32.1 (t), 29.6 (t), 23.2 (t), 14.5 (q) ppm.

**4,4'-(1,3,4-Thiadiazole-2,5-diyl-di-2,5-thiophenediyl)bis
[N,N-bis(4-hexylphenyl)benzeneamine] (XVIb, HxTPA-TThD)**



The synthesis of **XVIb** followed the general protocol GP3.

Boronic ester **I** (1619 mg, 3.0 mmol, 3 eq), thiadiazole **24b** (408 mg, 1.0 mmol, 1 eq), KO^tBu (337 mg, 3.0 mmol, 3 eq) and (NHC)Pd(allyl)Cl (11 mg, 20 μmol, 2 mol%) were refluxed in a mixture of ⁱPrOH/H₂O (3:1, 20 ml) for 2 h. Purification was performed by column chromatography (90 g SiO₂, PE:DCM ~ 50%, 667 mg, 62%) followed by separation from unconsumed **24a** via selective dissolving of the product in *n*-heptane yielding **XIII** as an orange solid (513 mg, 0.5 mmol, 48%).

¹H NMR (400 MHz, CD₂Cl₂, FID LUM063#F/50): δ = 7.49-7.46 (m, 6H), 7.22 (d, J = 4.1 Hz, 2H), 7.12 (m, 8H), 7.04-6.98 (m, 12H), 2.58 (t, J = 7.8 Hz, 8H), 1.63-1.58 (m, 8H), 1.34-1.32 (m, 24H), 0.90 (t, J = 6.7 Hz, 12H) ppm.

¹³C NMR (100 MHz, CD₂Cl₂, FID LUM063#F/53): δ = 161.3 (s), 149.4 (s), 149.0 (s), 145.3 (s), 139.3 (s), 131.3 (d), 130.2 (s), 129.9 (d), 127.2 (d), 126.2 (s), 125.7 (d), 123.1 (d), 122.8 (s), 122.0 (d), 35.9 (t), 32.3 (t), 32.1 (t), 29.6 (t), 23.2 (t), 14.5 (q) ppm.

E. Bibliography

-
- [1] M. Göppert-Mayer, *Annalen der Physik* **1931**, *401*, 273-294.
- [2] W. Kaiser, C. Garrett, *Physical Review Letters* **1961**, *7*, 229.
- [3] M. Pawlicki, H. A. Collins, R. G. Denning, H. L. Anderson, *Angewandte Chemie International Edition* **2009**, *48*, 3244-3266.
- [4] S. R. Marder, *Chemical communications* **2006**, 131-134.
- [5] M. Rumi, J. W. Perry, *Advances in Optics and Photonics* **2010**, *2*, 451-518.
- [6] M. Albota, D. Beljonne, J.-L. Brédas, J. E. Ehrlich, J.-Y. Fu, A. A. Heikal, S. E. Hess, T. Kogej, M. D. Levin, S. R. Marder, *Science* **1998**, *281*, 1653-1656.
- [7] B. H. Cumpston, S. P. Ananthavel, S. Barlow, D. L. Dyer, J. E. Ehrlich, L. L. Erskine, A. A. Heikal, S. M. Kuebler, I.-Y. S. Lee, D. McCord-Maughon, *Nature* **1999**, *398*, 51-54.
- [8] C. D. Andrade, C. O. Yanez, L. Rodriguez, K. D. Belfield, *The Journal of Organic Chemistry* **2010**, *75*, 3975-3982.
- [9] W. R. Zipfel, R. M. Williams, W. W. Webb, *Nature biotechnology* **2003**, *21*, 1369-1377.
- [10] W. L. Peticolas, *Annual Review of Physical Chemistry* **1967**, *18*, 233-260.
- [11] M. Rumi, S. Barlow, J. Wang, J. W. Perry, S. R. Marder, in *Photoresponsive Polymers I*, Springer, **2008**, pp. 1-95.
- [12] J. Lakowicz, *Principles of Fluorescence Spectroscopy*, 2nd ed., Kluwer Academic/Plenum Publishers, New York, **1999**.
- [13] G. S. He, L.-S. Tan, Q. Zheng, P. N. Prasad, *Chemical Reviews* **2008**, *108*, 1245-1330.
- [14] H. M. Kim, B. R. Cho, *Chemical communications* **2009**, 153-164.
- [15] A. Ajami, W. Husinsky, R. Liska, N. Pucher, *JOSA B* **2010**, *27*, 2290-2297.
- [16] N. S. Makarov, M. Drobizhev, A. Rebane, *Optics express* **2008**, *16*, 4029-4047.
- [17] C. N. LaFratta, J. T. Fourkas, T. Baldacchini, R. A. Farrer, *Angewandte Chemie International Edition* **2007**, *46*, 6238-6258.
- [18] D. A. Parthenopoulos, P. M. Rentzepis, *Science* **1989**, *245*, 843-845.
- [19] S. Kawata, Y. Kawata, *Chemical Reviews* **2000**, *100*, 1777-1788.
- [20] F. Helmchen, W. Denk, *Nature methods* **2005**, *2*, 932-940.
- [21] C. Spangler, *Journal of Materials Chemistry* **1999**, *9*, 2013-2020.
- [22] T.-C. Lin, S.-J. Chung, K.-S. Kim, X. Wang, G. S. He, J. Swiatkiewicz, H. E. Pudavar, P. N. Prasad, in *Polymers for Photonics Applications II*, Springer, **2003**, pp. 157-193.
- [23] W. Fisher, W. Partridge, C. Dees, E. Wachter, *Photochemistry and photobiology* **1997**, *66*, 141-155.
- [24] G. C. Ellis-Davies, *Nature methods* **2007**, *4*, 619-628.
- [25] F. Terenziani, C. Katan, E. Badaeva, S. Tretiak, M. Blanchard-Desce, *Advanced Materials* **2008**, *20*, 4641-4678.
- [26] P. Norman, Y. Luo, H. Ågren, *Optics communications* **1999**, *168*, 297-303.
- [27] E. Collini, *Physical Chemistry Chemical Physics* **2012**, *14*, 3725-3736.
- [28] M. Tromayer, Master thesis, Vienna University of Technology (Vienna, Austria), **2014**.

- [29] J. Torgersen, Diploma thesis, Vienna University of Technology (Vienna, Austria), **2010**.
- [30] B. Jia, J. Li, M. Gu, *Australian journal of chemistry* **2007**, *60*, 484-495.
- [31] S. Maruo, O. Nakamura, S. Kawata, *Optics letters* **1997**, *22*, 132-134.
- [32] J. Serbin, M. Gu, *Advanced Materials* **2006**, *18*, 221-224.
- [33] B.-B. Xu, Y.-L. Zhang, H. Xia, W.-F. Dong, H. Ding, H.-B. Sun, *Lab on a chip* **2013**, *13*, 1677-1690.
- [34] S. Krivec, N. Matsko, V. Satzinger, N. Pucher, N. Galler, T. Koch, V. Schmidt, W. Grogger, R. Liska, H. C. Lichtenegger, *Advanced Functional Materials* **2010**, *20*, 811-819.
- [35] S. J. Jhaveri, J. D. McMullen, R. Sijbesma, L.-S. Tan, W. Zipfel, C. K. Ober, *Chemistry of materials* **2009**, *21*, 2003-2006.
- [36] G. Odian, *New York [etc.]*. [41] PerkinElmer, *Pyris Software online help- Scanning Kinetics theory*.
- [37] H. Gruber, *Progress in polymer Science* **1992**, *17*, 953-1044.
- [38] L. Nguyen, M. Straub, M. Gu, *Advanced Functional Materials* **2005**, *15*, 209-216.
- [39] W. Zhou, S. M. Kuebler, K. L. Braun, T. Yu, J. K. Cammack, C. K. Ober, J. W. Perry, S. R. Marder, *Science* **2002**, *296*, 1106-1109.
- [40] H.-B. Sun, S. Kawata, *Journal of lightwave technology* **2003**, *21*, 624.
- [41] W. Haske, V. W. Chen, J. M. Hales, W. Dong, S. Barlow, S. R. Marder, J. W. Perry, *Optics express* **2007**, *15*, 3426-3436.
- [42] W. Teh, U. Dürig, G. Salis, R. Harbers, U. Drechsler, R. Mahrt, C. Smith, H.-J. Güntherodt, *Applied physics letters* **2004**, *84*, 4095-4097.
- [43] J. Torgersen, PhD thesis, Vienna University of Technology (Vienna, Austria), **2013**.
- [44] A. Ovsianikov, J. Viertl, B. Chichkov, M. Oubaha, B. MacCraith, I. Sakellari, A. Giakoumaki, D. Gray, M. Vamvakaki, M. Farsari, *Acs Nano* **2008**, *2*, 2257-2262.
- [45] K. J. Schafer, J. M. Hales, M. Balu, K. D. Belfield, E. W. Van Stryland, D. J. Hagan, *Journal of photochemistry and photobiology A: Chemistry* **2004**, *162*, 497-502.
- [46] K. D. Belfield, X. Ren, E. W. Van Stryland, D. J. Hagan, V. Dubikovsky, E. J. Miesak, *Journal of the American Chemical Society* **2000**, *122*, 1217-1218.
- [47] K. D. Belfield, K. J. Schafer, Y. Liu, J. Liu, X. Ren, E. W. V. Stryland, *Journal of Physical Organic Chemistry* **2000**, *13*, 837-849.
- [48] K. S. Lee, D. Y. Yang, S. H. Park, R. H. Kim, *Polymers for advanced technologies* **2006**, *17*, 72-82.
- [49] Y. Lu, F. Hasegawa, Y. Kawazu, K. Totani, T. Yamashita, W. Toshiyuki, *Sen'i Gakkaishi* **2004**, *60*, 165-172.
- [50] S. Zheng, L. Beverina, S. Barlow, E. Zojer, J. Fu, L. A. Padilha, C. Fink, O. Kwon, Y. Yi, Z. Shuai, *Chemical communications* **2007**, 1372-1374.

- [51] C. D. Entwistle, J. C. Collings, A. Steffen, L.-O. Pålsson, A. Beeby, D. Albesa-Jové, J. M. Burke, A. S. Batsanov, J. A. Howard, J. A. Mosely, *Journal of Materials Chemistry* **2009**, *19*, 7532-7544.
- [52] H. Zhou, F. Zhou, S. Tang, P. Wu, Y. Chen, Y. Tu, J. Wu, Y. Tian, *Dyes and pigments* **2012**, *92*, 633-641.
- [53] M. R. Harpham, O. z. n. Süzer, C.-Q. Ma, P. Bäuerle, T. Goodson III, *Journal of the American Chemical Society* **2009**, *131*, 973-979.
- [54] S. Huang, L.-Y. Zou, A.-M. Ren, J.-F. Guo, X.-T. Liu, J.-K. Feng, *New Journal of Chemistry* **2012**, *36*, 947-953.
- [55] M. Williams-Harry, A. Bhaskar, G. Ramakrishna, T. Goodson, M. Imamura, A. Mawatari, K. Nakao, H. Enozawa, T. Nishinaga, M. Iyoda, *Journal of the American Chemical Society* **2008**, *130*, 3252-3253.
- [56] O.-K. Kim, K.-S. Lee, H. Y. Woo, K.-S. Kim, G. S. He, J. Swiatkiewicz, P. N. Prasad, *Chemistry of materials* **2000**, *12*, 284-286.
- [57] C.-K. Wang, P. Macak, Y. Luo, H. Ågren, *The Journal of chemical physics* **2001**, *114*, 9813-9820.
- [58] E. Van Keuren, T. Wakebe, R. Andreaus, H. Möhwald, W. Schrof, V. Belov, H. Matsuda, R. Rangel-Rojo, *Applied physics letters* **1999**, *75*, 3312-3314.
- [59] P. Lind, M. Carlsson, B. Eliasson, E. Glimsdal, M. Lindgren, C. Lopes, L. Boman, P. Norman, *Molecular Physics* **2009**, *107*, 629-641.
- [60] G. Xia, P. Lu, S. Liu, *Acta chimica slovenica* **2005**, *52*, 336.
- [61] B. Holzer, Diploma thesis, Vienna University of Technology (Vienna, Austria), **2010**.
- [62] J. Binting, Diploma thesis, Vienna University of Technology (Vienna, Austria), **2011**.
- [63] D. Lumpi, Master thesis, Vienna University of Technology (Vienna, Austria), **2009**.
- [64] P. Kautny, D. Lumpi, Y. Wang, A. Tissot, J. Binting, E. Horkel, B. Stöger, C. Hametner, H. Hagemann, D. Ma, *Journal of Materials Chemistry C* **2014**, *2*, 2069-2081.
- [65] S.-J. Chung, K.-S. Kim, T.-C. Lin, G. S. He, J. Swiatkiewicz, P. N. Prasad, *The Journal of Physical Chemistry B* **1999**, *103*, 10741-10745.
- [66] A. Bhaskar, G. Ramakrishna, Z. Lu, R. Twieg, J. M. Hales, D. J. Hagan, E. Van Stryland, T. Goodson, *Journal of the American Chemical Society* **2006**, *128*, 11840-11849.
- [67] P.-H. Huang, J.-Y. Shen, S.-C. Pu, Y.-S. Wen, J. T. Lin, P.-T. Chou, M.-C. P. Yeh, *Journal of Materials Chemistry* **2006**, *16*, 850-857.
- [68] P.-Y. Gu, J. Gao, Q. Zhang, G. Liu, F. Zhou, Q.-F. Xu, J.-M. Lu, *Journal of Materials Chemistry C* **2014**, *2*, 1539-1544.
- [69] N. Miyaura, A. Suzuki, *J. Chem. Soc., Chem. Commun.* **1979**, 866-867.
- [70] N. Miyaura, K. Yamada, A. Suzuki, *Tetrahedron Letters* **1979**, *20*, 3437-3440.
- [71] N. Miyaura, T. Yanagi, A. Suzuki, *Synthetic Communications* **1981**, *11*, 513-519.
- [72] N. Miyaura, A. Suzuki, *Chemical Reviews* **1995**, *95*, 2457-2483.

E. Bibliography

- [73] S. Kotha, K. Lahiri, D. Kashinath, *Tetrahedron* **2002**, *58*, 9633-9695.
- [74] G. B. Smith, G. C. Dezeny, D. L. Hughes, A. O. King, T. R. Verhoeven, *The Journal of Organic Chemistry* **1994**, *59*, 8151-8156.
- [75] S. R. Chemler, D. Trauner, S. J. Danishefsky, *Angewandte Chemie International Edition* **2001**, *40*, 4544-4568.
- [76] N. Miyaura, *Journal of organometallic chemistry* **2002**, *653*, 54-57.
- [77] A. A. Braga, N. H. Morgon, G. Ujaque, F. Maseras, *Journal of the American Chemical Society* **2005**, *127*, 9298-9307.
- [78] A. Suzuki, *Journal of organometallic chemistry* **2002**, *653*, 83-90.
- [79] D. Milstein, J. Stille, *Journal of the American Chemical Society* **1978**, *100*, 3636-3638.
- [80] D. Milstein, J. Stille, *Journal of the American Chemical Society* **1979**, *101*, 4992-4998.
- [81] J. K. Stille, *Angewandte Chemie International Edition in English* **1986**, *25*, 508-524.
- [82] A. M. Echavarren, J. Stille, *Journal of the American Chemical Society* **1987**, *109*, 5478-5486.
- [83] A. L. Casado, P. Espinet, *Journal of the American Chemical Society* **1998**, *120*, 8978-8985.
- [84] C.-Y. Liu, H. Zhao, H.-h. Yu, *Organic Letters* **2011**, *13*, 4068-4071.
- [85] R. Anémian, D. C. Cupertino, P. R. Mackie, S. G. Yeates, *Tetrahedron Letters* **2005**, *46*, 6717-6721.
- [86] L.-C. Campeau, P. Thansandote, K. Fagnou, *Organic Letters* **2005**, *7*, 1857-1860.
- [87] O. Navarro, S. P. Nolan, *Synthesis* **2006**, *2006*, 366-367.
- [88] G. C. Fortman, S. P. Nolan, *Chemical Society Reviews* **2011**, *40*, 5151-5169.
- [89] J. Lv, Q. Liu, J. Tang, F. Perdih, K. Kranjc, *Tetrahedron Letters* **2012**, *53*, 5248-5252.
- [90] J. Lindley, *Tetrahedron* **1984**, *40*, 1433-1456.
- [91] S. V. Ley, A. W. Thomas, *Angewandte Chemie International Edition* **2003**, *42*, 5400-5449.
- [92] H. B. Goodbrand, N.-X. Hu, *The Journal of Organic Chemistry* **1999**, *64*, 670-674.
- [93] N. Marion, O. Navarro, J. Mei, E. D. Stevens, N. M. Scott, S. P. Nolan, *Journal of the American Chemical Society* **2006**, *128*, 4101-4111.
- [94] M. K. Kim, J. Kwon, T.-H. Kwon, J.-I. Hong, *New Journal of Chemistry* **2010**, *34*, 1317-1322.
- [95] P. Kautny, Master thesis, Vienna University of Technology (Vienna, Austria), **2013**.
- [96] N. Aizawa, Y.-J. Pu, H. Sasabe, J. Kido, *Organic Electronics* **2012**, *13*, 2235-2242.
- [97] W. F. Bailey, J. J. Patricia, *Journal of organometallic chemistry* **1988**, *352*, 1-46.
- [98] D. Seyferth, *Organometallics* **2006**, *25*, 2-24.

- [99] A.-S. Castanet, F. Colobert, P.-E. Broutin, *Tetrahedron Letters* **2002**, *43*, 5047-5048.
- [100] Y. Wu, Y. Li, S. Gardner, B. S. Ong, *Journal of the American Chemical Society* **2005**, *127*, 614-618.
- [101] T. Yasuda, T. Shimizu, F. Liu, G. Ungar, T. Kato, *Journal of the American Chemical Society* **2011**, *133*, 13437-13444.
- [102] H. C. Brown, S. Krishnamurthy, *Tetrahedron* **1979**, *35*, 567-607.
- [103] T. Kashiki, S. Shinamura, M. Kohara, E. Miyazaki, K. Takimiya, M. Ikeda, H. Kuwabara, *Organic Letters* **2009**, *11*, 2473-2475.
- [104] H. Sashida, K. Sadamori, T. Tsuchiya, *Synthetic Communications* **1998**, *28*, 713-727.
- [105] R. Søndergaard, M. Manceau, M. Jørgensen, F. C. Krebs, *Advanced Energy Materials* **2012**, *2*, 415-418.
- [106] D. L. Klayman, T. S. Griffin, *Journal of the American Chemical Society* **1973**, *95*, 197-199.
- [107] J. Gladysz, J. L. Hornby, J. E. Garbe, *The Journal of Organic Chemistry* **1978**, *43*, 1204-1208.
- [108] Y.-J. Hwang, N. M. Murari, S. A. Jenekhe, *Polymer Chemistry* **2013**, *4*, 3187-3195.
- [109] M. A. Leenen, F. Vian, F. Cucinotta, W. Pisula, H. Thiem, R. Anselmann, L. De Cola, *Macromolecular Chemistry and Physics* **2010**, *211*, 2286-2291.
- [110] B. Purushothaman, PhD thesis, University of Kentucky **2011**.
- [111] S. Haid, A. Mishra, M. Weil, C. Urich, M. Pfeiffer, P. Bäuerle, *Advanced Functional Materials* **2012**, *22*, 4322-4333.
- [112] G. Hua, Y. Li, A. L. Fuller, A. M. Slawin, J. D. Woollins, *European Journal of Organic Chemistry* **2009**, *2009*, 1612-1618.
- [113] F. N. Hayes, B. S. Rogers, D. G. Ott, *Journal of the American Chemical Society* **1955**, *77*, 1850-1852.
- [114] A. A. Kiryanov, P. Sampson, A. J. Seed, *The Journal of Organic Chemistry* **2001**, *66*, 7925-7929.
- [115] A. F. Littke, G. C. Fu, *Angewandte Chemie International Edition* **2002**, *41*, 4176-4211.
- [116] Z. Ge, T. Hayakawa, S. Ando, M. Ueda, T. Akiike, H. Miyamoto, T. Kajita, M. a. Kakimoto, *Advanced Functional Materials* **2008**, *18*, 584-590.
- [117] Z. Ge, T. Hayakawa, S. Ando, M. Ueda, T. Akiike, H. Miyamoto, T. Kajita, M.-a. Kakimoto, *Organic Letters* **2008**, *10*, 421-424.
- [118] Z. Li, PhD thesis, Vienna University of Technology (Vienna, Austria), **2013**.
- [119] Z. Li, N. Pucher, K. Cicha, J. Torgersen, S. C. Ligon, A. Ajami, W. Husinsky, A. Rosspeintner, E. Vauthey, S. Naumov, T. Scherzer, J. Stampfl, R. Liska, *Macromolecules* **2013**, *46*, 352-361.
- [120] Z. Li, M. Siklos, N. Pucher, K. Cicha, A. Ajami, W. Husinsky, A. Rosspeintner, E. Vauthey, G. Gescheidt, J. Stampfl, R. Liska, *Journal of Polymer Science Part A: Polymer Chemistry* **2011**, *49*, 3688-3699.

E. Bibliography

- [121] K. Cicha, Z. Li, K. Stadlmann, A. Ovsianikov, R. Markut-Kohl, R. Liska, J. Stampfl, *Journal of Applied Physics* **2011**, *110*, -.
- [122] H. Garoff, W. Ansorge, *Analytical biochemistry* **1981**, *115*, 450-457.
- [123] L. Doszczak, P. Kraft, H.-P. Weber, R. Bertermann, A. Triller, H. Hatt, R. Tacke, *Angewandte Chemie International Edition* **2007**, *46*, 3367-3371.
- [124] M. W. Andersen, B. Hildebrandt, G. Köster, R. W. Hoffmann, *Chemische Berichte* **1989**, *122*, 1777-1782.
- [125] R. A. Bredeweg, L. D. Rothman, C. D. Pfeiffer, *Analytical Chemistry* **1979**, *51*, 2061-2063.

F. Appendix

F.1 NMR-spectra

NMR-spectra unknown to literature are displayed in the first part of the Appendix.

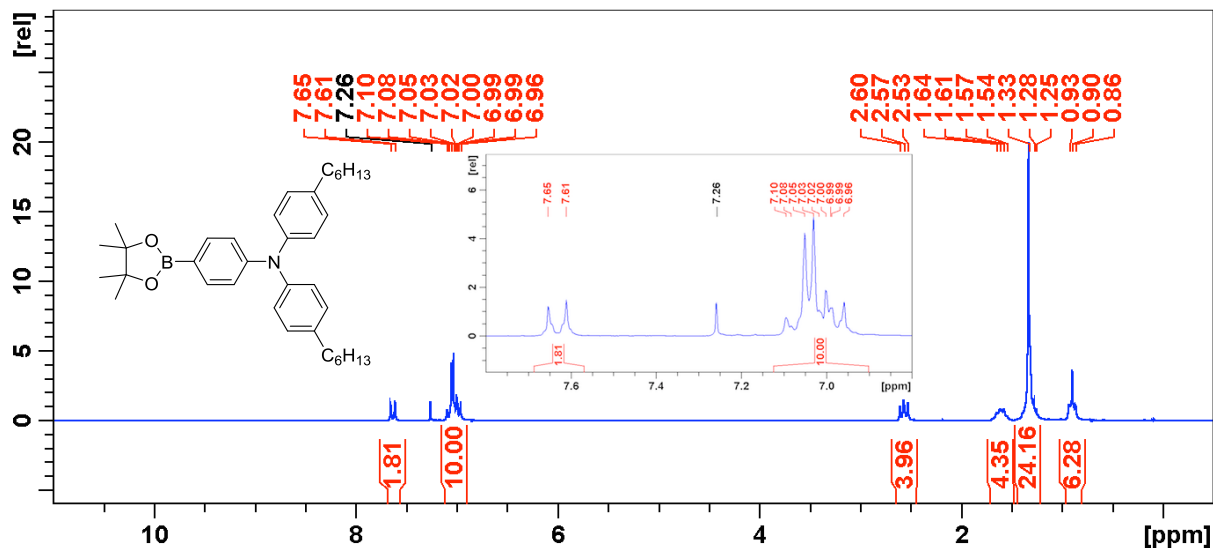


Figure 21: ¹H NMR (200 MHz, CDCl₃) of compound I

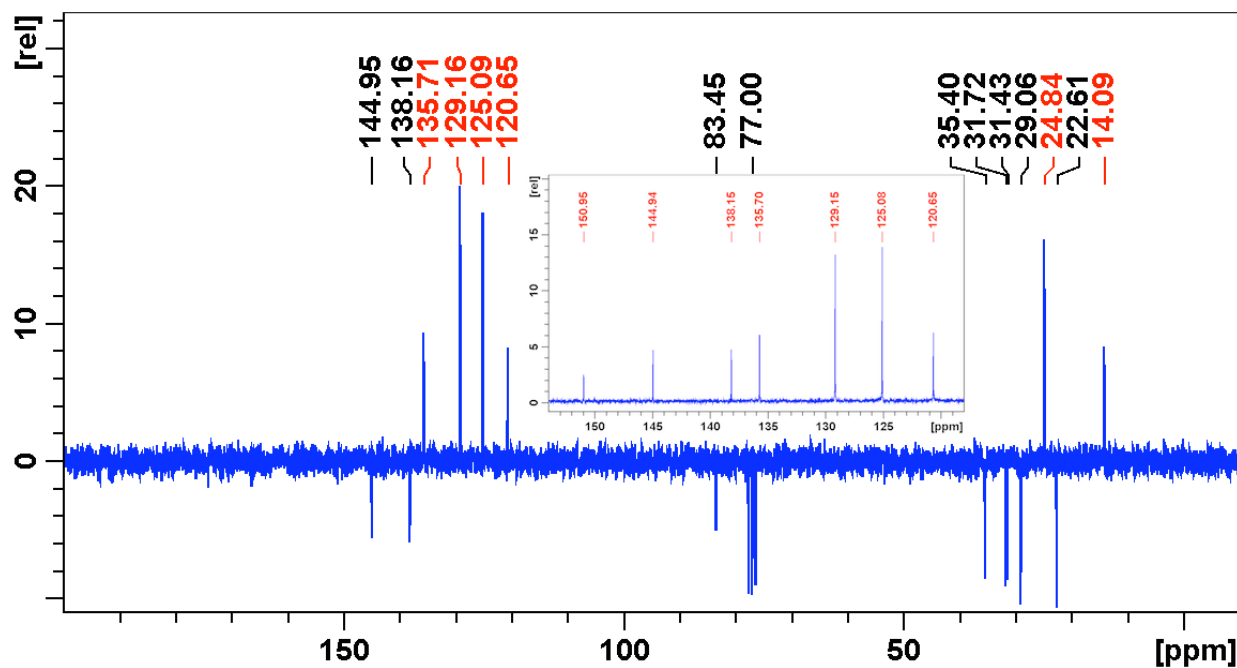


Figure 22: ¹³C NMR (50 MHz, CDCl₃) of compound I

F. Appendix

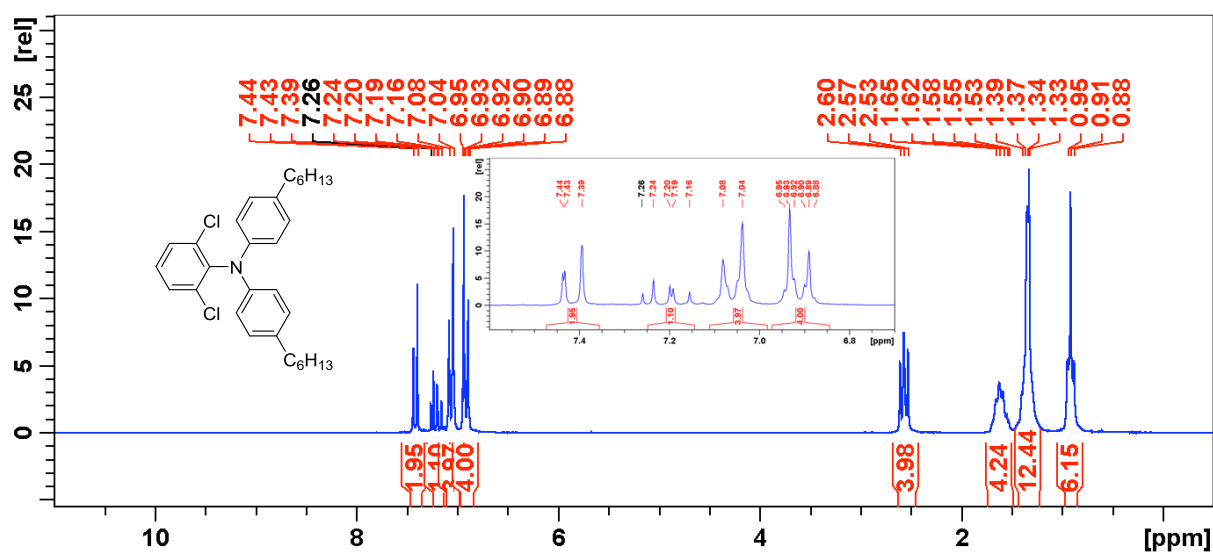


Figure 23: ^1H NMR (200 MHz, CDCl_3) of compound II

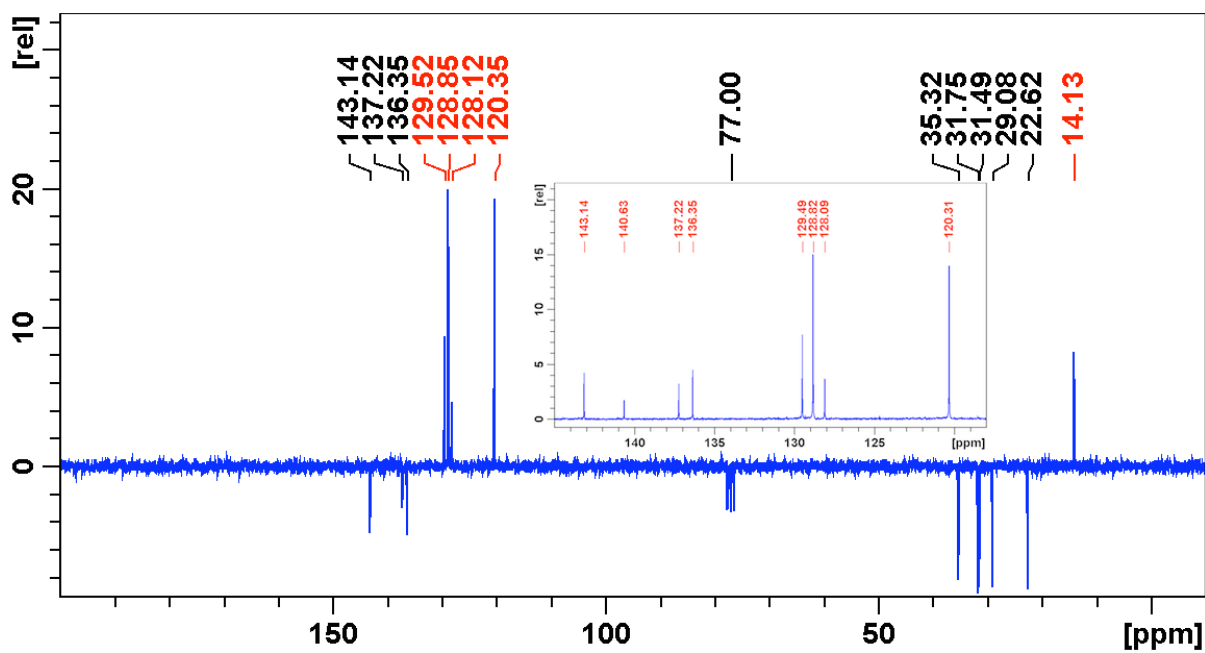


Figure 24: ^{13}C NMR (50 MHz, CDCl_3) of compound II

D. Experimental Part

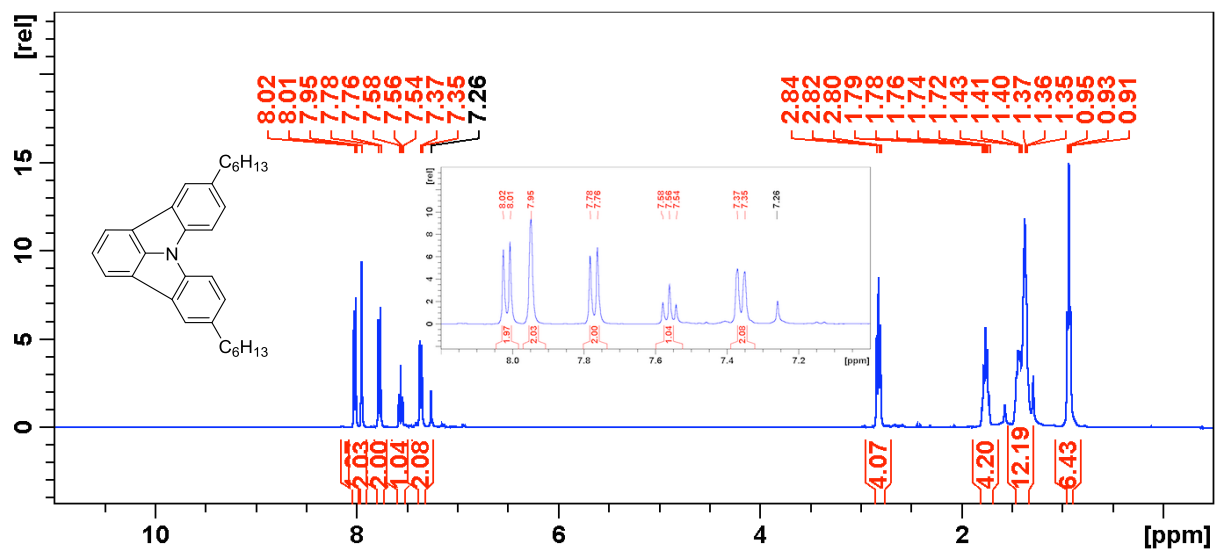


Figure 25: ^1H NMR (400 MHz, CDCl_3) of compound III

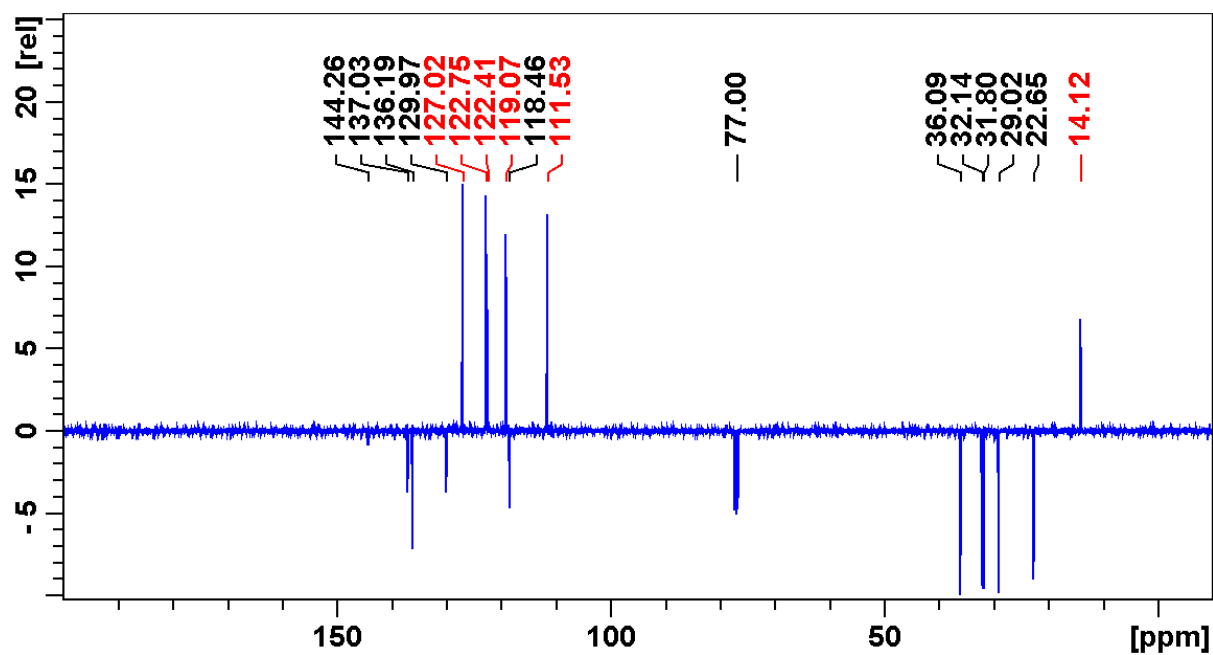
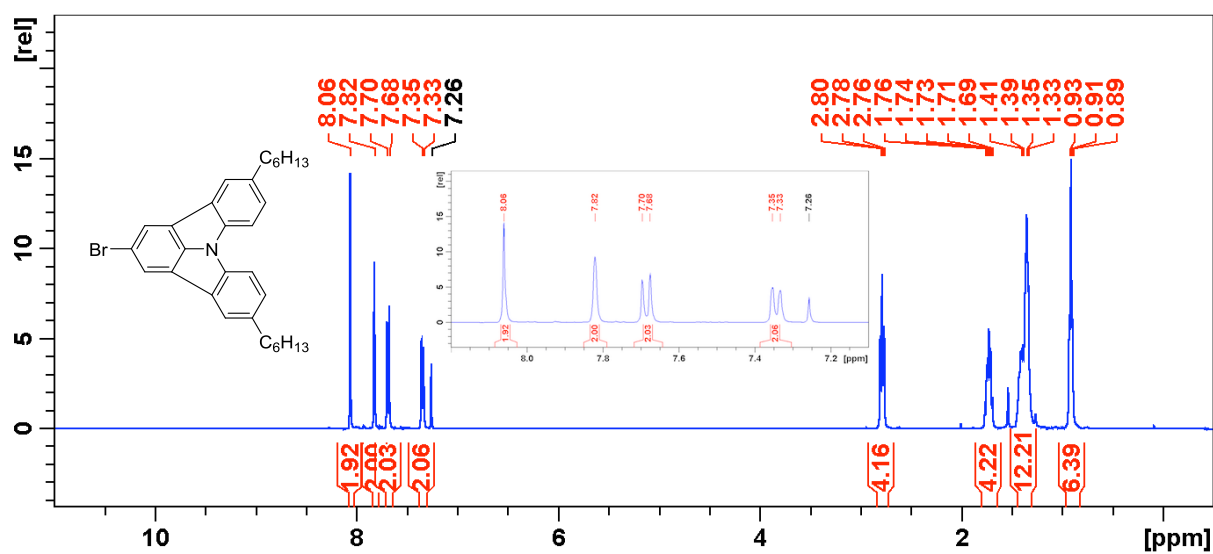
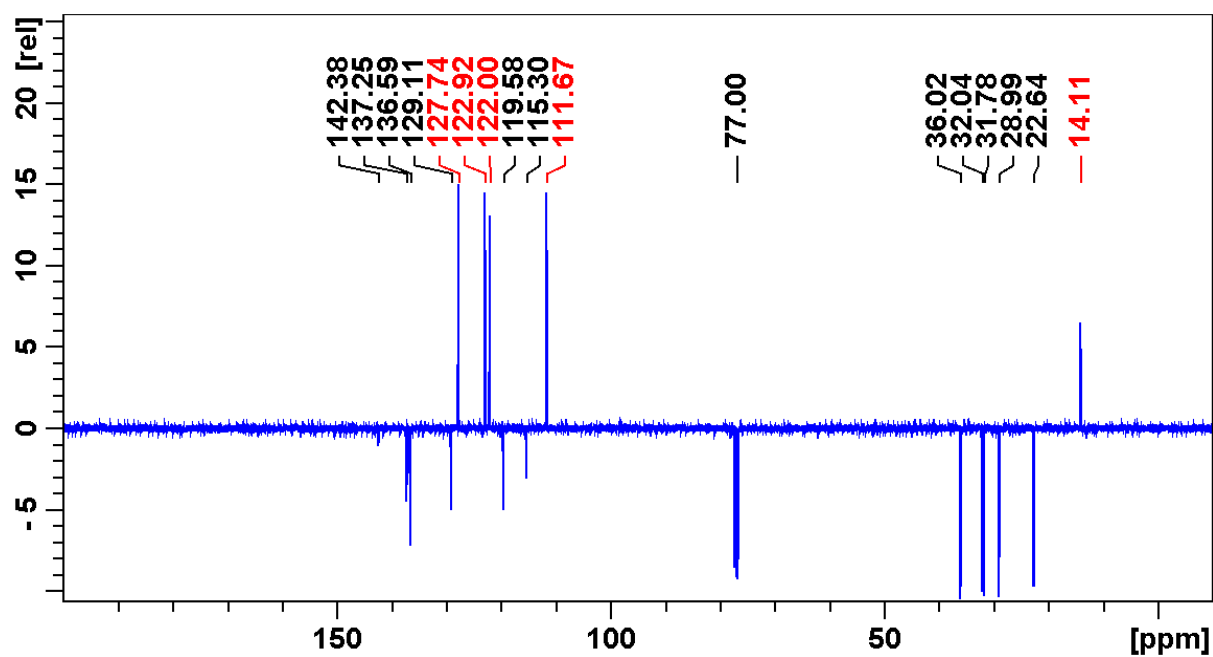


Figure 26: ^{13}C NMR (100 MHz, CDCl_3) of compound III

Figure 27: ^1H NMR (400 MHz, CDCl_3) of compound IVFigure 28: ^{13}C NMR (100 MHz, CDCl_3) of compound IV

D. Experimental Part

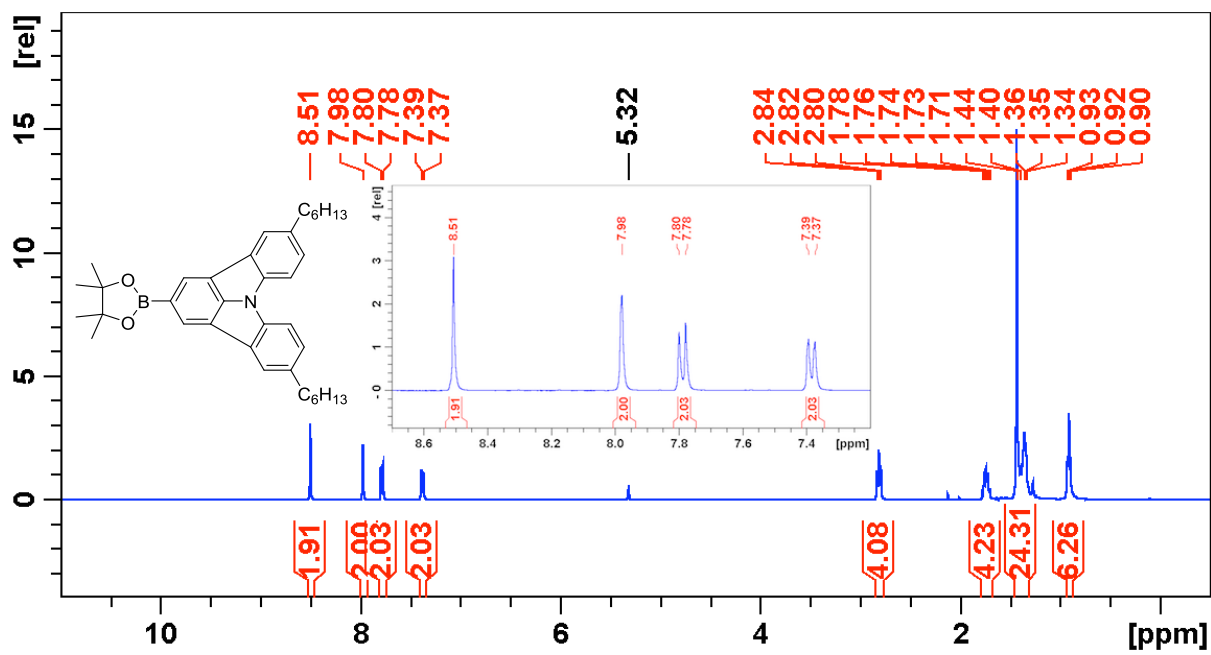


Figure 29: ¹H NMR (400 MHz, CDCl₃) of compound V

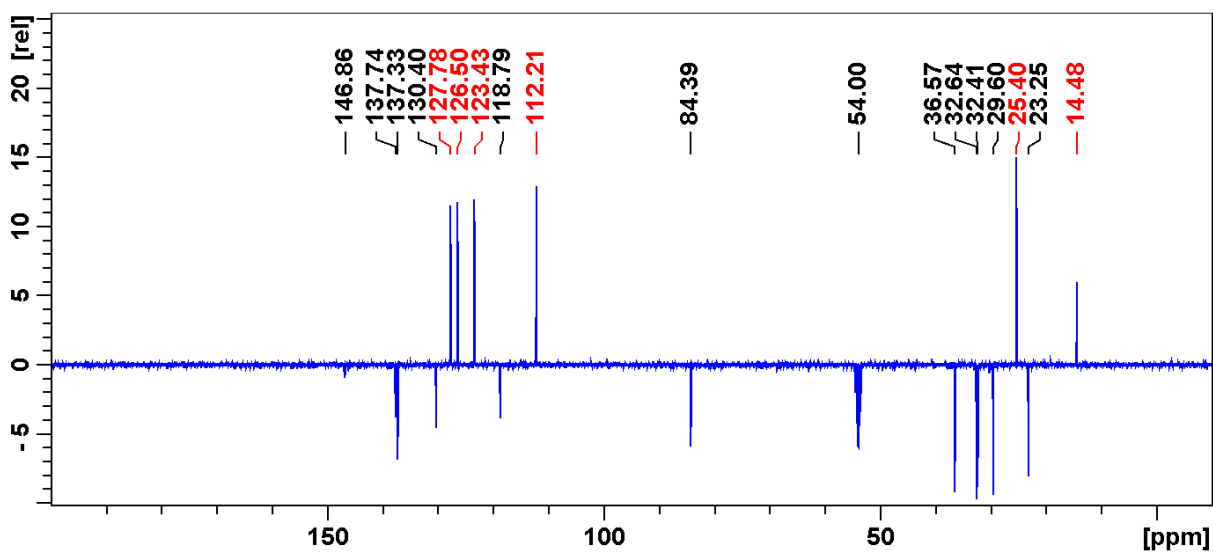
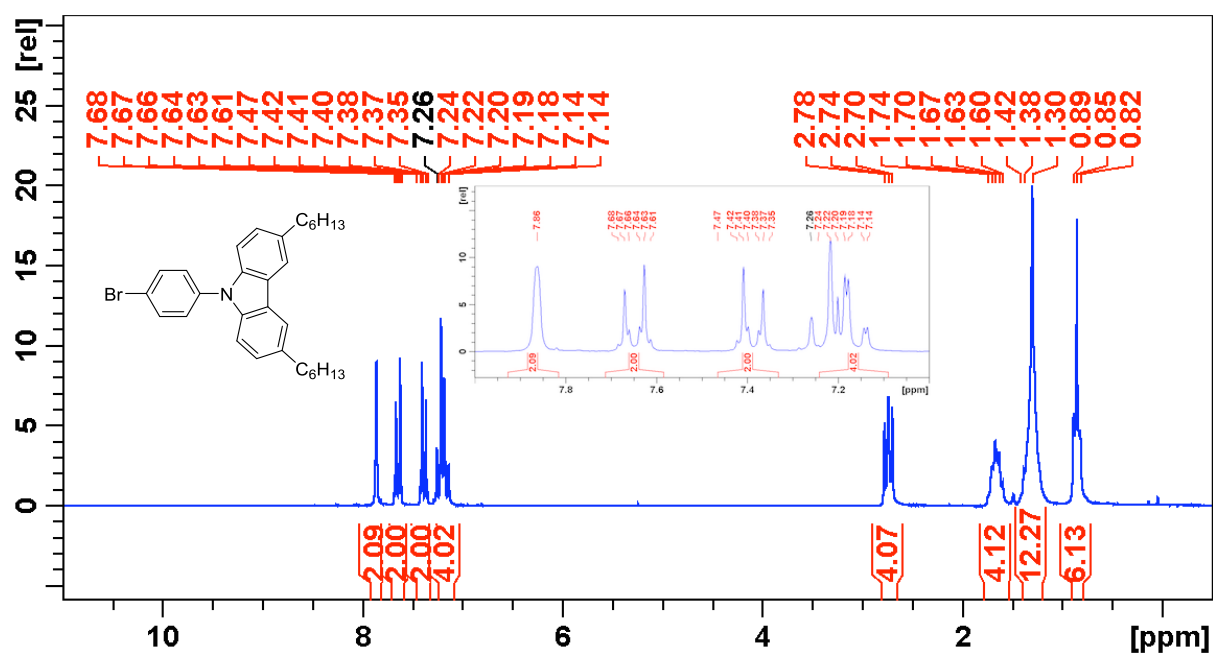
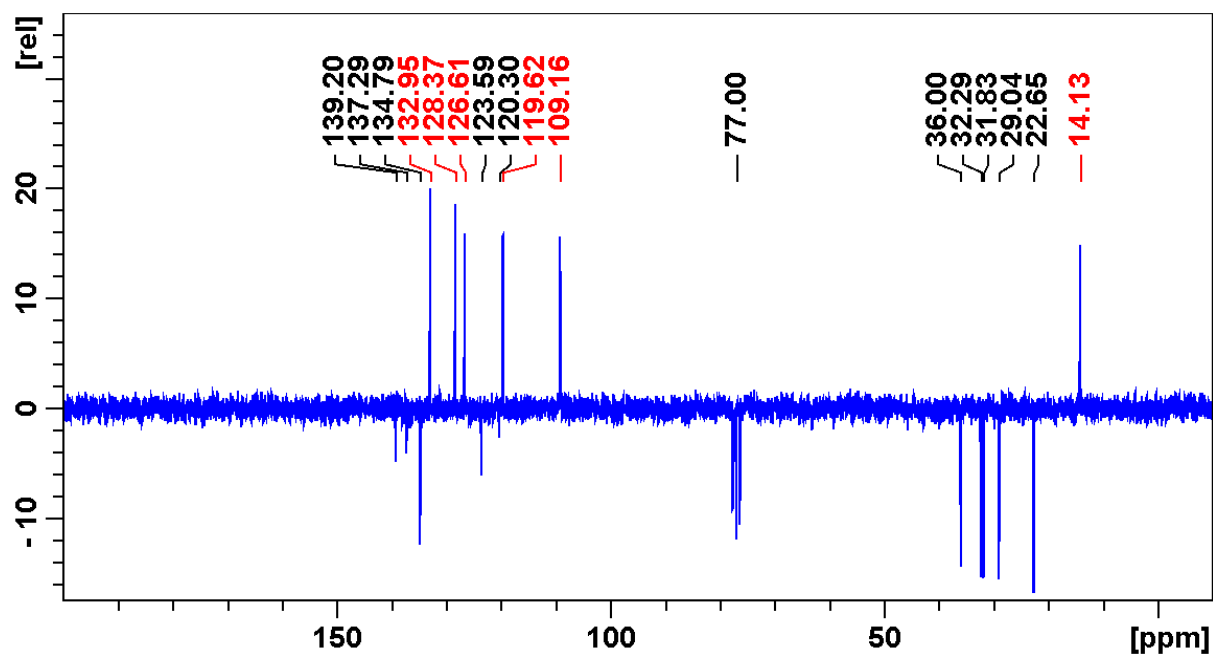


Figure 30: ¹³C NMR (100 MHz, CDCl₃) of compound V

Figure 31: ^1H NMR (200 MHz, CDCl_3) of compound VIFigure 32: ^{13}C NMR (50 MHz, CDCl_3) of compound VI

D. Experimental Part

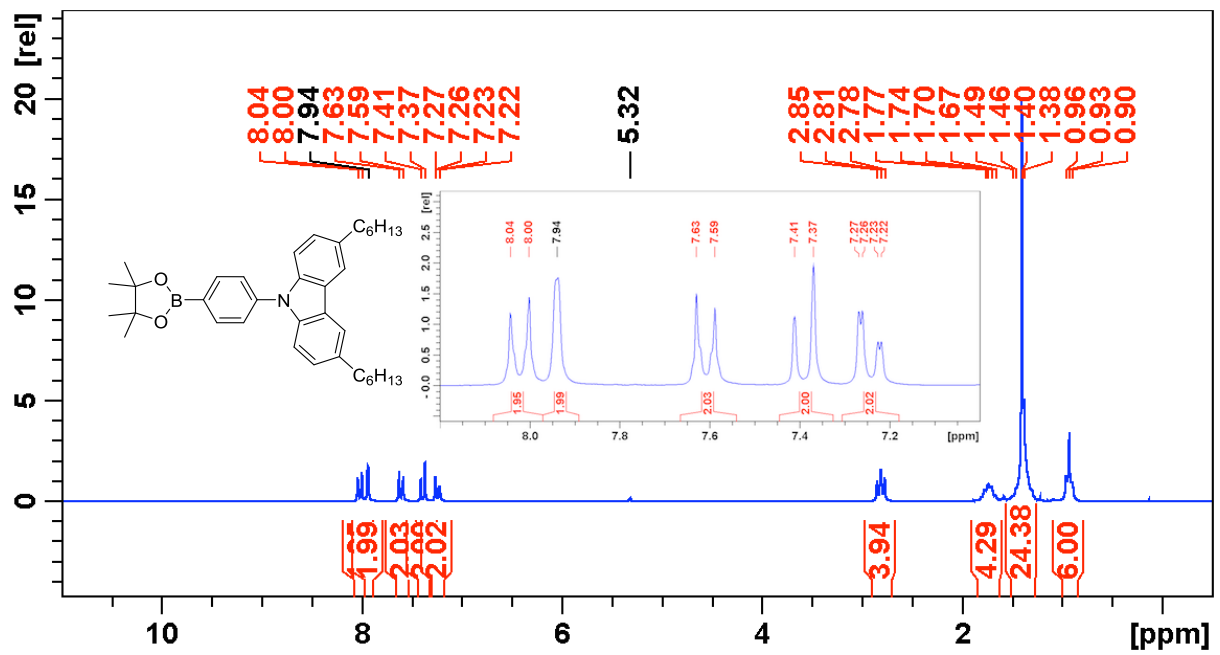


Figure 33: ^1H NMR (200 MHz, CDCl_3) of compound VII

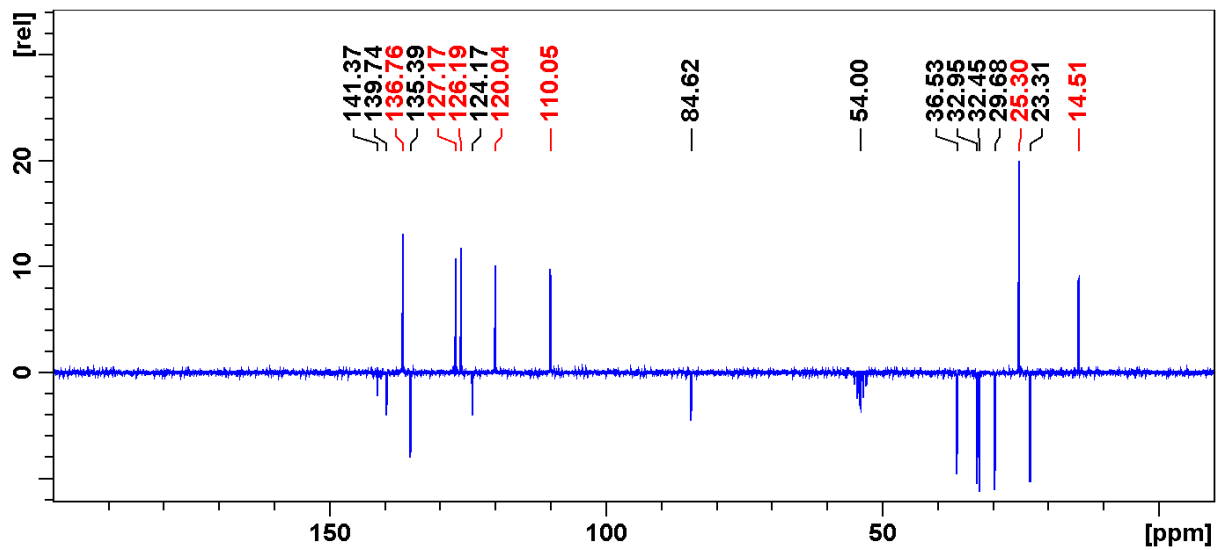
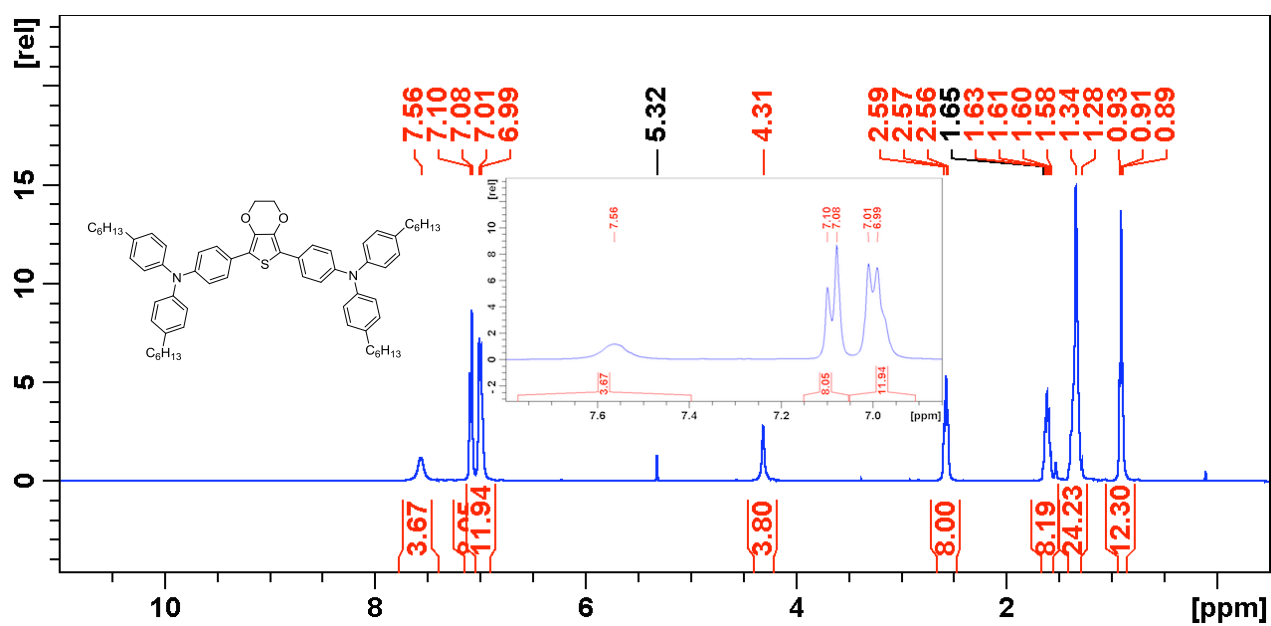


Figure 34: ^{13}C NMR (50 MHz, CDCl_3) of compound VII

Figure 35: ^1H NMR (400 MHz, CD_2Cl_2) of compound VIII

D. Experimental Part

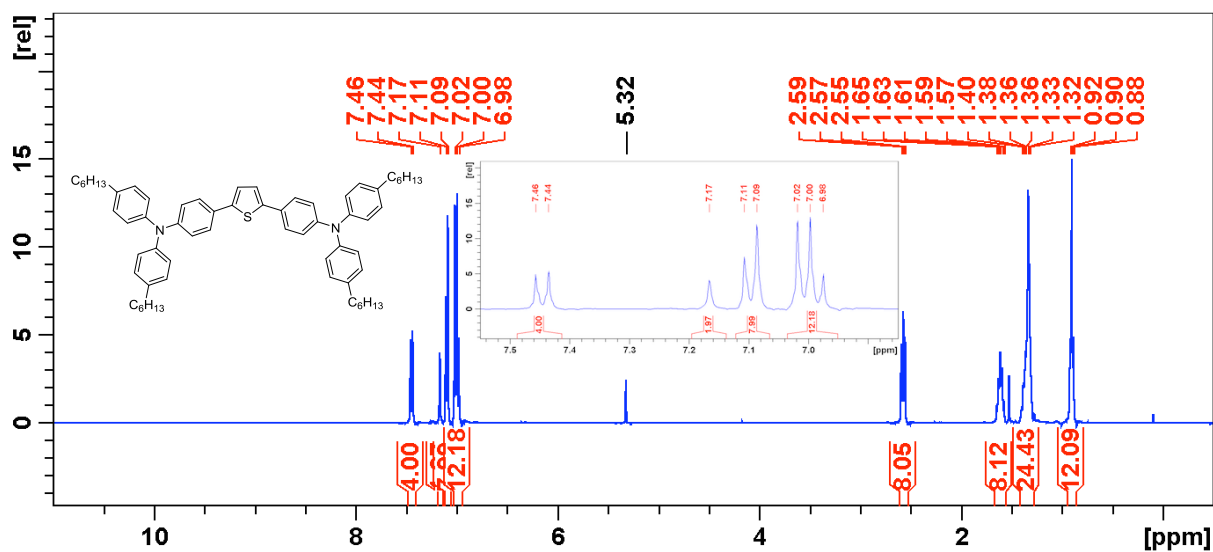


Figure 36: ^1H NMR (400 MHz, CD_2Cl_2) of compound IXa

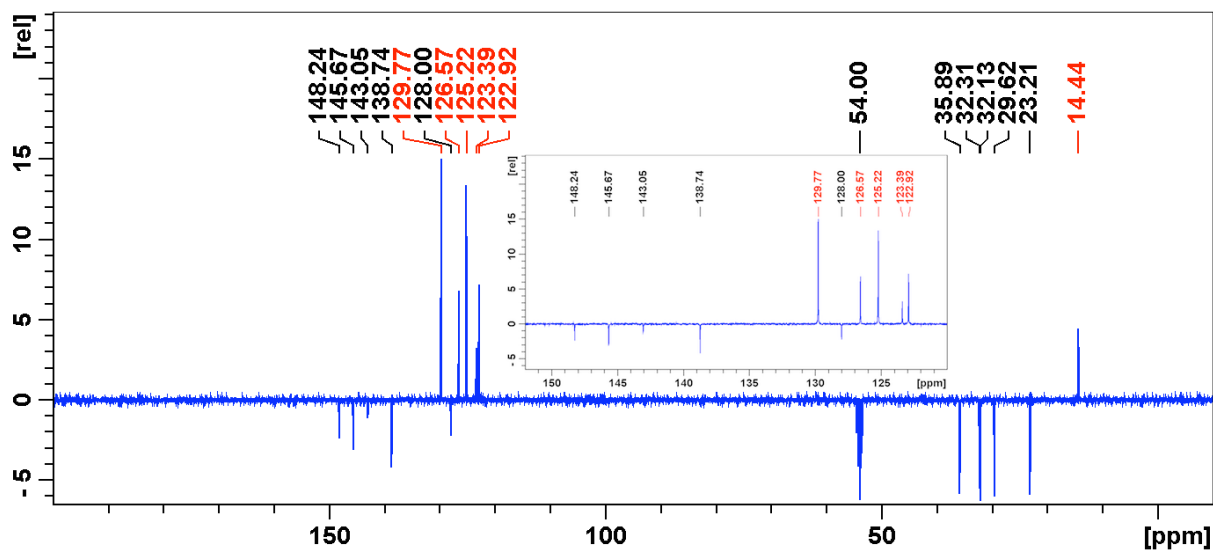


Figure 37: ^{13}C NMR (100 MHz, CD_2Cl_2) of compound IXa

D. Experimental Part

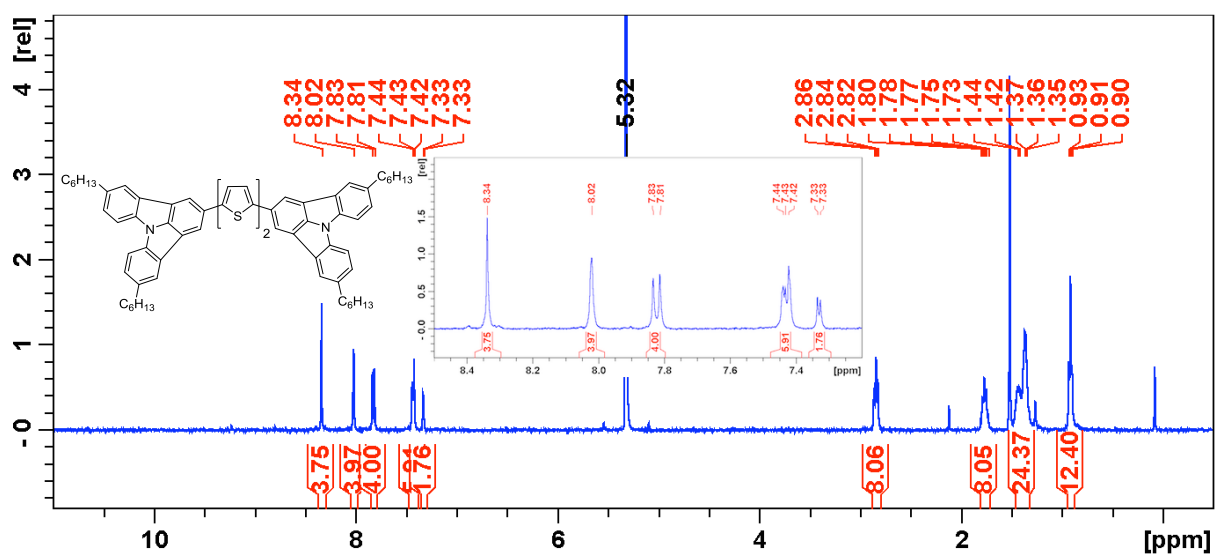
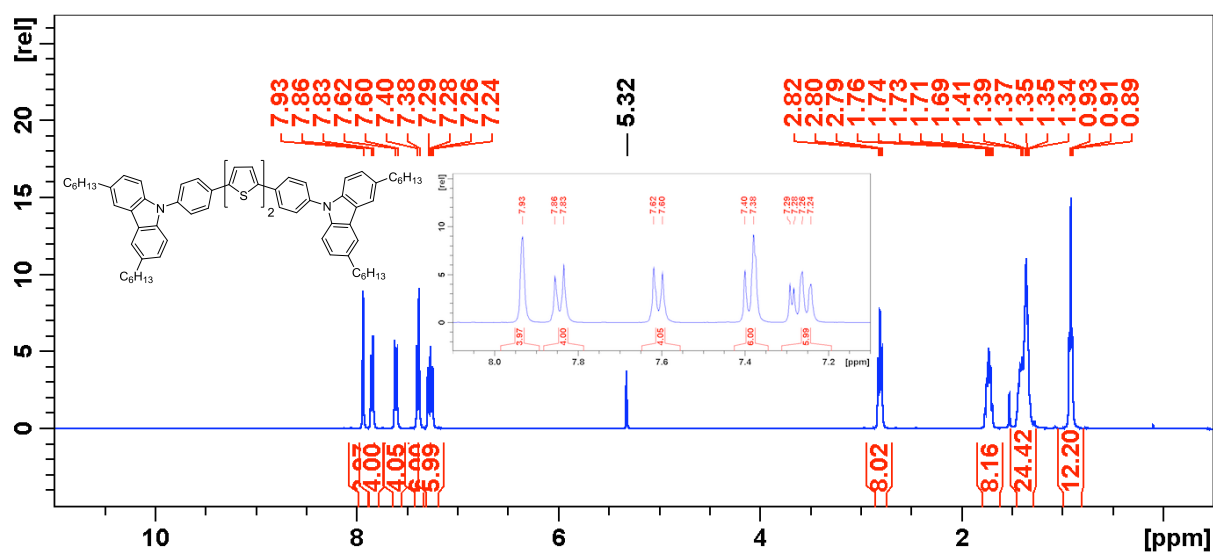
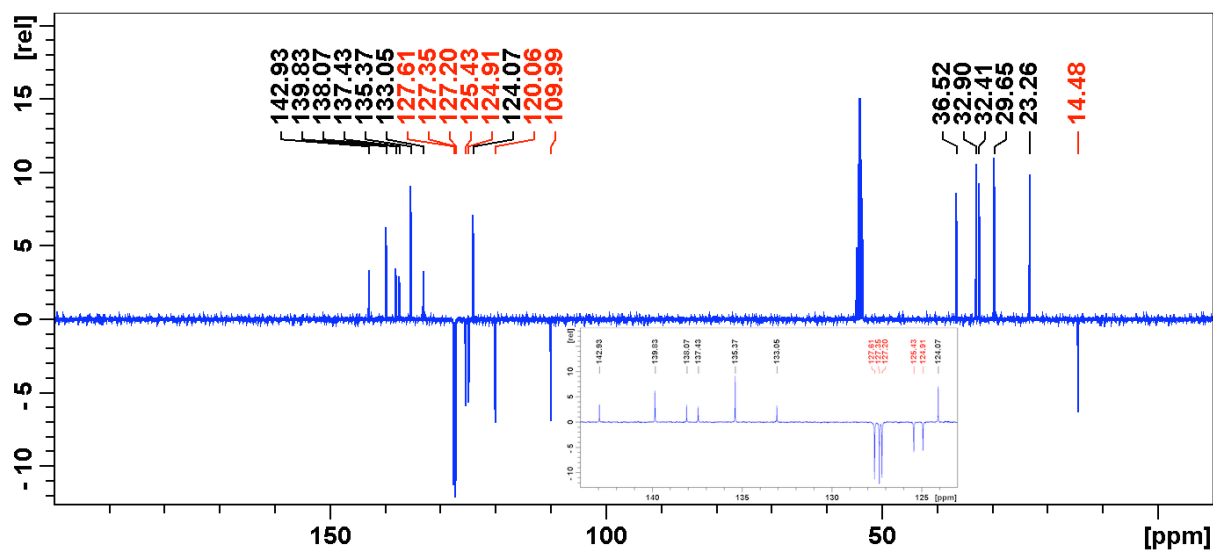


Figure 40: ^1H NMR (400 MHz, CD_2Cl_2) of compound X

Figure 41: ^1H NMR (400 MHz, CD_2Cl_2) of compound XIFigure 42: ^{13}C NMR (100 MHz, CD_2Cl_2) of compound XI

D. Experimental Part

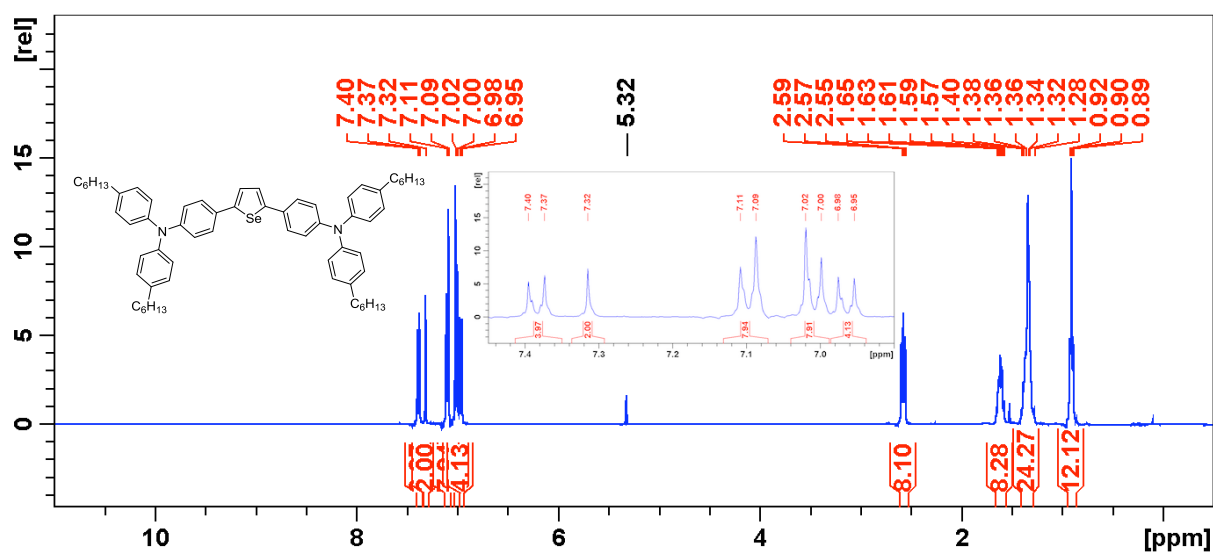


Figure 43: ¹H NMR (400 MHz, CD₂Cl₂) of compound XII

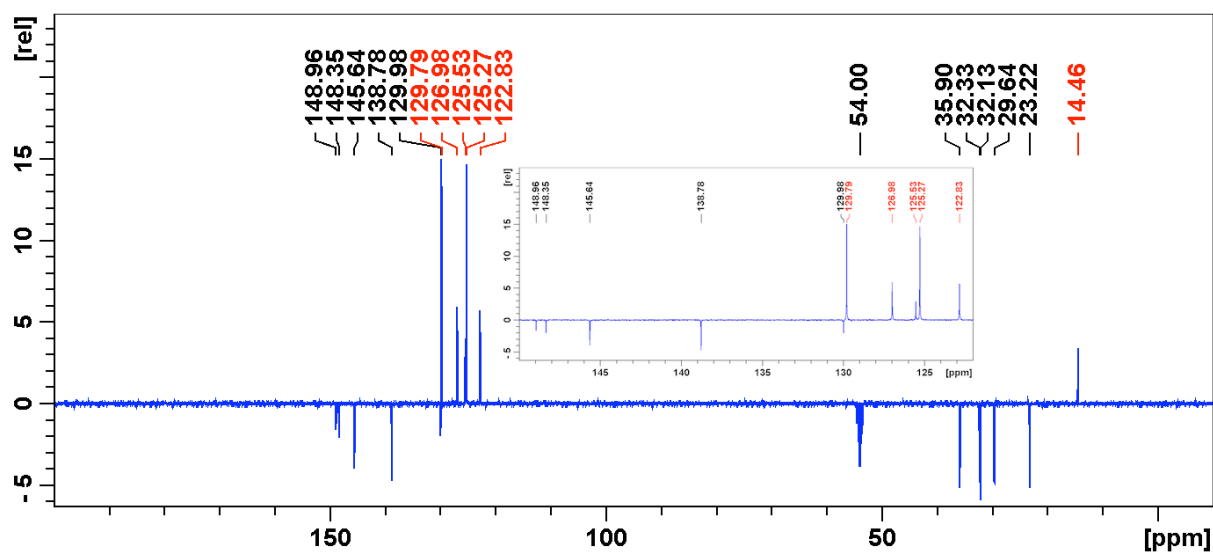


Figure 44: ¹³C NMR (100 MHz, CD₂Cl₂) of compound XII

F. Appendix

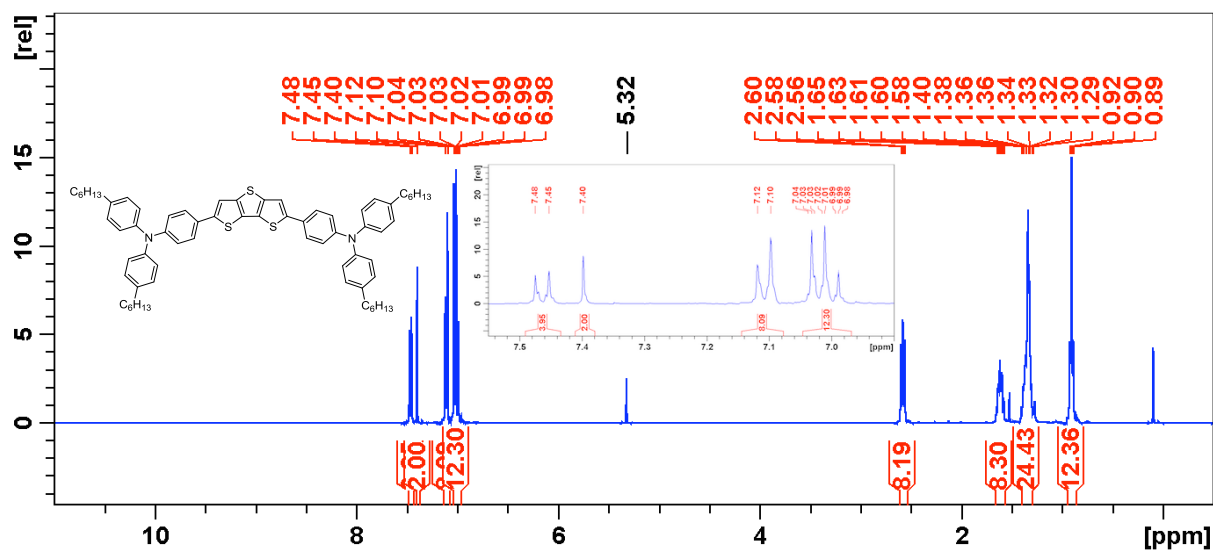


Figure 45: ¹H NMR (400 MHz, CD₂Cl₂) of compound XIII

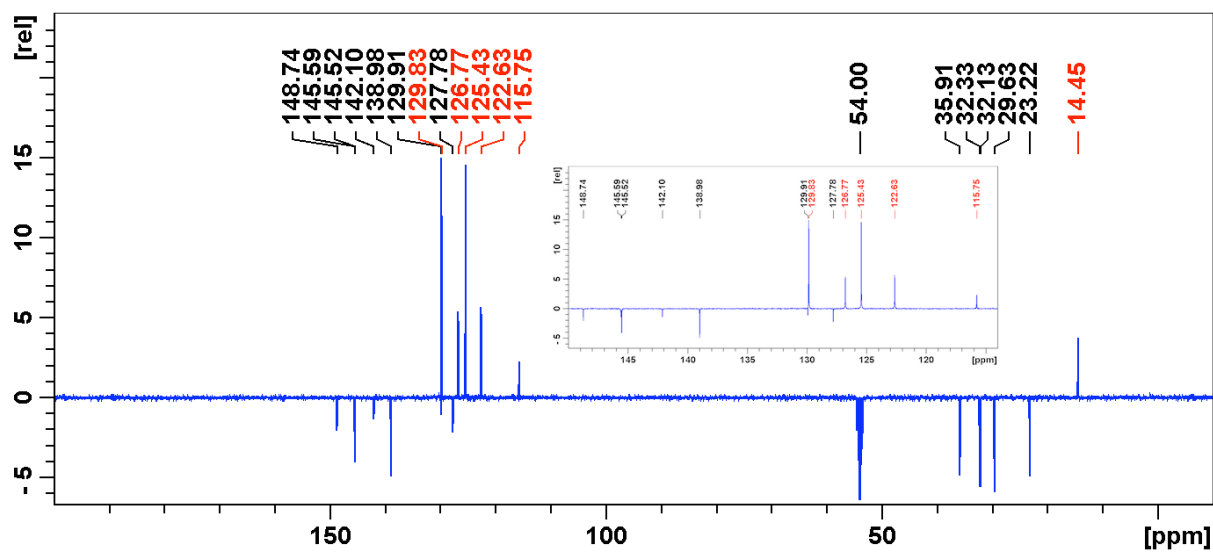


Figure 46: ¹³C NMR (100 MHz, CD₂Cl₂) of compound XIII

D. Experimental Part

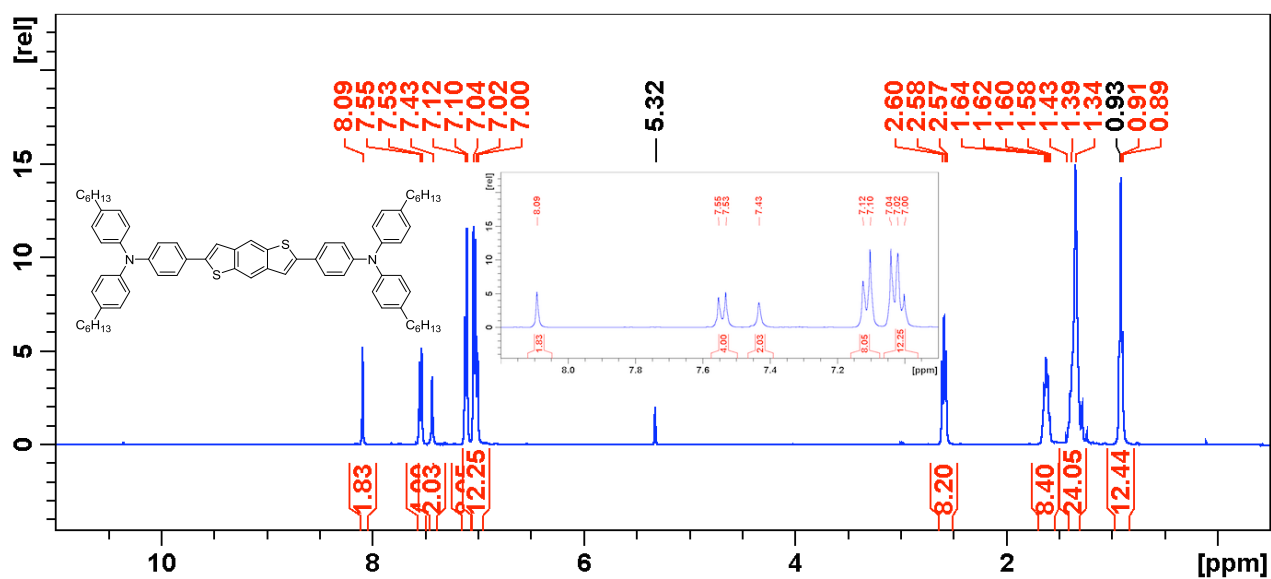


Figure 47: ^1H NMR (400 MHz, CD_2Cl_2) of compound XIVa

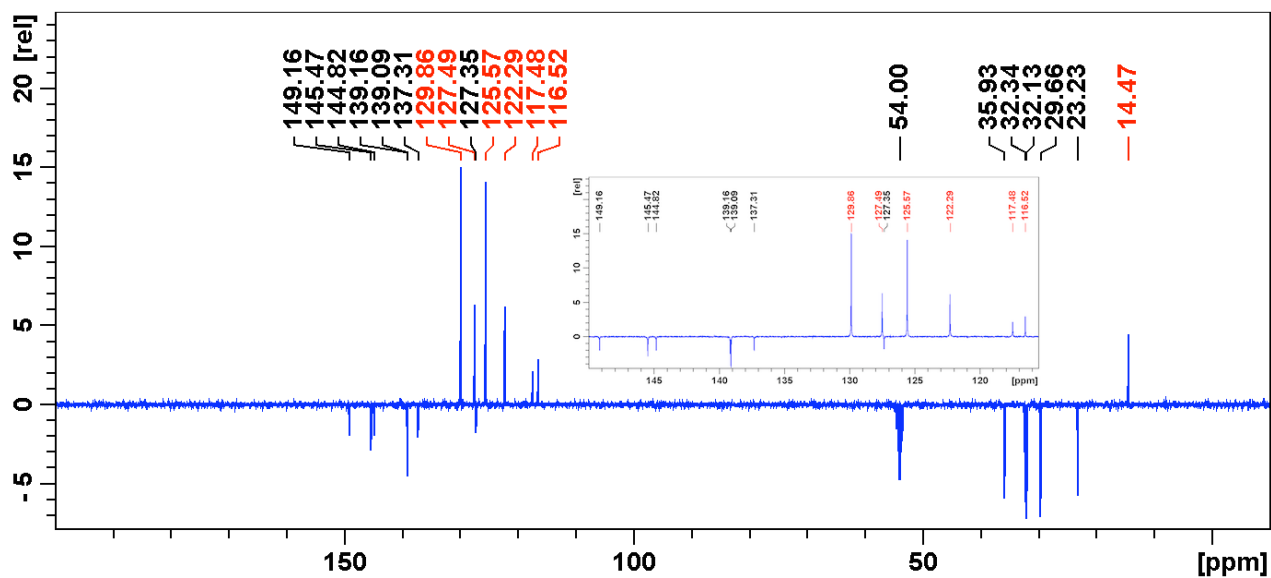
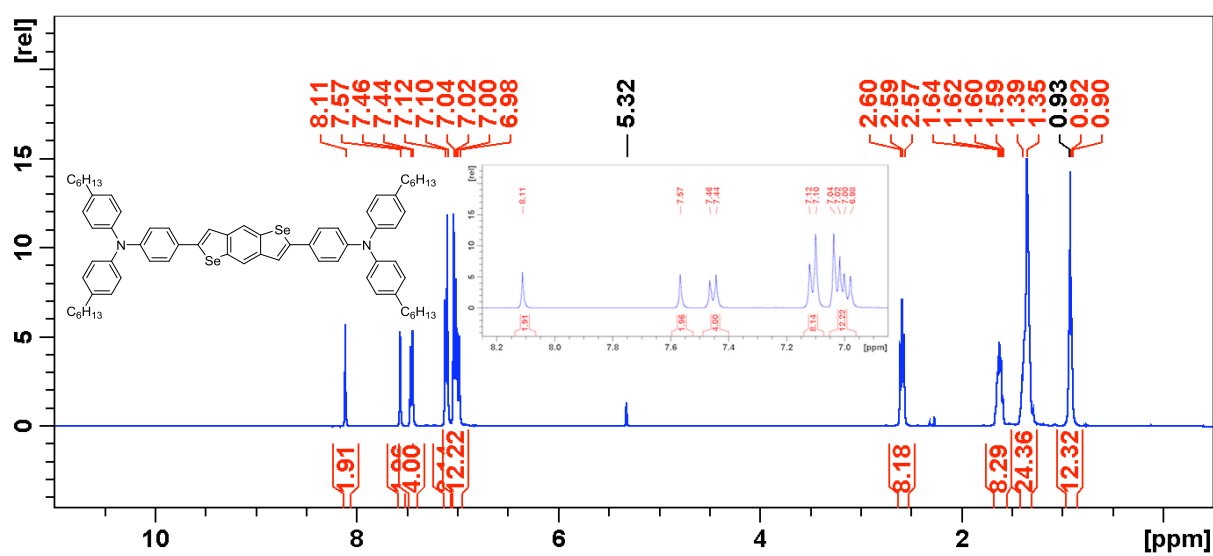
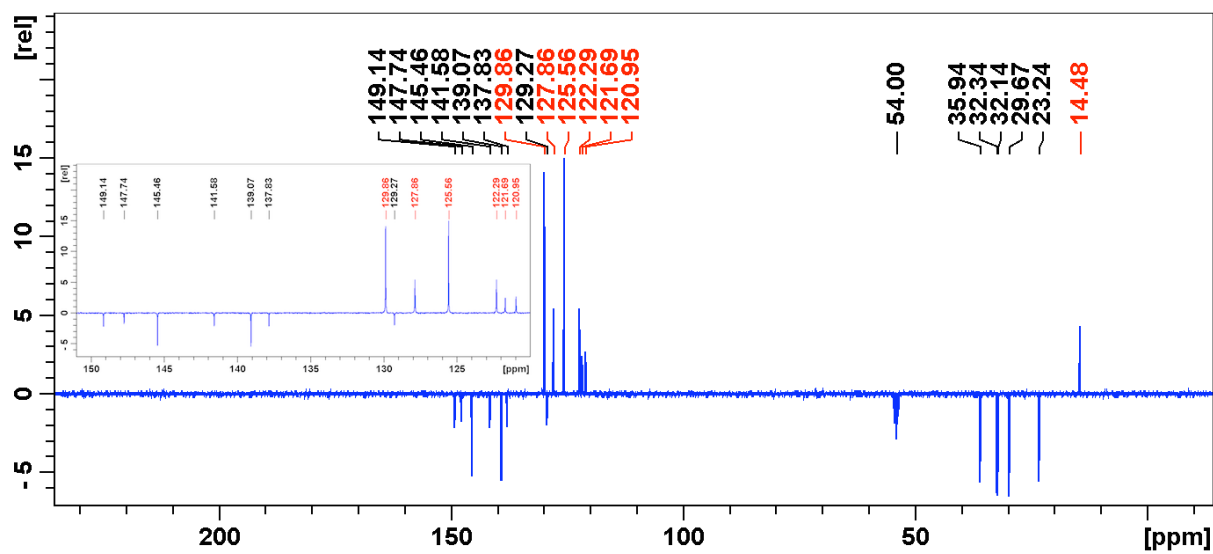


Figure 48: ^{13}C NMR (100 MHz, CD_2Cl_2) of compound XIVa

Figure 49: ¹H NMR (400 MHz, CD₂Cl₂) of compound XIVbFigure 50: ¹³C NMR (100 MHz, CD₂Cl₂) of compound XIVb

D. Experimental Part

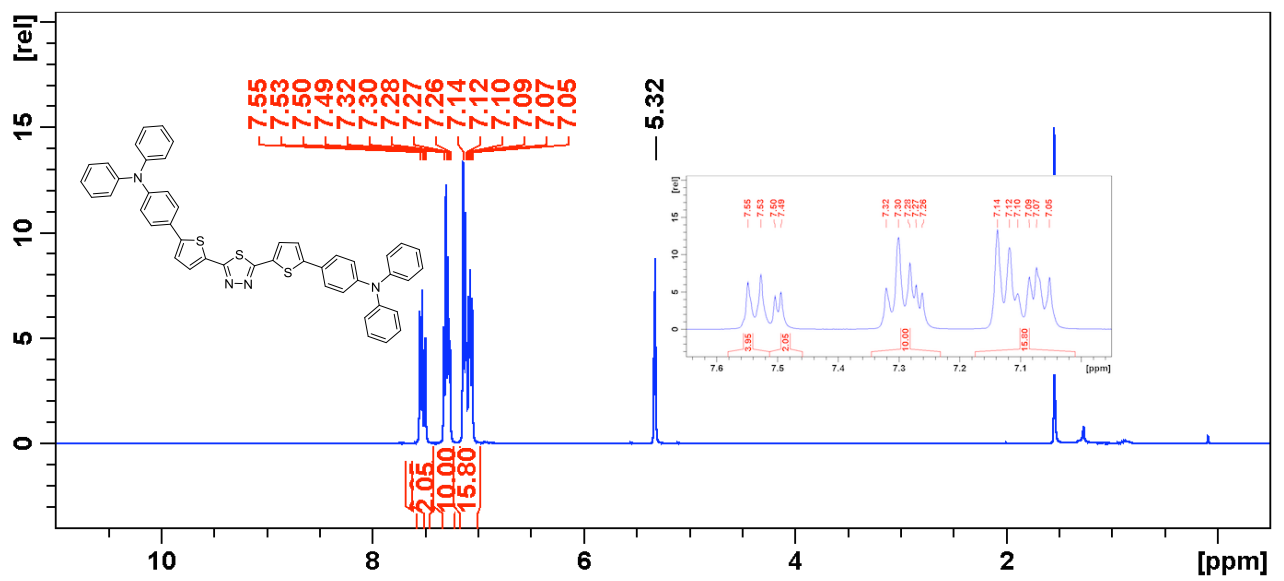


Figure 51: ^1H NMR (400 MHz, CD_2Cl_2) of compound **XVb**

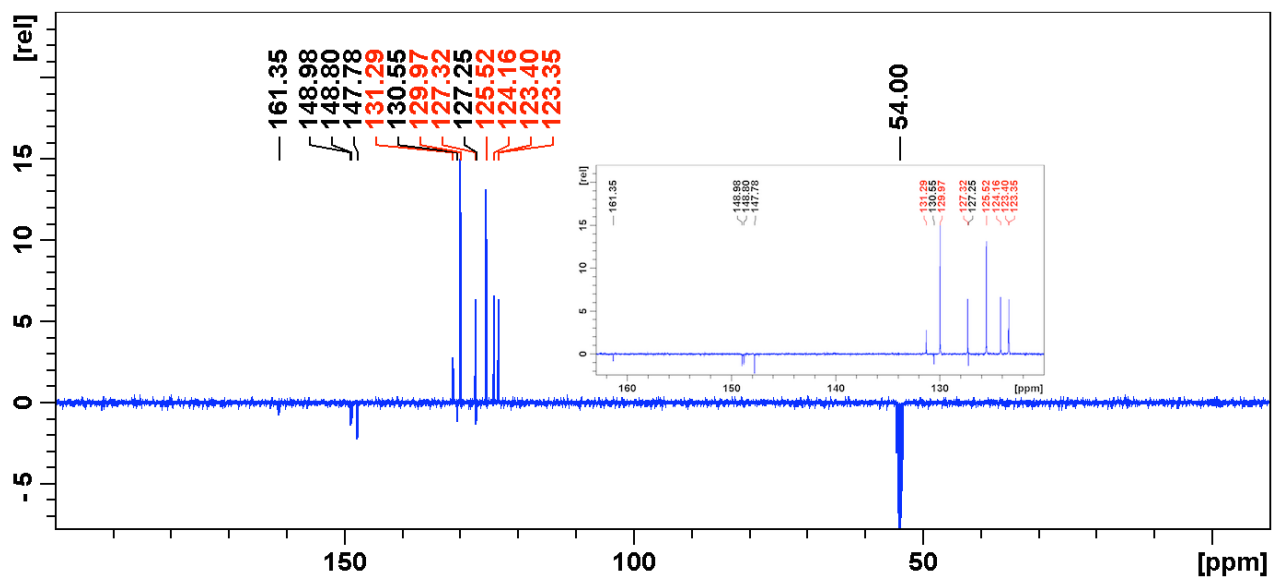


Figure 52: ^{13}C NMR (100 MHz, CD_2Cl_2) of compound **XVb**

F. Appendix

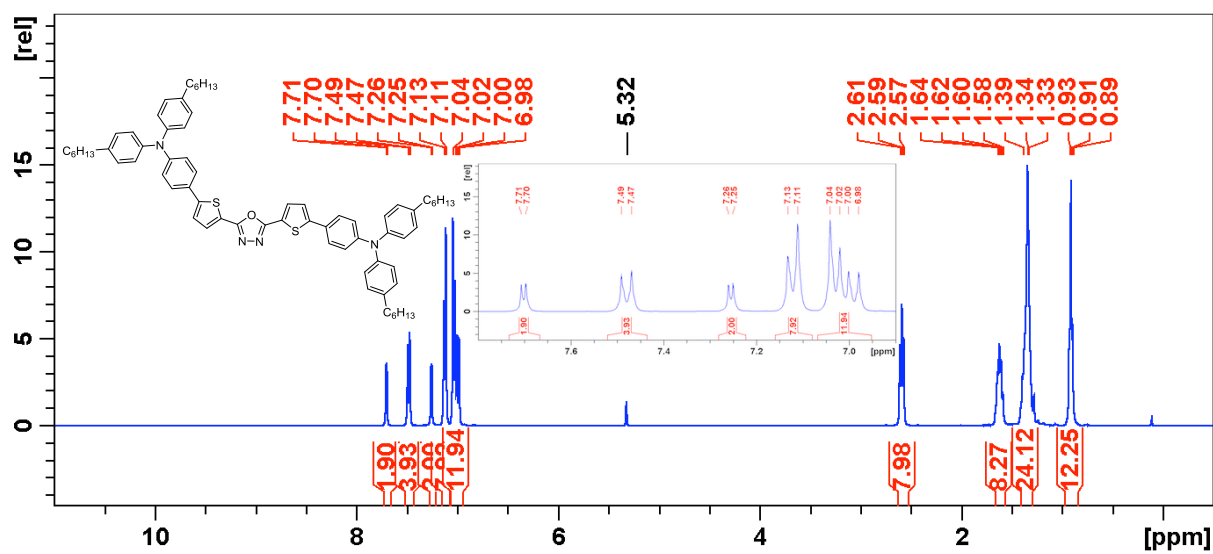


Figure 53: ¹H NMR (400 MHz, CD₂Cl₂) of compound XVIa

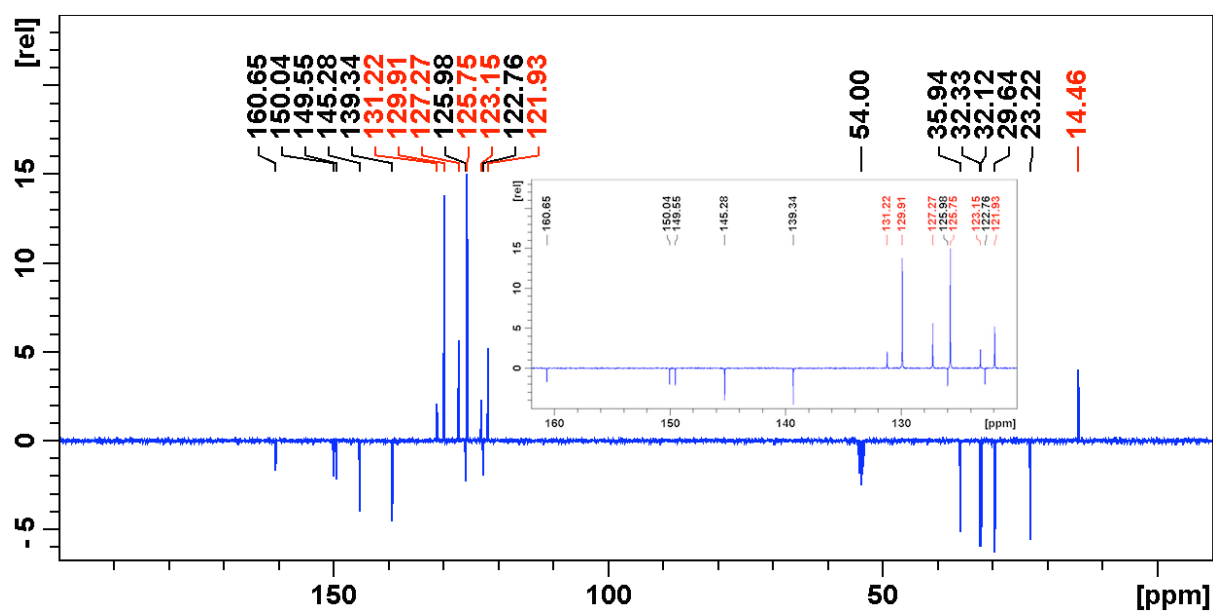


Figure 54: ¹³C NMR (100 MHz, CD₂Cl₂) of compound XVIa

D. Experimental Part

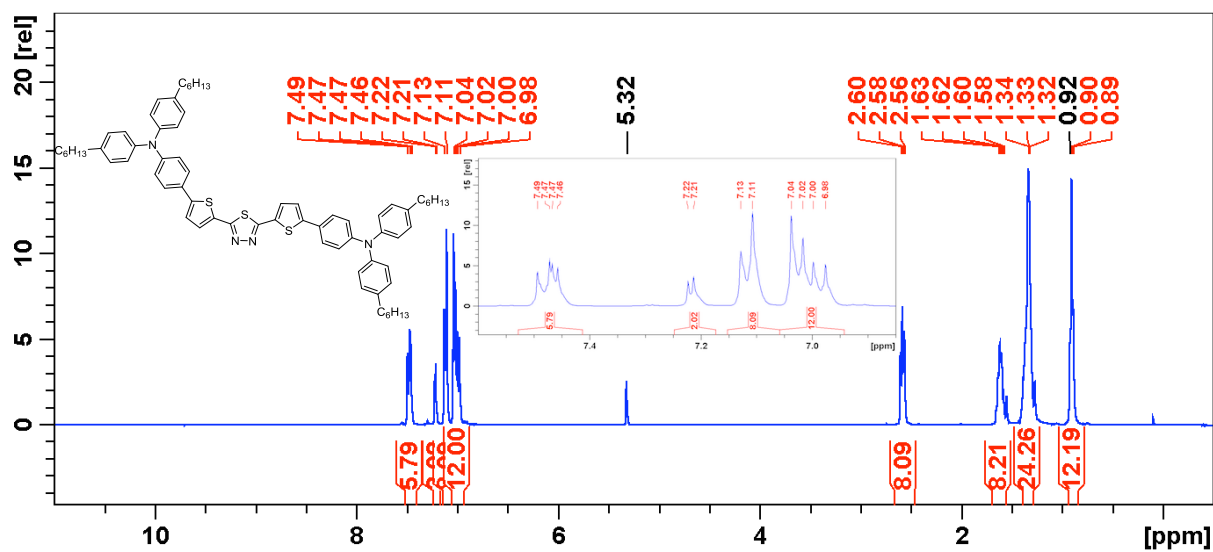


Figure 55: ¹H NMR (400 MHz, CD₂Cl₂) of compound XVIIb

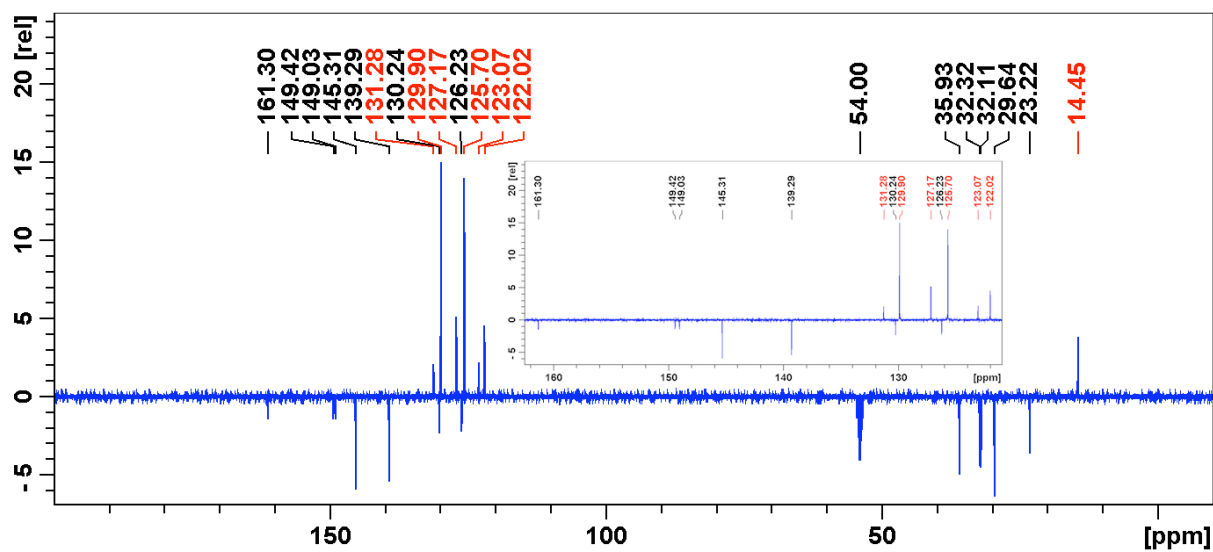


Figure 56: ¹³C NMR (100 MHz, CD₂Cl₂) of compound XVIIb

F.2 SEM-images of 2PIP-structuring tests

SEM-images of 2PIP-structuring tests are displayed in the second part of the Appendix.

B3FL

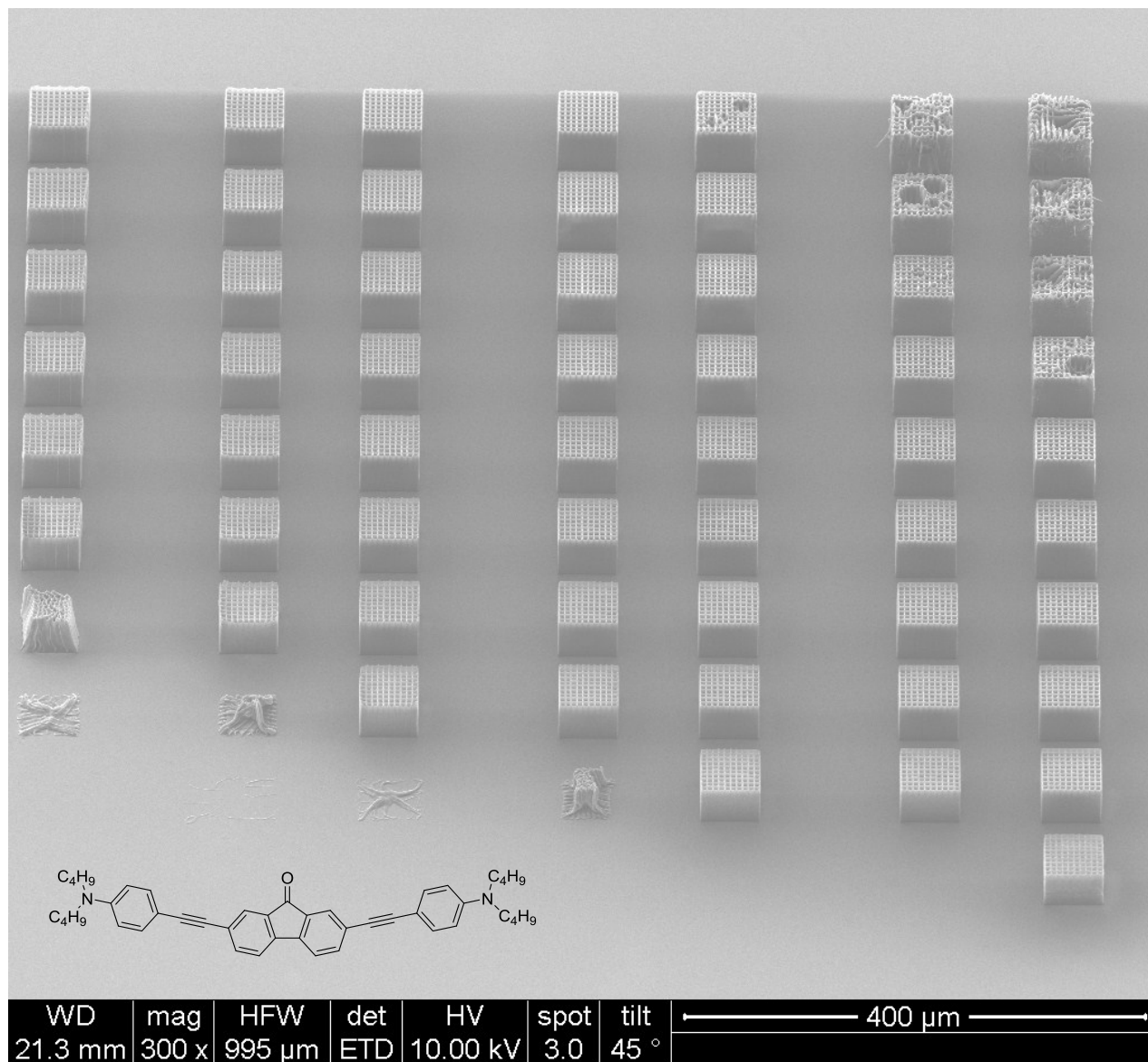


Figure 57: SEM-image of 2PIP-structuring test of reference compound **B3FL**; magnification: 300x; 45 $^{\circ}$ tilt.

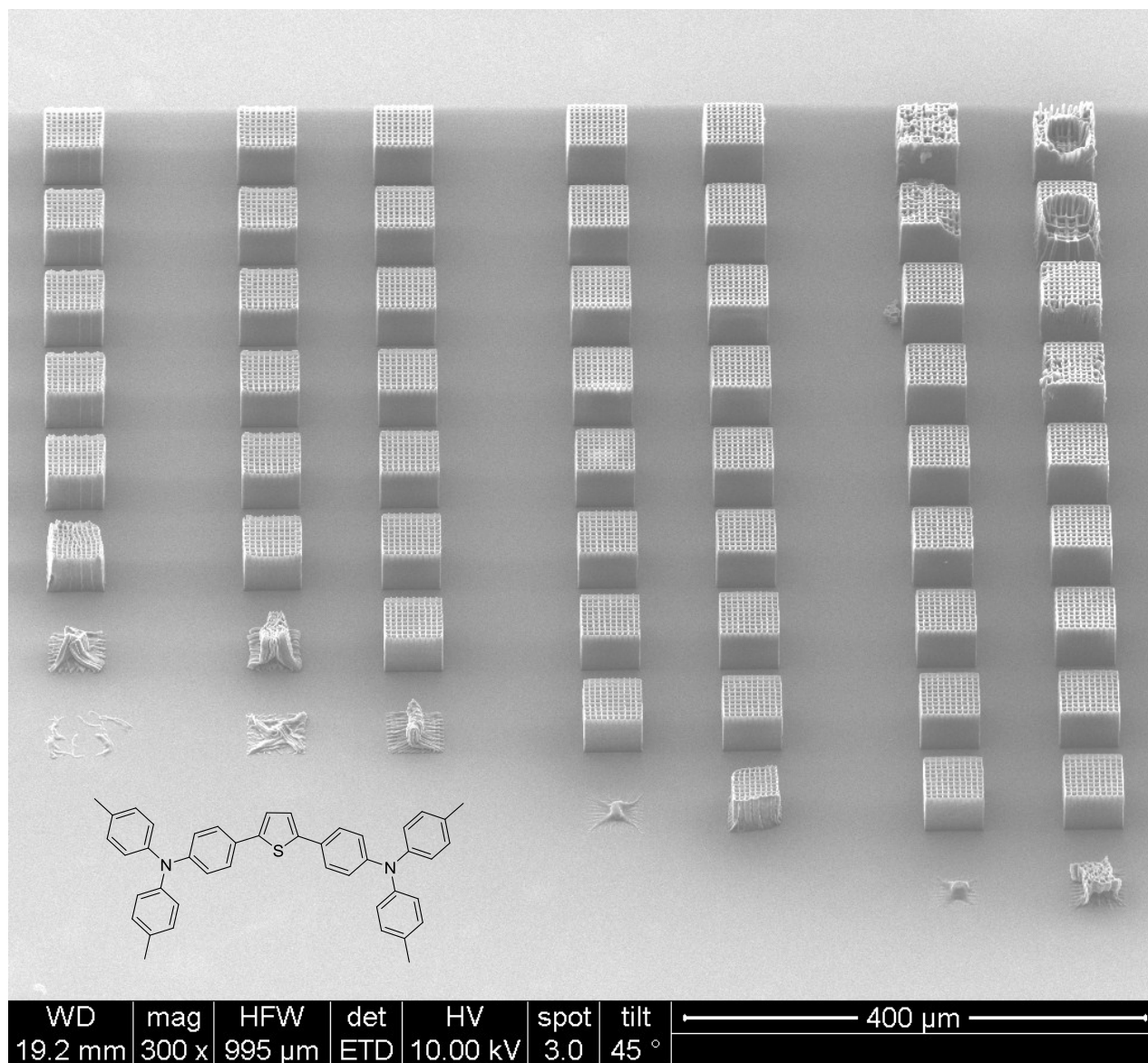
BMA-1T

Figure 58: SEM-image of 2PIP-structuring test of reference compound **BMA-1T**; magnification: 300x; 45° tilt.

IXa, HxTPA-1T

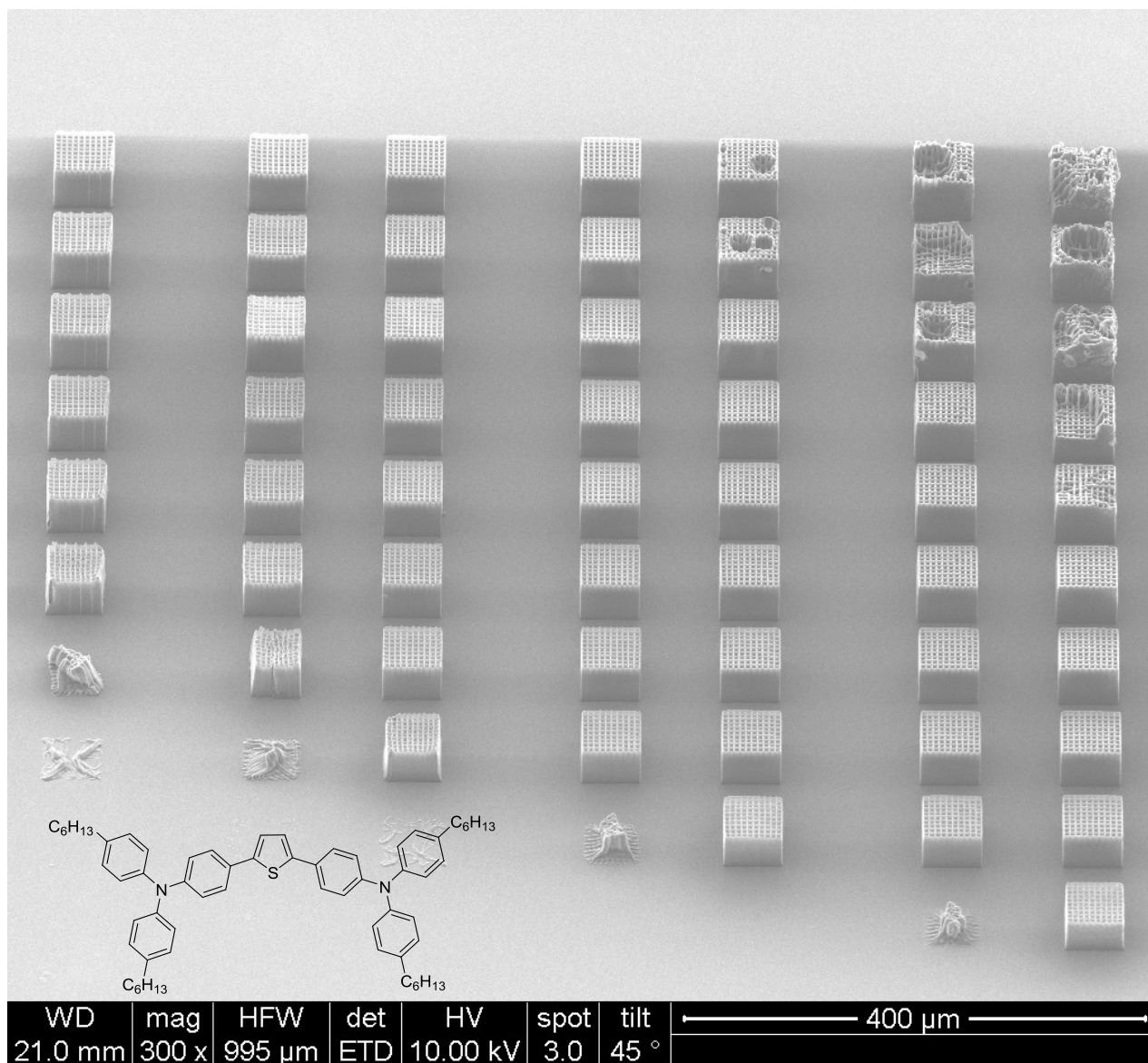


Figure 59: SEM-image of 2PIP-structuring test of compound IXa, HxTPA-1T; magnification: 300x; 45° tilt.

VIII, HxTPA-1E

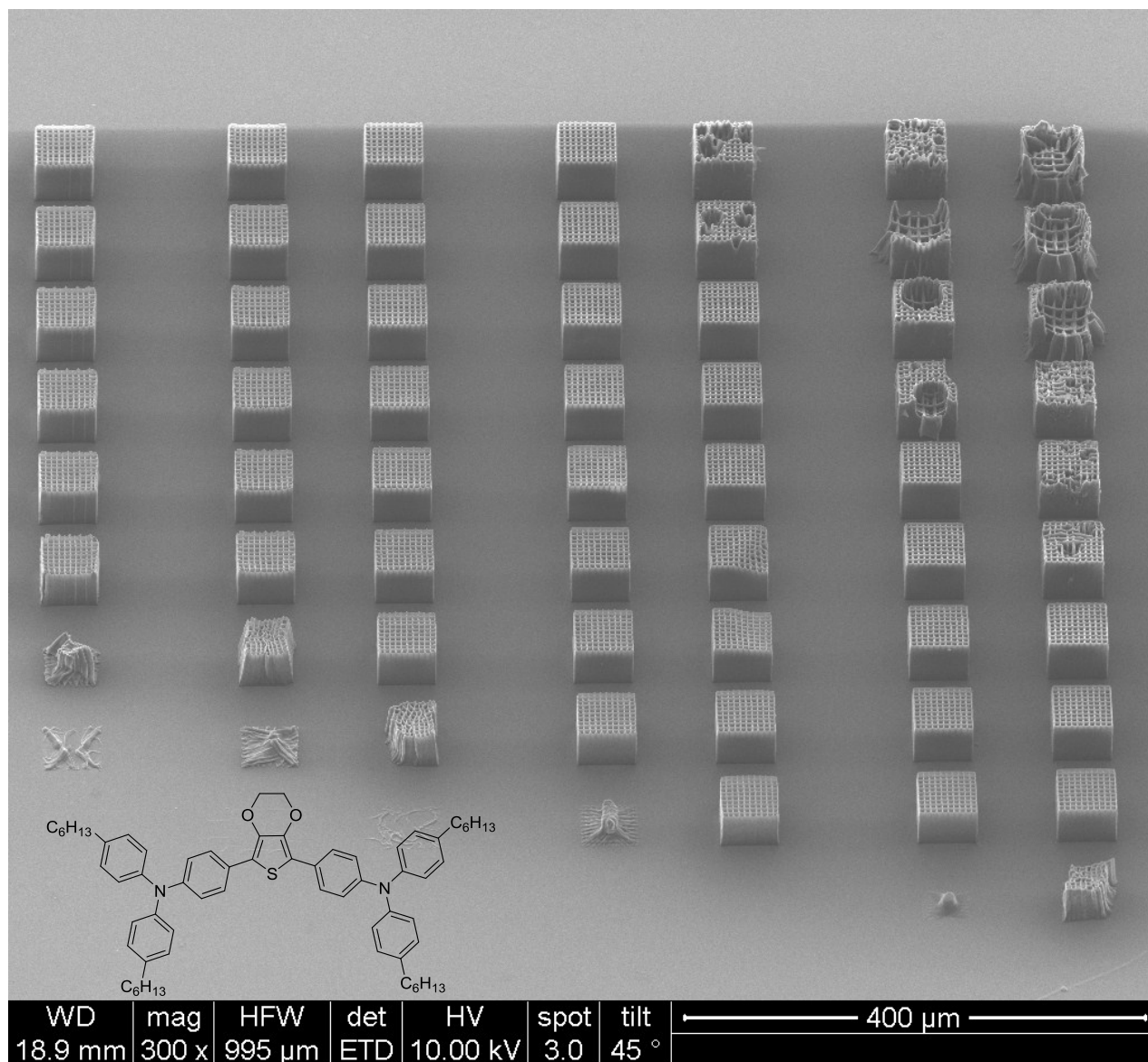


Figure 60: SEM-image of 2PIP-structuring test of compound **VIII, HxTPA-1E**; magnification: 300x; 45° tilt.

XII, HxTPA-1S

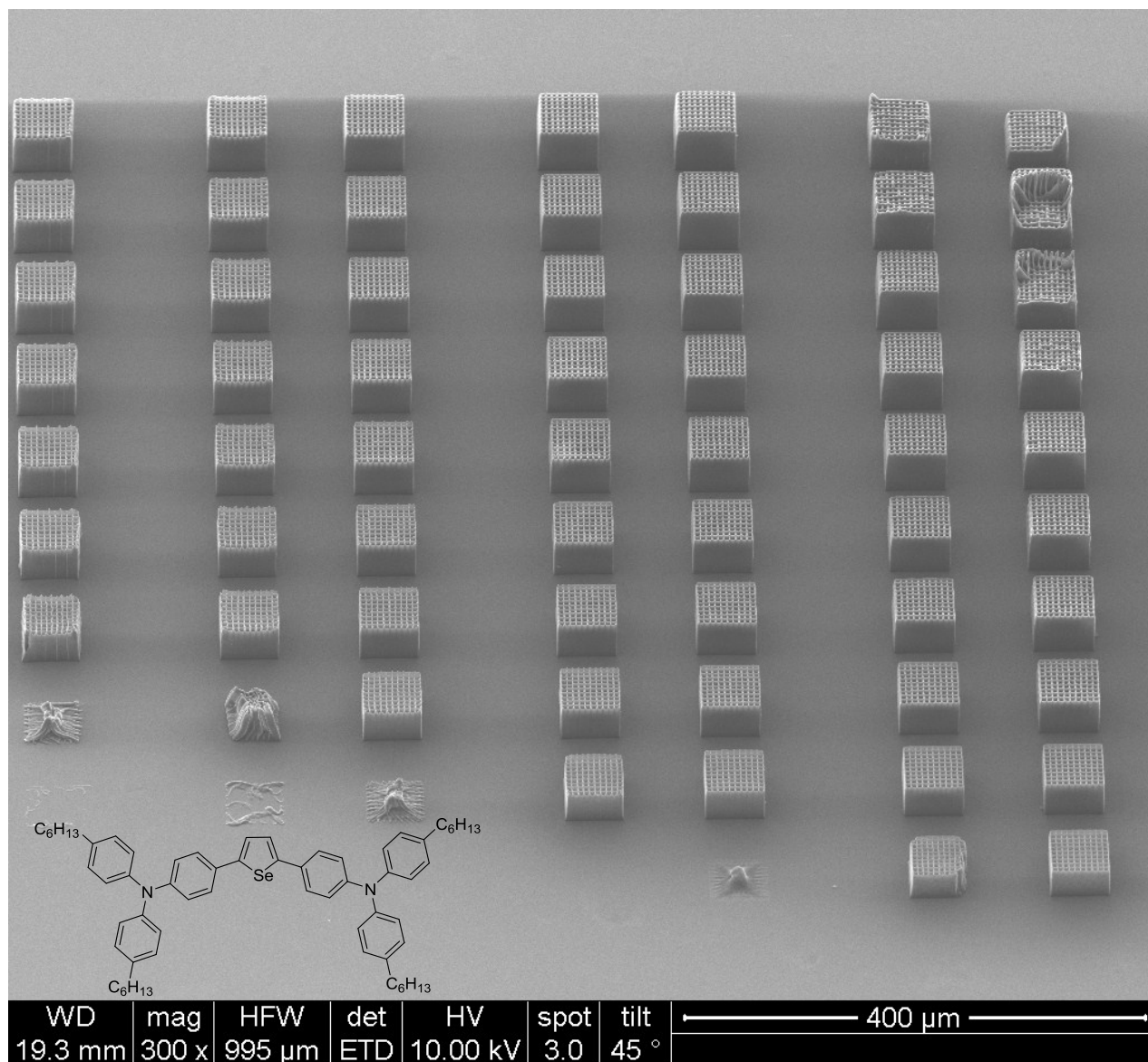


Figure 61: SEM-image of 2PIP-structuring test of compound **XII, HxTPA-1S**; magnification: 300x; 45° tilt.

XIII, HxTPA-1DTT

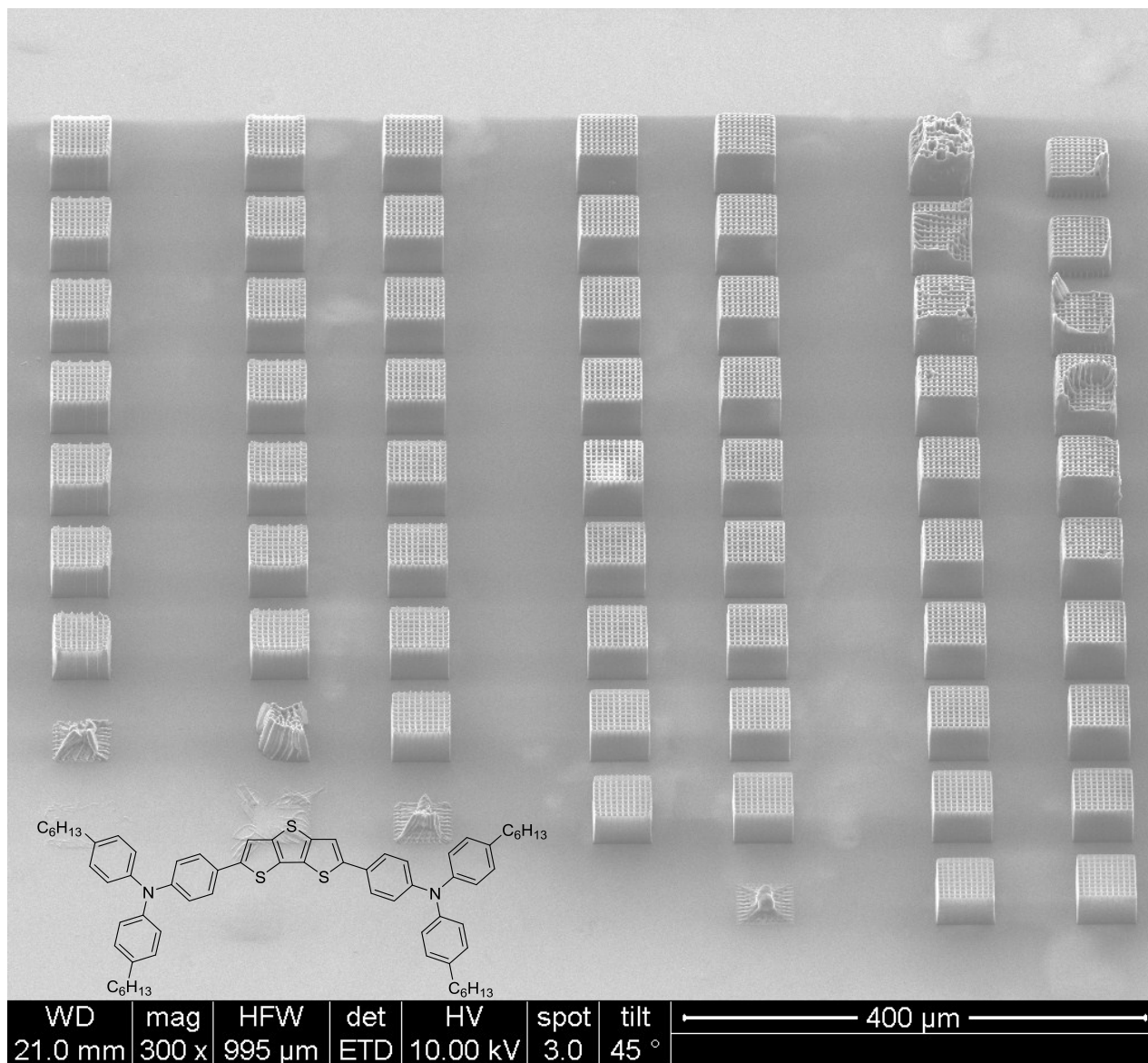


Figure 62: SEM-image of 2PIP-structuring test of compound **XIII**, HxTPA-1DTT; magnification: 300x; 45° tilt.